ROBUST CONTROL OF A TRIPLE-EFFECT EVAPORATOR

Pierre Greeff

ROBUST CONTROL OF A TRIPLE-EFFECT EVAPORATOR

by

PIERRE GREEFF

A dissertation submitted in partial fulfilment
of the requirements for the degree

MASTER OF ENGINEERING (CONTROL ENGINEERING)

in the

FACULTY OF ENGINEERING

UNIVERSITY OF PRETORIA

April 1998

ROBUST CONTROL OF A TRIPLE-EFFECT EVAPORATOR

Author: Pierre Greeff
Supervisor: Prof. P.L. de Vaal
Department: CHEMICAL ENGINEERING
UNIVERSITY OF PRETORIA
Degree: Master of Engineering (Control Engineering)

SYNOPSIS

The aim of this study was to test the applicability and utility of linear multivariable robust analysis techniques to a typical chemical process control problem. The fundamental issue in feedback control is robustness in the face of uncertainty. The integrated nature of the process studied leads to interaction between process variables, necessitating a multivariable approach.

It was found that robust analysis techniques provide a useful source of information: the traditional use of safety margins to ensure robustness based on rules of thumb can be replaced by precisely calculated margins. Robustness of a feedback loop with regard to stability and performance is evaluated by considering an upper bound on a scalar-valued function of frequency, namely the structured singular value.

An obvious requirement for the testing of robustness is a description bounding the expected uncertainty. A description encompassing the entire range of possible plant operating conditions using a linear nominal plant model with associated bounded perturbation for the system under study, was derived. The uncertainty description used, independent norm-bounded additive uncertainty in the transfer function matrix elements, reduces this multivariable description to a number of single input single output process identification problems. A novel algorithm was used to calculate the least conservative nominal plant model with norm-bounded uncertainty description.

The calculation algorithm employed for robust analysis requires that the problem statement be given a specific structure, the so called MΔ-structure. It was found that it is possible to transform the evaluation of robust stability and robust performance to this structure.

The major weakness of robust analysis techniques are strong dependence on the validity and tightness of the uncertainty description. Techniques exist which allow a tighter linear description of plant uncertainty than the technique used in this study. It is however so that a significant portion of the uncertainty stems from the fact that a linear model is used to describe an inherently (known) non-linear plant. It is believed that linear robust analysis techniques provide a significant aid to the

control engineer, but that what is needed in reality is an approach which allows for non-linear process descriptions.

Keywords: robust control, process control, structured singular value, triple-effect evaporator, multivariable control, norm-bounded uncertainty, additive uncertainty, process modelling

ROBUUSTE BEHEER VAN 'N DRIE-STADIUM VERDAMPER

Outeur: Pierre Greeff
Studieleier: Prof P.L. de Vaal
Departement: CHEMIESE INGENIEURSWESE
UNIVERSITEIT VAN PRETORIA
Graad: Magister in Ingenieurswese (Beheeringenieurswese)

SINOPSIS

Die doel van hierdie ondersoek was om die toepaslikheid en bruikbaarheid van lineêre multiveranderlike robuustheidsanalise metodes vir chemiese prosesbeheer te ondersoek. Die kern saak by terugvoerbeheer is robuustheid ten spyte van onsekerheid. Die geïntegreerde aard van die proses onder beskouing gee aanleiding tot interaksie tussen prosesveranderlikes. Hierdie interaksie vereis die gebruik van 'n multiveranderlike benadering.

Daar is gevind dat robuustheidsanalisetegnieke 'n bruikbare bron van inligting is: die tradisionele gebruik van veiligheidsfaktore gebaseer op duimreëls ten einde robuustheid te verseker word vervang deur presies berekende stabiliteitsgrense. Die robuustheid van 'n terugvoerlus, met betrekking tot stabiliteit en werkverrigting, word geëvalueer deur van 'n bogrens van 'n skalaar-waardige funksie van frekwensie, nl. die gestruktureerde singuliere waarde, gebruik te maak.

'n Vereiste vir die evaluering van robuustheid is 'n beskrywing van die verwagte onsekerheid. 'n Lineêre nominale model met geassosieerde begrensde afwyking is gebruik om 'n beskrywing te verkry wat die totale moontlike bedryfsgebied van die aanleg dek. Die gebruikte onsekerheidsbeskrywing, nl. onafhanklike norm-begrensde sommerende onsekerheid in die elemente van die oordragsfunksiematriks, reduseer hierdie multiveranderlike beskrywing tot 'n aantal enkel-inset enkel-uitset prosesidentifikasie probleme. 'n Oorspronklike algoritme is gebruik om die mins konserwatiewe nominale aanlegmodel met norm-begrensde onsekerheidsbekrywing te bepaal.

Die berekeningsalgoritme wat gebruik is vir robuustheidsanalise, vereis die probleemstelling in 'n baie spesifieke struktuur, die MΔ-struktuur. Daar is gevind dat dit moontlik is om die evaluering van robuuste stabiliteit en werkverrigting te transformeer na hierdie struktuur.

Die belangrikste beperking van die robuustheidsanalisetegnieke is dat dit sterk afhanklik is van die geldigheid en noukeurigheid van die onsekerheidsbeskrywing. Daar bestaan tegnieke wat 'n minder konserwatiewe lineêre beskrywing van die onsekerheid moontlik maak as die tegniek wat in hierdie studie gebruik is. 'n Betekenisvolle deel van die onsekerheid is egter die gevolg van die feit dat 'n lineêre model gebruik is om 'n inherent (bekende) nie-lineêre aanleg te beskryf. Hoewel lineêre

robuustheidsanalise 'n bruikbare hulpmiddel is vir die beheeringenieur, is die werklike behoefte om 'n benadering te vind wat nie-lineêre prosesbeskrywings toelaat.

Sleutelwoorde: robuuste beheer, prosesbeheer, gestruktureerde singuliere waarde, prosesmodellering, drie-stadium verdamper, multiveranderlike beheer, norm-begrensde onsekerheid, sommerende onsekerheid

ACKNOWLEDGEMENTS

I wish to thank:

Prof. P.L. de Vaal for guidance and supervision. Also the rest of the Chemical Engineering staff for providing an enjoyable working environment.

The Chamber of Mines for financial assistance.

AECI for allowing me the opportunity to pursue my interest.

My family for providing me with a safe haven and unconditional love and support: my father for his interest, my mother for her uncanny insight, my brother for his example, my sister for her understanding and motivation and Isabelle for her companionship.

TABLE OF CONTENTS

LIST OF SYMBOLS

BD_a Δ with $\sigma^*(\Delta) \leq a$

CL Characteristic Locus

$C_{p,s}$ heat capacity of dissolved substance

$C_{p,w}$ heat capacity of liquid water

d external disturbance

d_b tube diameter

F_{con} condensate flowrate

F_{feed} feed flowrate

$F_{p,j}$ product flowrate from effect j

G true plant

G_0 nominal plant

$H_{bvf,j}$ enthalpy of vapour formed in tube section j

H_{bv} enthalpy of vapour

h_j liquid level in effect j

H_{st} enthalpy of steam on shell-side

H_{vup} enthalpy of steam fed to effect

H_{21} $\left(I + G_0K\right)^{-1} G_0$

INA Inverse Nyquist Array

k_0 cross-condition-criterion

K controller

M or M_{22} interconnection matrix

M molar mass

m noise

N_b number of tubes in effect

P pressure

P_{down} down-stream pressure

P_w^{vap} vapour pressure of water

q controller detuning

$Q_{in,j}$ heat transfer into tube section j

r reference signal

R gas constant

S sensitivity: $\left(I + GK\right)^{-1}$

S_0 nominal sensitivity: $\left(I + G_0K\right)^{-1}$

SSV structured singular value

T complimentary sensitivity: $\left(I + GK\right)^{-1} GK$

T temperature

T_0 nominal complimentary sensitivity: $(I + G_0K)^{-1} G_0K$

T_{ref} reference temperature

u manipulated variable

V volume

$V_{bf,j}$ rate of vapour production in tube section j

V_{down} vapour flowrate from effect

V_{st} flowrate of fresh steam

V_{st} hold-up of steam on shell-side of evaporator

V_{up} vapour flowrate into effect

$W_{1 \text{ or } 2}$ weighting in M

$W_{b,j}$ liquid hold-up in tube section j

W_P performance weighting

W_s sump hold-up

x_w mole fraction of water

$X_{b,j}$ weight fraction dissolved substance in tube section j

X_{feed} weight fraction dissolved substance in feed

$X_{p,j}$ weight fraction dissolved substance in product stream from effect j

X_s sump weight fraction dissolved substance

y output

z tube length

Greek and other symbols

δ element of uncertainty with specific bound

$\tilde{\delta}$ elements of $\tilde{\Delta}$

$\hat{\delta}$ norm-bound imposed on $\tilde{\delta}$

Δ structured block-diagonal uncertainty matrix

$\tilde{\Delta}$ full uncertainty matrix

$\lambda(A)$ eigenvalue of A

μ structured singular value

μ_l liquid viscosity

ρ_l liquid density

ρ_v vapour density

$\rho(A)$ spectral radius of A, max $|\lambda(A)|$

σ^* maximum singular value

$\Im\{\ \}$ Fourier transform

$\| \ \|_\infty$ $\sup_\omega \|A(j\omega)\|$

$\|M\|_\mu = \sup_\omega \{\mu(M(j\omega))\}$

$\mathcal{L}$ (M,Δ)linear fractional transformation: $\mathcal{L}(M,\Delta) = M_{11} + M_{12}\Delta(I - M_{22}\Delta)^{-1} M_{21}$

LIST OF FIGURES

Chapter 2

Chapter 3

Chapter 4

LIST OF TABLES

Chapter 3

Chapter 4

CHAPTER 1: INTRODUCTION

The fundamental issue in feedback design is robustness in the face of uncertainty (Doyle, 1982). This uncertainty has several sources including, among others, processes which are not fully understood, application of linearised models to inherently non-linear processes and the variation of process parameters over time. The analysis is complicated by the fact that the uncertainty is structured.

Tools for the robustness analysis of linear systems have been developed by several workers (Doyle, 1982; Postlethwaite, Edmunds & MacFarlane, 1982; Kouvaritakis&Latchman, 1985a&b; among others). The uncertainty is described by perturbing a linear, nominal plant model with an uncertainty matrix with some sort of bounds on the values the plant model is allowed to assume. It is then possible to determine the robust stability and performance characteristics of the family of plants allowed by the uncertainty description. The utility of the results are of course heavily dependent on the tightness and validity of the uncertainty description.

Increasing cost of energy, stricter environmental and quality standards, as well as increased competition in the global market has led to more integrated process designs. Integrated process designs however result in significant interaction between process variables. Interaction necessitates the use of a multivariable approach.

The main aim of this work was to test the applicability of linear multivariable robust analysis techniques to general chemical engineering systems. Issues considered were:

- The relevancy of the plant description used (linear model with bounded perturbation).
- The difficulties associated with obtaining such a description and whether it can be achieved in practice.
- Whether these techniques render a framework for typical stability and performance evaluation.
- Applicability of linear robust analysis as an aid in controller design.
- Whether, from a chemical process control point of view, these techniques should be further developed and tested to the stage where they can be applied in day to day industrial practice.

In order to facilitate investigation in a fast, cost-effective, safe and efficient manner, it was decided to create a rigorous dynamic computer model of a typical chemical engineering process. A falling film triple-effect evaporator was chosen. It is capacious in the ability to store mass and energy, the system is non-linear and yields a stable, overdamped response (typically modelled as first order lag + deadtime). The energy integration in multiple-effect evaporators (boil-off from one effect is used as heating source for another), leads to significant interaction between process variables, necessitating the use of multivariable analysis techniques. The model was derived by considering time-dependent

mass and energy balances, as well as the associated algebraic equations (e.g. equilibrium, heat transfer, etc.) needed to describe the system behaviour.

The computer model was created in the *Matlab/Simulink* environment. After implementation the model was regarded as a "black box" in subsequent work. This ensured preventing use of information that would not be available when applying the techniques to a real situation. A range of conditions were identified over which the "plant" could possibly operate.

The rest of the project proceeded in three stages. In the first stage a linear, nominal plant description with associated uncertainty was obtained. This plant and uncertainty description is required to cover the entire possible operating range.

Secondly, linear multivariable controllers were designed for the nominal plant model obtained in stage one, using two well-established approaches, namely the Inverse Nyquist Array and Characteristic Locus methods.

Thirdly, robust analysis techniques were applied to the controllers obtained. In particular the effect of various controller detunings on the stability and performance of the actual system were investigated in a quantitative manner as opposed to the normal qualitative investigation.

CHAPTER 2: LITERATURE REVIEW AND THEORY

1. LINEAR ROBUST ANALYSIS

The fundamental issue in feedback design is to provide stability and performance in the face of uncertainty (Doyle, 1982). Uncertainty is the result of mismatch between plant model and actual plant. The necessary tools for the evaluation of nominal, perfectly known linear systems are well-known. This section traces the development of the necessary tools for the evaluation of uncertain systems, i.e. linear robust analysis. Use is made of frequency domain techniques. A first attempt at rigorous analysis of this problem was made by (Doyle&Stein, 1981) in their now classic paper.

In order to accomplish robust analysis two requirements must be met: Firstly, the ability to describe the uncertainty. This is done by perturbing a nominal plant model. Secondly, the tools with which to analyse all possible perturbed systems allowed by the uncertainty description.

The multivariable nature of the problem adds to its complexity. It is possible that different sources of uncertainty may act simultaneously on specific parts of the plant. This leads to the conclusion that plant uncertainty has structure. Two methods of analysing the robustness is immediately apparent (Doyle, 1982). The first is to consider the effect of the perturbations one at a time. This may however yield arbitrarily optimistic results. The second approach is to lump all perturbations into a single, larger perturbation. This may however yield arbitrarily conservative results. Optimistic results are obtained, because the scope of possible perturbations is reduced; conservative results are obtained, because the known structure of the perturbations is ignored, thereby increasing the scope of possible perturbations. To obtain meaningful results the combined effect of all possible perturbations have to be considered simultaneously, without disregarding the structure of the uncertainty.

The theory discussed below is further explained by its actual application to the triple-effect evaporator. This is presented in paragraph 3, chapter 4.

1.1 NOMINAL FEEDBACK SYSTEMS

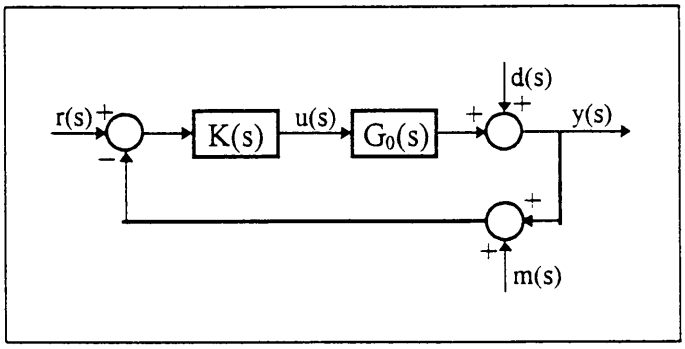

Figure 1: *Standard feedback configuration*

In the following nominal systems, i.e. perfectly known linear systems, are analysed. Reference is made throughout to the feedback system shown in figure 1. Considering figure 1 it easily follows that (Maciejowski, 1989):

$$y = S_0(s)d(s) + T_0(s)r(s) - T_0(s)m(s)$$

where the nominal sensitivity, S_0, is given by

$$S_0 = (I + G_0K)^{-1}$$

and the nominal complementary sensitivity, T_0, is given by

$$T_0 = I - S_0 = (I + G_0K)^{-1} G_0K$$

In general S and T would refer to the sensitivity and complimentary sensitivity of the real plant, G.

The following treatment is brief and only serves as background for the subsequent discussion on robustness.

1.1.1 STABILITY

The stability of feedback systems is normally checked by employing Nyquist-like tests. However, these tests are insensitive to right half-plane pole-zero cancellations between the plant, $G_0(s)$, and controller, K(s). Such cancellations can cause feedback systems to become unstable when any disturbance occurs between K(s) and $G_0(s)$ in the feedback loop shown in figure 1.

Internal stability tests the stability of any input- output pair in the feedback configuration and is therefore sensitive to pole-zero cancellations. Two important results from internal stability is the following (Maciejowski, 1989):

I. If K(s) is stable, the feedback configuration shown in figure 1 is internally stable if and only if

$$H_{21}(s) = [I + G_0(s)K(s)]^{-1} G_0(s)$$

is stable.

II. If K(s) is exponentially stable, then H_{21} as defined above is stable if and only if $\det[I + G_0(s)K(s)]$ has no zeros in the closed right half-plane, and $[I + G_0(s)K(s)]^{-1} G_0(s)$ has no poles at every closed right half-plane pole of $G_0(s)$.

The second part of II is needed to pick up on possible right half plane pole zero cancellations. If it is known that no such cancellations have been introduced, it suffices to check the first part of the theorem. If a positive feedback convention is used similar results are obtained in terms of

$$H_{21}(s) = [I - G_0(s)K(s)]^{-1} G_0(s)$$

and det[I-$G_0(s)K(s)$].

The generalised Nyquist stability theorem can now be derived using the first part of II. In this development use is made of the following identity (Maciejowski, 1989):

$$\det[I + G_0 K] = \prod_i [1 + \lambda_i (G_0 K)]$$

The principle of argument along the Nyquist contour is now applied to this identity to pick up on zeros of det [I+G_0K] in the right half plane. Should any zeros occur on the imaginary axis, they are excluded from the contour, by making small indentations in the contour (Skogestad&Postlethwaite, 1996). The result of this is the generalised Nyquist stability theorem (Maciejowski, 1989):

> If $G_0(s)$ has P_o unstable poles and K(s) is stable, then the closed-loop system formed by $G_0(s)$ and K(s) is stable if and only if the characteristic loci of $G_0(s)K(s)$, taken together, encircle the point -1 + j0 P_o times anticlockwise, assuming that no pole-zero cancellations have occurred.

This may also be stated directly in terms of det [I+G_0K]. (Skogestad&Postlethwaite, 1996):

> If $G_0(s)$ has P_o unstable poles and K(s) is stable, then the closed-loop system formed by $G_0(s)$ and K(s) is stable if and only if the Nyquist plot of det [I+G_0K] encircles the origin P_o times anticlockwise and does not pass through the origin, assuming that no pole-zero cancellations have occurred.

1.1.2 PERFORMANCE

As shown in paragraph 1.1, the relationship between external disturbances and output is given by

$$y = (I + G_0 K)^{-1} d = S_0 d$$

where S_0 is termed the nominal sensitivity. The ability of the feedback system to reject disturbances may be evaluated by considering its sensitivity. Nominal performance is therefore commonly evaluated by considering the following condition (Skogestad&Postlethwaite, 1996):

$$\|W_P S_0\|_\infty < 1$$

where $W_P(s)$ is a diagonal matrix containing weighting functions, i.e.

$$W_P = diag\{w_{P,i}\}$$

A typical weighting function is:

$$w_P = \frac{s/M + \omega_B}{s + \omega_B A}$$

This places the following restrictions on sensitivity in each loop ($1/w_P$):

- it has a high frequency asymptote of M and this constrains the peak in sensitivity to < M; typically values of 2 are used
- the sensitivity crosses 1 at ω_B; approximately the bandwidth requirement
- it is equal to A at low frequencies; a small number such as 0,03 is typically used
- it has a slope below the high frequency asymptote of -1/decade

1.2 UNCERTAINTY

In order to design controllers a plant model is required. It is however so that mismatch exists between the model and actual plant. Uncertainty refers to this mismatch.

1.2.1 SOURCES OF UNCERTAINTY

Uncertainty is a result of several factors (Skogestad&Morari, 1987; Morari&Zafiriou, 1989)

- Real processes are non-linear. If models are obtained through linearisation, then the model is only accurate in the region of the reference state chosen for linearisation. This statement holds even if the linear approximation is very accurate around the reference point. The same is valid for linear models obtained around a specific operating point using process identification techniques. Saturation of manipulated variables represents an important type of non-linearity (Skogestad&Postlethwaite, 1996).
- Processes may be inadequately understood to be modelled, even non-linearly. Process identification may alleviate this by adopting a black-box approach. Fundamental insight is however sacrificed.
- Model parameters may be known inaccurately, or may vary with operating conditions, e.g. dead times vary with flowrates. Process parameters may vary with time, e.g. heat transfer coefficients decrease with time due to fouling.
- Fast dynamic phenomena, e.g. valve dynamics, are usually neglected and this leads to model uncertainty at higher frequencies. There is also a high frequency limit imposed on process identification techniques.

1.2.2 DESCRIPTION

The exact mathematical description of the plant, G(s), is unknown. It is however known that the plant lies in the neighbourhood of some nominal system, $G_0(s)$, whose mathematical model is known exactly. This nominal plant coupled with uncertainty descriptions are now used to define the set of

all possible plants (Skogestad&Morari, 1987). Given a nominal system G_0, there are three commonly used perturbations. They are

$$G(s) = G_0(s) + \delta_a(s)$$
$$G(s) = G_0(s)\left[I + \delta_i(s)\right]$$
$$G(s) = \left[I + \delta_o(s)\right]G_0(s)$$

where δ_a represents an additive perturbation, δ_i an input multiplicative perturbation and δ_o an output multiplicative perturbation (Maciejowski, 1989). The δ's referred to here are assumed to be proper, stable transfer function matrices and are functions of frequency. In order to describe the family of possible plants, the elements of δ are allowed to vary within boundaries imposed by considering the available information regarding the uncertainty. In general these bounds can refer to both the magnitude and phase of either the elements of δ, or δ as a whole. Magnitude and phase bounds are applicable, since we are dealing with numbers in the complex plane. Subsequently δ will refer to the smallest element with a specific bound; either the entire matrix or its individual elements. A useful class of perturbations is obtained by restricting the spectral norm of δ. This is considered further in paragraph 1.3.2. Of course setting δ equal to zero yields the nominal system.

In order to fully utilise the known structure of the uncertainty, it may be necessary to employ more than one of the uncertainty descriptions simultaneously (Doyle, 1982).

Depending on the amount of information available regarding the exact structure of the perturbation, the perturbation can be classified as either structured or unstructured.

1.2.3 REPRESENTATION: LINEAR FRACTIONAL TRANSFORMATIONS (LFT'S)

It is always possible to isolate all sources of uncertainty into a single block-diagonal matrix in which each block represents a source of uncertainty (Doyle, 1982). In other words a number of uncertainty matrices, δ_j, is combined into a single block diagonal matrix, Δ. Δ may be represented as:

$$\Delta = diag\left\{\delta_1, \delta_2, \ldots, \delta_j, \ldots, \delta_m\right\}$$

Of course each of the δ matrices has a specific size. The only allowed Δ matrices are the ones with the correct block-diagonal structure that satisfy the conditions on the individual δ's. If there is only one δ, the uncertainty is termed unstructured, otherwise it is termed structured.

This is schematically depicted in figure 2. M is known exactly since it only incorporates the nominal plant model and the controller, both of which are known exactly.

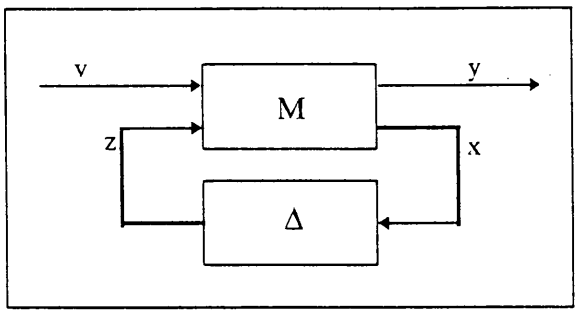

Figure 2: *Isolating uncertainty yielding an M-Δ feedback structure*

Partitioning M so that

$$\begin{bmatrix} y \\ x \end{bmatrix} = \begin{bmatrix} M_{11} & M_{12} \\ M_{21} & M_{22} \end{bmatrix} \begin{bmatrix} v \\ z \end{bmatrix}$$

it follows that

$$y = \left\{ M_{11} + M_{12}\Delta(I - M_{22}\Delta)^{-1} M_{21} \right\} v$$

The above leads to the following definition (Packard&Doyle, 1993):

$$\mathcal{L}(M,\Delta) = M_{11} + M_{12}\Delta(I - M_{22}\Delta)^{-1} M_{21}$$

where $\mathcal{L}(M,\Delta)$ is called a linear fractional transformation (LFT).

For an MΔ-structure with the Δ-matrix above M, and partitioning of M in such a way that M_{11} is compatible with Δ, leads to the following linear fractional transformation:

$$\mathcal{L}(\Delta,M) = M_{22} + M_{21}\Delta(I - M_{11}\Delta)^{-1} M_{12}$$

1.2.4 Independent Uncertainty in the Transfer Function Matrix Elements

In certain cases exact bounds on the individual elements in the transfer function matrix are known. This typically occurs in cases where such bounds are determined by means of experimental system identification, or can arise because of specific knowledge during the modelling stage (Kouvaritakis& Latchman, 1985b). In order to incorporate these bounds into a matrix setting it is necessary to make use of an additive uncertainty description. This is because matrix summation is performed element-wise, whereas matrix-multiplication is performed as a row and column operation.

These descriptions are potentially very conservative, since they do not allow for correlations between elements, but allow them to vary independently from each other (Morari&Zafiriou, 1989). Consider the case where a perturbation in more than one element is caused by the same factor, e.g.

an input multiplicative uncertainty will result in the same relative perturbation in each matrix element in one of the system matrix columns. Independent uncertainty bounds on the transfer matrix elements will allow the elements to vary independently from each other; a situation that is not possible in practice. Plants are therefore included in the set of possible plants that can never occur in practice. This may lead to conservative results.

It is possible to transform this uncertainty description to block-diagonal form (each block being 1×1). The resulting Δ-matrix is however $n^2\times n^2$ (Morari&Zafiriou, 1989). This is the approach adopted in this study (see paragraph 3, chapter 4).

1.3 ROBUST STABILITY

It is important to realise that the results derived in this section assume nominal stability. Before checking for robust stability, it is imperative to firstly assure that the controller stabilises the nominal plant.

1.3.1 DEVELOPMENT

From paragraph 1.2.3 it should be clear that the uncertain feedback system shown in figure 2 will remain stable if

$$\mathcal{L}(M,\Delta) = M_{11} + M_{12}\Delta(I - M_{22}\Delta)^{-1}M_{21}$$

is stable for all allowed Δ. Assuming that the controller stabilises the nominal plant, it follows that M, and therefore M_{11}, M_{12}, M_{21} and M_{22}, are stable. Δ has been assumed stable. The only possible source of instability in the above expression is therefore

$$\Delta(I - M_{22}\Delta)^{-1} = (I - \Delta M_{22})^{-1}\Delta$$

The reader will notice that this form corresponds to the H_{21} transfer function matrix used in the derivation of internal stability in paragraph 1.1.1. Robust stability can therefore be checked by considering the stability of the feedback connection of M_{22} and Δ for all allowed Δ.

The Nyquist stability theorem will now be applied to the feedback connection of M_{22} and Δ. Since both M_{22} and Δ are stable, right half plane pole zero cancellations are impossible and the Nyquist criterion is therefore valid. For the same reason $M_{22}\Delta$ has no unstable poles, and therefore no encirclements of $-1 + j0$ is required for closed loop stability. What is therefore required is a way to analyse the characteristic loci (the eigenvalues as a function of frequency) of $M_{22}\Delta$ for all allowed Δ. This problem is complicated by the fact that no simple relation exists between the eigenvalues of M_{22} and Δ, and those of $M_{22}\Delta$.

The above may also be stated in terms of det[I-M_{22} Δ] by using the alternative form of the Nyquist stability criterion. The result is (Skogestad&Postlethwaite, 1996):

> Assume that the nominal system $M_{22}(s)$ and $\Delta(s)$ are stable. Consider the convex set of perturbations Δ (convexity: if Δ' is an allowed perturbation then so is $c\Delta'$, where c is any real scalar with $|c| \leq 1$). Then the feedback system in figure 2 is stable for all allowed perturbations if and only if
>
> Nyquist plot of det[$I - M_{22}\Delta$] does not encircle the origin
>
> $\Leftrightarrow$ $\det[I - M_{22}\Delta] \neq 0$, for all ω and all allowed Δ

The proof of the first statement is a direct application of the Nyquist stability criterion to stable M_{22} and Δ. The second part of the theorem makes use of the convexity property of the set Δ. This convexity property makes the determinant a continuous function of the set Δ. (This follows since $\det[cA] = c^n \cdot \det[A]$, where A is n×n (O'Neill, 1991).) If a Δ' exists such that the Nyquist contour of det[I - $M_{22}\Delta'$] encircles the origin, then another perturbation exists in the set, $\Delta'' = \varepsilon\Delta'$ with $\varepsilon < 1$, and an ω' such that

$$\det[I - M_{22}(\omega')\Delta''(\omega')] = 0.$$

1.3.2 Structured Singular Value (SSV) and Norm Bounded Perturbations

In this section the structured singular value (SSV) is introduced and its use discussed. This is the robust analysis tool used throughout in this work.

1.3.2.1 Norm Bounded Perturbations and Scaling

Use of the SSV is restricted to the class of norm bounded, block-diagonal perturbations. The only bound imposed on δ is a restriction on its spectral norm δ (e.g. $\sigma^*(\delta) \leq a$, where a is some real constant), ignoring any possible phase information. This results in disk-shaped uncertainty regions. Considering a block-diagonal uncertainty matrix, Δ, as introduced in paragraph 1.2.3, these bounds correspond to:

$$\Delta = diag\{\delta_1, \delta_2, \ldots, \delta_i, \ldots, \delta_m\} \quad , \quad \sigma^*(\delta_i(\omega)) \leq a_i(\omega)$$

It is customary to include scaling matrices into matrix M in figure 2, paragraph 1.2.3, such that the norm bounds become

$$\sigma^*(\delta_i(\omega)) \leq 1$$

1.3.2.2 SSV: MOTIVATION FOR USE

An important property of norm bounded perturbations as discussed above is that it is convex (i.e. if Δ' is an allowed perturbation then so is $c\Delta'$, where c is any real scalar with $|c| \leq 1$). It follows from paragraph 1.3.1 that a necessary and sufficient criterion for robust stability is therefore given by:

$$\det[I - M_{22}\Delta] \neq 0 \quad \text{for all } \omega \text{ and all allowed } \Delta$$

A workable, sufficient criterion is now derived (Maciejowski, 1989).

$$\det[I - M_{22}\Delta] = \prod_i (1 - \lambda_i(M_{22}\Delta))$$

In other words stability is ensured as long as

$$\lambda_j(M_{22}\Delta) \leq 1$$

Further

$$\lambda_j(M_{22}\Delta) \leq \rho(M_{22}\Delta) \leq \sigma^*(M_{22}\Delta) \leq \sigma^*(M_{22})\sigma^*(\Delta)$$

It is also true that

$$\sigma^*(\Delta) \leq a \text{ if and only if } \sigma^*(\delta_i) \leq a \text{ for all i}$$

If scaling has been introduced such that a = 1 (this ensures that $\sigma^*(\Delta) = 1$), it follows from the above arguments that stability is guaranteed if

$$\sigma^*(M_{22}) \leq 1$$

This criterion is however conservative for the following reasons:

- the sequence of inequalities between $\lambda_j(M_{22}\Delta)$ and $\sigma^*(M_{22})\sigma^*(\Delta)$
- the fact that the known structure of Δ is not used

This motivates the definition of the structured singular value presented in the next section which yields necessary and sufficient stability conditions.

1.3.2.3 SSV: DEFINITION AND APPLICATION

In order to simplify the notation in what follows the following definition is introduced. BD_a is the set of stable block-diagonal matrices with structure corresponding to the known structure of the

uncertainty, and $\|\delta_i\|_\infty \leq a$, i = 1,2...m. Using this terminology the allowed perturbations, after scaling , belong to the set BD_1.

The structured singular value of a matrix is now defined as (Doyle, 1982):

$$\mu(M_{22}(j\omega)) = \begin{cases} 0 \text{ if } \det[I - M_{22}(j\omega)\Delta(j\omega)] \neq 0 \text{ for any } \Delta \in BD_\infty \\ \dfrac{1}{\min\limits_{\Delta \in BD_\infty} [\sigma^*(\Delta(j\omega)) : \det[I - M_{22}(j\omega)\Delta(j\omega)] = 0} \end{cases} \text{otherwise}$$

In other words the structured singular value is the inverse of the magnitude of the smallest Δ, with the required block-diagonal structure, needed to destabilise the process. An obvious necessary and sufficient condition for robust stability is now given in (Doyle et al, 1982): The feedback system will remain stable for all $\Delta \in BD_1$ if and only if

$$\|M_{22}\|_\mu < 1$$

where

$$\|M_{22}\|_\mu = \sup_\omega \{\mu(M_{22}(j\omega))\}$$

1.3.2.4 SSV: CALCULATION

Although the definition and theorem given in paragraph 1.3.2.3 yield a simple working framework, a real test for robust stability has not been provided, since no means to calculate the structured singular value has been presented and the optimisation mentioned in the definition is not convex. A number of useful properties of the structured singular value is presented in (Doyle, 1982). Among them is the following upper bound

$$\mu(M_{22}) \leq \inf_D \sigma^*(DM_{22}D^{-1})$$

where D is the set of positive real matrices given by $D = \text{diag}\{d_i I_i\}$ where the size of each block, i.e. the size of I_i, corresponds to the structure of Δ. This optimisation problem is convex, and for three or fewer blocks equality is obtained. Numerical experiments however indicate that the results calculated are reasonably tight for even more blocks (Maciejowski, 1989). What is required to ensure robust stability is an upper bound on μ and this has now been provided.

Another property is (Doyle, 1982)

$$\rho(M_{22}) \leq \mu(M_{22}) \leq \sigma^*(M_{22})$$

This means that the stability bounds calculated using structured singular values are less conservative than those using the technique presented in paragraph 1.3.2.2 using only singular values. Of course

$$\mu(M_{22}) = \sigma^*(M_{22})$$

for unstructured perturbations.

1.3.3 ALTERNATIVE APPROACHES

The drawback of the approach presented above is that the bounds derived are norm-bounded, disregarding any possible phase information. This description results in disk-shaped uncertainty regions, whereas the true shape of the uncertainty may be quite different. The amount of conservatism introduced can be easily visualised as shown in figure 3.

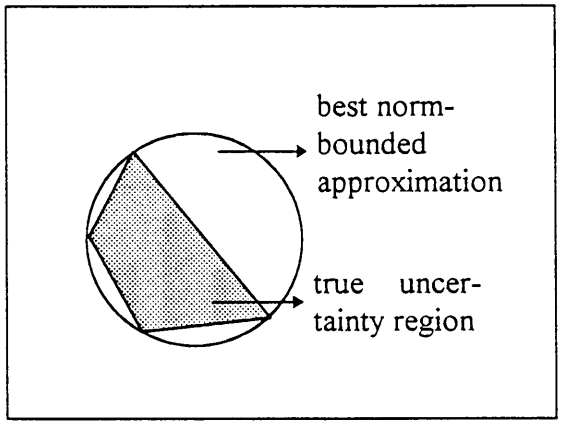

Figure 3: *Possible conservatism introduced using only norm-bounds*

The majority of the alternative approaches presented below aims at describing the true uncertainty region more accurately, utilising both gain and phase information.

1.3.3.1 GAIN PHASE METHOD

This approach was put forward by (Postlethwaite, Edmunds & MacFarlane, 1982). Use is made of a curvilinear rectangular or annular region in the complex plane which contains the eigenvalues of a matrix. This region is termed the principal region and its boundaries are described by the minimum and maximum principal gains and the minimum and maximum principal phases (if the principal phases have a spread of more than π radians the region becomes annular).

Using the following well-known result

$$\sigma^*(M_{22}\Delta) \geq \sigma^*(M_{22})\sigma^*(\Delta)$$

a small gain theorem is derived in the reference.

A novel bound on the phase of the principal region of the product of two matrices is then derived in terms of the phases of the individual matrices. This is then used to derive a small phase theorem.

The small gain and small phase theorems are now combined into a single robust stability theorem utilising both gain and phase information. The theorem argues that in order to achieve instability an encirclement of the critical point by the characteristic loci of $M_{22}\Delta$ is required, as shown in paragraph 1.3.1. Such an encirclement is only possible if the phase and gain of the principal region simultaneously exceed $-\pi$ radians and one respectively.

This theorem utilises both gain and phase information describing the uncertainty. The drawback is that only unstructured perturbations are allowed.

1.3.3.2 CROSS-CONDITION CRITERION AND E-CONTOURS

This approach was first put forward by (Kouvaritakis&Latchman, 1985a). A unified approach, namely maximum principle direction alignment (MPDA), yielding the same results was later put forward by (Kouvaritakis&Latchman, 1985b).

The class of perturbations considered is a matrix with norm-bounds on the individual elements, i.e.

$$\left\{\tilde{\Delta}: \tilde{\Delta}^{+} \leq P\right\}$$

where $\leq$ refers to element-by-element comparison and P is a matrix with all positive elements. It is also possible to transform this problem to block-diagonal form (each block being 1×1) and then to analyse it using the SSV methods discussed in paragraph 1.3.2. This approach is followed in this study and demonstrated in paragraph 3, chapter 4.

Stability is guaranteed if

$$\rho(M_{22}P) < 1$$

since any encirclements of the critical point are now impossible. This can be developed to

$$\rho(M_{22}P) \leq \sigma^{*}(M_{22}P) \leq \sigma^{*}(M_{22})\sigma^{*}(P) < 1$$

This stability bound can be easily calculated. Conservatism has however been introduced by:

- moving from the spectral radius to the maximum singular value

- the Schwartz inequality, in this case $\sigma^*(M_{22}P) \le \sigma^*(M_{22})\sigma^*(P)$

It is now shown (Kouvaritakis & Latchman, 1985b) that all this conservatism can be removed (equality obtained in the above sequence of inequalities), if maximum principal direction alignment (MPDA) is valid. Non-similarity scaling is now employed to approximate MPDA.

$$\rho(M_{22}P) = \rho\left(R^{-1}M_{22}L^{-1}LPR\right) \le \sigma^*\left(R^{-1}M_{22}L^{-1}LPR\right) \le \sigma^*\left(R^{-1}M_{22}L^{-1}\right)\sigma^*(LPR) = \frac{\sigma^*(LPR)}{\sigma_*\left(LM_{22}{}^{-1}R\right)}$$

L and R are real, diagonal matrices used to approach MPDA as closely as possible. The cross condition number, k, is defined as:

$$k = \frac{\sigma^*(LPR)}{\sigma_*(LM_{22}R)}$$

Robust stability is therefore guaranteed if

$$k_0 = \inf_{L,R} \frac{\sigma^*(LPR)}{\sigma_*(LM_{22}R)} < 1$$

It is further shown that MPDA is achievable so that the above bound becomes sufficient and necessary. This optimisation is computable.

An analogous approach yields graphical results. Regions in the complex plane, termed E-contours, are calculated which enclose all allowed characteristic loci (Kouvaritakis & Latchman, 1985a, 1985b). Eigenvalue exclusion results are derived which make computation of these regions possible. An algorithm for the construction of E-contours is given. This approach has the advantage that the traditional form of the Nyquist graphical approach is retained; no new information is however added.

The E-contour approach has been further adapted by (Kouvaritakis, Rossiter & Wang, 1991), by allowing a more accurate description of the uncertainty region. Norm-bounded uncertainty descriptions yield disk-shaped uncertainty regions. These regions are now refined to ellipses with major axis, minor axis and rotation with regard to the real axis fitted to the uncertainty. This means that gain and phase information are employed and tighter stability bounds calculated. The resulting E-contours are referred to as highly structured.

1.3.3.3 Highly Structured Stability Margins

This approach was put forward by (Rotstein, Desages & Romagnoli, 1989). Complete phase and gain information can be employed and the allowed uncertainty region can have an arbitrary shape.

In this work use is made of the concepts of expansion function and gain margin. The gain margin is defined as the extent to which the uncertainty region has to be expanded, using the expansion function, in order to yield a robustly unstable system.

An implementable algorithm is derived which converges to the gain margin of the exact uncertainty region of arbitrary shape. The idea is to cover the uncertainty region in circles. The gain margin for this larger uncertainty region is then calculated and the original uncertainty region is then expanded or compressed proportional to this value. The new uncertainty region is then further subdivided and new gain margins calculated for all possible combinations of uncertainty regions. This procedure converges to a number of circular bounds which closely describes the exact uncertainty region.

The drawback of this approach is that the algorithm is cumbersome. The fact that all the available phase and gain information is utilised results in tighter stability margins being derived.

1.3.3.4 NUMERICAL RANGE

The numerical range of a matrix has the properties that it is amiable to computation and contains the eigenvalues of a matrix (Palazoglu&Khambanonda, 1990). There also exists a simple relation between the numerical range of the sum of two matrices, and the numerical ranges of the individual matrices.

Owens (1984) made first use of the numerical range concept to allow a more detailed description of plant perturbations including gain and phase information. These ideas were further developed by (Palazoglu&Khambanonda, 1989), who derived a stability criterion used to detune filter constants in the internal model control (IMC) controller structure.

In (Palazoglu&Khambanonda, 1990) the numerical range is combined with singular value theory to yield refined eigenvalue inclusion regions (REIR). Numerical range eigenvalue inclusion results are superimposed on singular value inclusion results in order to yield these regions. A general robust stability criterion is now derived in terms of encirclements by the REIR as the frequency parameter is varied. In order to facilitate computation the relevant matrices are factored into normal matrices, since this yields easily calculable numerical ranges (the numerical range of a normal matrix is a polygon with vertices the eigenvalues of the matrix).

1.4 ROBUST PERFORMANCE

In this section it is shown that no new tools are required for the analysis of robust performance. The approach is simply to add another block to the Δ-matrix. Robust performance is equivalent to robust stability with regard to an appended Δ-matrix, $\text{diag}\{\Delta_P,\Delta\}$ (Doyle et al, 1982).

1.4.1 NOMINAL PERFORMANCE AS A ROBUST STABILITY PROBLEM

As stated before, paragraph 1.2, an often used performance specification takes the form

$$\|W_P S_0\|_\infty = \left\|W_P (I + G_0 K)^{-1}\right\|_\infty < 1 .$$

Consider the following feedback loop with uncertainty shown in figure 4. $\tilde{\Delta}_P$ is a norm-bounded unstructured uncertainty; the norm-bound is given by

$$\sigma^*\left(\tilde{\Delta}_P W_P^{-1}\right) \leq 1$$

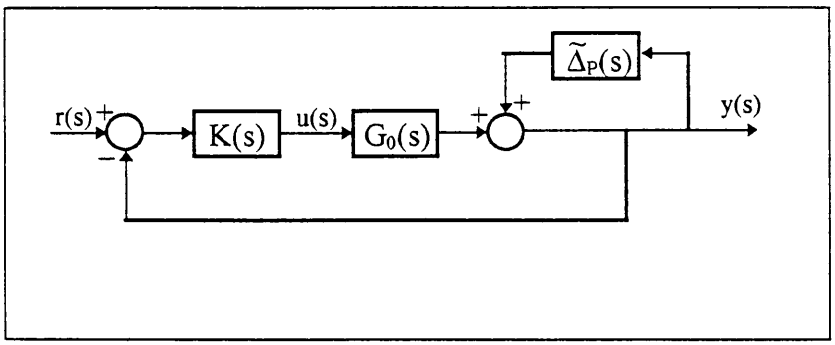

Figure 4: *Feedback loop for nominal performance*

Following the procedure outlined above this can be cast into the following MΔ-structure:

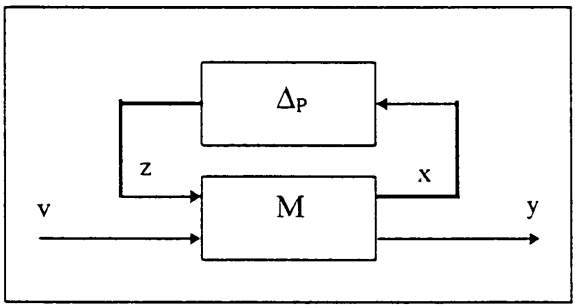

Figure 5: *MΔ-structure for nominal performance*

In the above structure the bound is given by

$$\sigma^*(\Delta_P) \leq 1$$

and W_P, the performance weighting, has been included in M. This structure can be represented by the following LFT:

$$y = \left(\Delta_P, M\right)v = \left\{M_{22} + M_{21}\Delta_P\left(I - M_{11}\Delta_P\right)^{-1} M_{12}\right\}v$$

Robust stability of the feedback loop in figure 5 corresponds to the following condition

$$\|M_{11}\|_{\mu} = \sup_{\omega}\{\mu(M_{11}(j\omega))\} < 1$$

Since Δ_P is unstructured, it follows that

$$\mu(M_{11}) = \sigma^*(M_{11})$$

In this case M_{11} is given by

$$M_{11} = W_P(I + G_0K)^{-1}$$

The above leads to the following condition for robust stability of the feedback loop

$$\sigma^*\left[W_P(I + G_0K)^{-1}\right] < 1$$

This is precisely the condition for nominal performance given at the start of this section. It has therefore been shown that nominal performance is equivalent to robust stability with regard to the uncertainty description used in this paragraph.

1.4.2 Robust Performance and the Main Loop Theorem

What is needed to establish robust performance is to show that

$$\|W_PS\|_{\infty} = \left\|W_P(I + GK)^{-1}\right\|_{\infty} < 1.$$

is valid for all possible plants, G, allowed by the uncertainty description. Consider the appended MΔ-structure shown in figure 6.

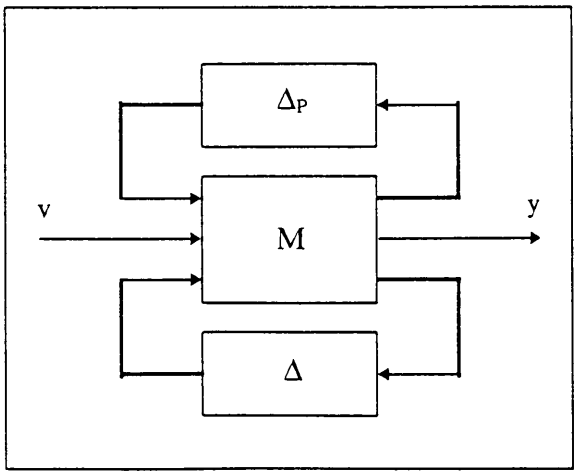

Figure 6: *Appended MΔ-structure for robust performance*

The bottom part of this structure generates all possible plants allowed by the uncertainty description, denoted by $\mathcal{L}(M,\Delta)$, while the top part represents the performance criterion. Analogous to the development in paragraph 1.4.1, robust performance is guaranteed if

$$\left\| \max_{\Delta} \mu\left(M_{11}\left[\mathcal{L}(M,\Delta)\right]\right) \right\|_{\infty} < 1$$

The following result is the main loop theorem from (Packard&Doyle, 1993):

$$\mu_{\Delta_P,\Delta}(M) < 1 \Leftrightarrow \begin{cases} \mu(M_{22}) < 1 \\ \max\limits_{\Delta} \mu\left(M_{11}\left[\mathcal{L}(M,\Delta)\right]\right) < 1 \end{cases}$$

It is thus clear that robust performance is guaranteed if the system perturbed by the appended Δ_P-Δ-structure is robustly stable. It is also obvious that robust performance implies robust stability.

1.5 APPLICATION

In order to apply the robust analyis techniques developed above, it is required to always ensure nominal stability before proceeding. The technique establishes robust stability by checking that the number of encirclements of the critical point remains unchanged from the nominal case. Clearly the incorrect number of encirclements for the nominal case, renders the robust stability test results invalid. Performance is analysed by checking the robust stability of a very specific MΔ-structure. The same argument therefore holds for robust performance analysis. Nominal stability is checked using the Nyquist stability criterion (paragraph 1.1.1).

The next step is to cast the problem into the standard MΔ-structure. This is illustrated by means of an example in chapter 4 for the robust stability, nominal performance and robust performance cases.

The designer now checks that the robust condition set in the MΔ-structure is satisfied by ensuring that $\|M_{22}\|_{\mu} < 1$. The smaller the value of $\|M_{22}\|_{\mu}$, the greater the margin of safety. A useful source of information for the designer is provided by considering a graph of structured singular value against frequency. The main design aim is to minimise $\|M_{22}\|_{\mu}$, i.e. the peak value of SSV.

In (Agamennoni et al, 1989) a simple application of robust analysis to controller tuning is introduced. It is first proved that the structured singular value (SSV) is a continuous function of M. It is hereafter shown that if M has no poles on the imaginary axis, the SSV is a continuous function of frequency. In the final step of controller design the SSV of the controller designed with nominal

plant considerations is calculated. Through a detuning of the controller, i.e. K(s) = q·K(s) (q is a constant scalar), the SSV of the system is now minimised to yield a controller with maximum robust stability bounds. The utility of this approach is of course independent of the manner in which the initial K is obtained.

It would also be possible to incorporate robust analysis techniques as the final step in an iterative controller design loop. One would redesign the controller until satisfactory robust behaviour is obtained. The most advanced application of these techniques corresponds to μ-synthesis; the so called DK-iteration (Skogestad&Postlethwaite, 1996). Here robustness is considered explicitly during the actual controller design step.

2. PROCESS IDENTIFICATION: FREQUENCY RESPONSE FROM PULSE TESTING

Obtaining of dynamic relationships between plant variables, i.e. transfer functions, based on experimental dynamic data is the realm of process identification (Luyben, 1990). This approach can only be employed where processes are already in operation. It is often used where the process is deemed to be too complex to warrant modelling attempts from first principles, or where uncertainty exists regarding certain model parameters. It is also used for model validation. In this study process identification is applied over a range of operating conditions, in order to determine a nominal plant model and uncertainty description.

Pulse testing is one of a number of techniques that can be applied for process identification. It has the following advantages when one considers the objective of the identification and the nature of the process:

- results are obtained directly in the frequency domain
- the disturbance can be applied to processes containing pure integrators and still yield bounded responses

Pulse testing is performed by applying a pulse disturbance to the process at steady state (Luyben, 1990). The pulse starts and ends at the same value and square pulses are often used. The process output is now recorded until steady state is once again obtained.

2.1 MATHEMATICAL CONSIDERATIONS

The frequency response of an output variable to an input variable can be calculated by (Luyben, 1990)

$$G(jw) = \frac{\int_0^\infty y^*(t)e^{-j\omega t}dt}{\int_0^\infty u^*(t)e^{-j\omega t}dt}$$

The process inputs and outputs are defined in terms of perturbation variables, that is y^* and u^* in the above equation. Since a pulse input is used, u^* returns to zero and therefore the integral in the denominator is finite. For systems where the initial steady state and the final steady state correspond (y^* returns to zero) the integral in the numerator is also bounded. In such cases the results are easily computable. For systems containing pure integrators the final steady state will however not correspond to the initial steady state and the integral in the numerator becomes unbounded.

One method of addressing this problem is presented by (Seborg, Edgar & Mellichamp, 1989). It is proposed that the output data be differentiated numerically. The frequency response of the differentiated data is now computed. If G_1 represents the frequency response of the original data set and G_2 the response of the differentiated data, G_1 and G_2 are related by

$$G_1(j\omega) = \frac{G_2(j\omega)}{j\omega}$$

This follows from (O'Neill, 1991)

$$\Im\{f'(t)\} = j\omega \cdot \Im\{f(t)\}$$

2.2 Practical Considerations

2.2.1 *Digital Evaluation of Fourier Transforms*

It is shown in (Luyben, 1990) that the Fourier transform can be approximated by

$$\int_0^\infty f(t)e^{-j\omega t}dt \approx \sum_{k=1}^{N} e^{-j\omega t_{k-1}}\left\{x_k\left(\frac{e^{-j\omega\Delta t_k}-1}{\omega^2\Delta t_k}-\frac{e^{-j\omega\Delta t_k}}{j\omega}\right)-x_{k-1}\left(\frac{e^{-j\omega\Delta t_k}-1}{\omega^2\Delta t_k}-\frac{1}{j\omega}\right)\right\}$$

where subscript k refers to sampling instant and $\Delta t_k = t_k - t_{k-1}$. This approach is convenient since the sampling time need not be constant. The Fast Fourier Transform reduces the computational effort, it however requires equally-spaced sample-times, which is not the case for the application considered here.

2.2.2 *Pulse Width and Height*

Consider a rectangular input pulse of width D and height h. The Fourier transform of this pulse is given by

$$\begin{aligned} U(\omega) &= \frac{h}{j\omega}(1-e^{-j\omega D}) \\ &= \frac{h}{j\omega}\left(1-\cos(\omega D)+j\sin(\omega D)\right) \\ &= \frac{h\sin(\omega D)}{\omega}-\frac{hj}{\omega}\left(\cos(\omega D)-1\right) \end{aligned}$$

From this last expression it follows that at $\omega = 2\pi/D$ the frequency response of the pulse becomes zero. Since this frequency response appears in the denominator of the system frequency response, the system frequency response becomes unbounded. For this reason the experimentally determined frequency response of the system becomes meaningless at frequencies close to $2\pi/D$, and the smaller the pulse width can be made, the higher the frequencies at which the frequency response can be determined.

As far as pulse height is concerned there are two conflicting requirements. Due to the non-linear nature of the processes, a too big pulse may drive the system away from the operating point around which an experimental linear model is to be determined. Too small a pulse may however have such a negligible effect on the process, that it may well be indiscernible given process noise (or in this case the error tolerance of the integration algorithm used). (Luyben, 1990)

3. CONTROLLER DESIGN METHODS

The Characteristic Locus and Inverse Nyquist Array design methods were employed. Both directly employ the nominal plant frequency response. Neither of them allows for directly incorporating uncertainty information during the design. Robustness needs to be checked in a subsequent step employing the techniques described in paragraph 1.

These design methods were favoured since they directly employ the frequency response. The results obtained from the process identification step are already in the frequency domain. This means that conservatism that would have been introduced due to inaccurate fitting of transfer function models or state space models was avoided.

A controller design technique such as μ-synthesis would however yield superior results, since robustness is considered explicitly during the controller design step (Skogestad&Postlethwaite, 1996). This technique has the disadvantage that state space plant descriptions are required. This would introduce further conservatism in the uncertainty description as explained above. Furthermore a state space description cannot deal directly with deadtime and an approximation (e.g. the Padé approximation) is required. The resulting controllers are also high order and controller order reduction techniques are in general required.

3.1 INVERSE NYQUIST ARRAY METHOD

The Inverse Nyquist array technique was first put forward by (Rosenbrock, 1974). The technique directly uses the frequency response of the plant for design of the controller. In a first step it is aimed to decouple the plant, i.e. to reduce the multivariable nature of the problem to a number of SISO design problems. After this decoupling a diagonal controller, effectively a number of SISO-controllers, is now added in series with the decoupler in order to give the desired response in each

loop. The decoupling is however never 100% efficient, and the effect of interaction has to be taken into account when designing the SISO controllers. There are both inverse and direct Nyquist array methods and the inverse technique was used in this study. When use is made of the inverse technique, simple relations exist to take the effect of interaction into account when designing the SISO controllers. The inverse method uses the inverse of the plant frequency response, G_0^{-1}. The major drawback of the inverse approach is that the compensator that is yielded by this design approach has to be inverted for implementation. The approach followed here yields controllers that can be simply inverted.

As stated above the aim of this design method is to decouple the system in a first design step and thereafter implement a number of SISO controllers. The controller K is therefore designed as

$$K^{-1} = K_b^{-1} K_a^{-1}$$

where K_a^{-1} serves to decouple G_0^{-1} and K_b^{-1} is a diagonal controller shaping the decoupled loops. The controller is realised and implemented as

$$K = K_a K_b$$

3.1.1 Decoupling the System: Quasi-Gauss Elimination

In this approach use is made of an analogy to Gauss-elimination, commonly employed when solving systems of linear equations (Burden&Faires, 1993), to eliminate the non-diagonal elements (Hulbert&Braae, 1982). In general the i,jth element can be eliminated from a constant matrix, Z, by pre-multiplying with an identity matrix with the i,jth element replaced with

$$m_{ij} = -\frac{z_{ij}}{z_{jj}}$$

The only difference when applying this technique to a transfer function matrix is that the elements of Z (in practice Z is the inverse frequency response of the plant), and therefore m, are functions of frequency. In order to proceed the value of m_{ij} is calculated at a number of discrete frequency points and this frequency response fitted to a low order transfer function. Hereafter a performance criterion is optimised by varying the parameters in order to ensure optimal fitting. A few general guidelines to aid in the initial choice of m_{ij} are given by (Hulbert&Braae, 1982). In order to yield a decoupled system all the non-diagonal elements are eliminated in this fashion. As already stated the inverse design technique requires that the controller be inverted. The inverse of the matrices used for elimination is however easily obtained as an identity matrix with the i,jth element replaced by $-m_{ij}$.

3.1.2 Diagonal Controller Design

Since inverse frequency responses are being used, inverse Nyquist or Whiteley loci are being shaped. The interpretation of Whiteley loci are discussed in (Rosenbrock, 1974; Maciejowski, 1989).

3.2 CHARACTERISTIC LOCUS METHOD

This design approach has developed from the work by (MacFarlane&Belletruti, 1973) and (MacFarlane and Kouvaritakis, 1977). This design method is based on the extension of the classical works of Bode and Nyquist on the frequency response of single-input single-output feedback loops to the multivariable case (MacFarlane&Belletruti, 1973). In this extension it is shown that the well-known scalar results are a special case of a completely general vector theory.

The aim of the design method is to directly shape the characteristic loci of the plant. The reason for this is obvious if one considers the Nyquist stability criterion. This is made possible by employing approximate commutative controllers (Maciejowski, 1989). Consider the spectral decomposition

$$G_0 = W\Lambda W^{-1}$$

where W is a matrix whose columns are the eigenvectors of G_0 and Λ is a diagonal matrix with entries the eigenvalues of G_0, λ_i. Consider a compensator K with spectral decomposition

$$K = W\mathrm{M}W^{-1}$$

In this case M is a diagonal matrix with entries the eigenvalues of K, μ_i. It is clear that

$$G_0K = W\Lambda W^{-1}W\mathrm{M}W^{-1} = W\mathrm{N}W^{-1}$$

where N is a diagonal matrix with entries the eigenvalues of G_0K, ν_i, given by

$$\nu_i = \lambda_i\mu_i$$

In other words the eigenvalues have been directly shaped by using a compensator, termed commutative, which shares the same eigenvectors as G_0. To directly implement this strategy for control purposes is not feasible, since the pant, G_0, and therefore its eigenvector matrix, W, is a function of frequency. What can however be achieved is to find real constant matrices which can be physically implemented and which approximate W and W^{-1} at a specific frequency. The algorithm to calculate this approximation is termed the ALIGN algorithm and was developed by (MacFarlane&Kouvaritakis, 1977). Such a compensator is termed an approximate commutative compensator.

The design now proceeds by designing three compensators (Maciejowski, 1989):

- Compute a real $K_h \approx G_0^{-1}$ at some high frequency using the ALIGN algorithm. This serves to decouple the plant at high frequencies where high gains can no longer be relied on to ensure little

interaction. The loci are also manipulated at this stage by multiplying with a constant diagonal matrix to make it easier to achieve the desired number of encirclements of the critical point in later design stages.

- An approximate commutative compensator, $K_m(s)$, is then designed at some medium frequency to shape the loci of $G_0(s)K_h$ around crossover, without undoing the decoupling achieved in the previous design step.
- An approximate commutative compensator, $K_h(s)$, is then designed at some low frequency to ensure satisfactory low frequency behaviour, e.g. zero steady-state offset. A parameter α is used to ensure that low frequency compensation does not continue into the medium frequency domain (MacFarlane&Kouvaritakis, 1977).
- The complete compensator is finally realised as

$$K = K_h K_m(s) K_l(s)$$

CAPTER 3: DATA ACQUISITION

1. APPARATUS

All calculations were performed on a personal computer in the *Matlab/Simulink* environment. A dynamic model of the process was created and used as a "black box" plant in the subsequent work. What is presented below is a short process description and the range of operating conditions considered. A fuller exposition of the model development is presented in appendix A.

1.1 PROCESS DESCRIPTION

The process consists of a triple-effect falling film evaporator used for concentrating solutions of water and a non-volatile solute. The steam fed to the process is high pressure steam. Given that the solute is heat-sensitive, operation is under vacuum. The nature of the upstream processing causes step changes in the overall load to the plant, i.e. F_{feed}, to be the most important disturbance to take cognisance of. The process flowsheet is shown in figure 1.

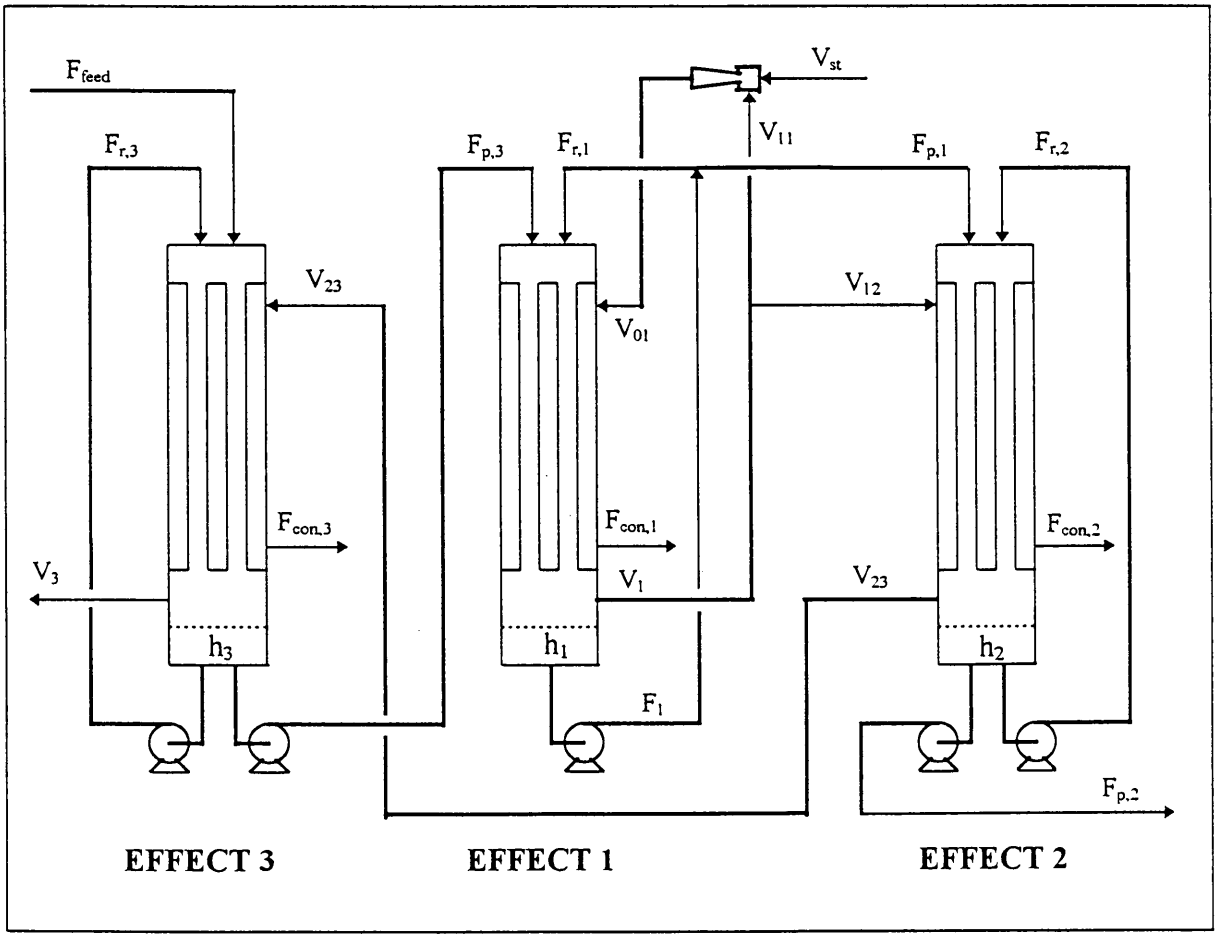

Figure 1. *Process flowsheet*

- *Controlled variables*
  - ⇒ final product composition, $X_{p,2}$
  - ⇒ heights in all the sumps: h_1, h_2 and h_3
- *External disturbances*
  - ⇒ feed flowrate, F_{feed}
  - ⇒ feed composition, X_{feed}
  - ⇒ feed temperature, T_{feed}

  (These are not all possible external disturbances allowed in the model, but the ones considered)
- *Manipulated variables*
  - ⇒ V_{st}
  - ⇒ $F_{p,1}$
  - ⇒ $F_{p,2}$
  - ⇒ $F_{p,3}$

1.2 RANGE OF OPERATING CONDITIONS

The range of operating conditions of the controlled- and manipulated variables and the external disturbances considered is listed in table 1.

Table 1: *Range of operating conditions*

Input/ Output	Units	Minimum	Maximum	Scaling
F_{feed}	kg/s	2,3777	4,4157	1,019
T_{feed}	K	310	340	15
X_{feed}	mass/mass	0,075	0,100	0,0125
V_{st}	kg/s	0,1983	0,7583	0,28
$F_{p,1}$	kg/s	0,2001	2,2001	1
$F_{p,2}$	kg/s	0,1184	1,1184	0,5
$F_{p,3}$	kg/s	0,8942	4,8942	2
$X_{p,2}$	mass/mass	0,392	0,557	0,0844
h_1	m	0,20	0,50	0,15
h_2	m	0,24	0,54	0,15
h_3	m	0,24	0,54	0,15

The scalings referred to in the above table were used to normalise all variables to $|a| \leq 1$. Scaling is required so that valid conclusions can be drawn from system analysis (Skogestad&Postlethwaite, 1996). Consider for example investigating the extent of interaction between loops. With all loops normalised, valid conclusions can be drawn.

2. PLANNING AND METHODS

2.1 PROCESS IDENTIFICATION AND UNCERTAINTY DESCRIPTION

The aim of process identification was to obtain a nominal plant model with uncertainty description which fully describes the entire range of possible plant behaviour, to be used subsequently for controller design and robustness analysis. Since the uncertainty description used was independent, additive, norm-bounded uncertainty in the transfer function matrix elements, this goal can be represented as:

$$\begin{pmatrix} X_2 \\ h_1 \\ h_2 \\ h_3 \end{pmatrix} = G_0 \begin{pmatrix} V_{st} \\ F_{p,1} \\ F_{p,2} \\ F_{p,3} \end{pmatrix} + \tilde{\Delta} \begin{pmatrix} V_{st} \\ F_{p,1} \\ F_{p,2} \\ F_{p,3} \end{pmatrix}$$

where

$$G_0 = \begin{pmatrix} g_{011} & g_{012} & g_{013} & g_{014} \\ g_{021} & g_{022} & g_{023} & g_{024} \\ g_{031} & g_{032} & g_{033} & g_{034} \\ g_{041} & g_{042} & g_{043} & g_{044} \end{pmatrix}$$

and

$$\tilde{\Delta} = \begin{pmatrix} \tilde{\delta}_{11} & \tilde{\delta}_{12} & \tilde{\delta}_{13} & \tilde{\delta}_{14} \\ \tilde{\delta}_{21} & \tilde{\delta}_{22} & \tilde{\delta}_{23} & \tilde{\delta}_{24} \\ \tilde{\delta}_{31} & \tilde{\delta}_{32} & \tilde{\delta}_{33} & \tilde{\delta}_{34} \\ \tilde{\delta}_{41} & \tilde{\delta}_{42} & \tilde{\delta}_{43} & \tilde{\delta}_{44} \end{pmatrix}$$

G_0 is the nominal transfer function and $\tilde{\Delta}$ the uncertainty. The aim is therefore to determine the elements of G_0 and norm bounds on the elements of $\tilde{\Delta}$ that fully describe the plant behaviour. Both G_0 and $\tilde{\Delta}$ are functions of frequency. G_0 and $\tilde{\Delta}$ are complex matrices. Real valued norm bounds are imposed on the elements of $\tilde{\Delta}$.

The controller design and robust analysis methods used exclusively employ the frequency domain. This served as motivation to suffice with frequency domain results, without fitting a transfer function model to it. As will be shown shortly, this choice allowed the least conservative uncertainty description for the method of description used.

2.1.1 SOURCES OF UNCERTAINTY

Possible sources of uncertainty will now be discussed to serve as motivation for the pulse tests performed. This section should be read together with the equations used to describe the model (see appendix A) in order to understand the causes of the various effects mentioned here. The process

under consideration is non-linear. This results in process uncertainty away from the reference state used for linearisation. The non-linearity has several origins:

- the relations used to model boiling point data is non-linear; vapour pressure is calculated using the Antoine equation
- the relationship between flow rate and film thickness (and as a consequence heat transfer) is non-linear; this effect is reduced by the constant recycle flow (it is only a minor portion of the total flow down the tube that varies)
- one of the controlled variables is a mass fraction of solute; this results in non-linearities between amount of water evaporated and mass fraction
- a square root relationship exists between steam flowrate and pressure difference

Varying flowrates affect the following process parameters:

- higher flowrates generally correspond to faster dynamic response, i.e. smaller time constants and dead-times
- flowrate also affects film thickness; higher flowrates corresponding to thicker films. This reduces the heat transfer coefficients. It also increases the hold-up in the tubes, slowing the response of the solute balance. This effect is again reduced by the constant recycle flow.
- increased hold-up in the sumps of the effects results in slower response of the solute balance

Possible uncertainty that may have resulted from inaccurate fitting of transfer functions to the frequency response generated, is not applicable as fitting was not done.

2.1.2 Pulse Tests

2.1.2.1 Steady State Starting Conditions

In order to fully describe the plant behaviour the entire range of operating conditions had to be investigated. The range of operating conditions were bounded by investigating all possible combinations of the extremes of process variables. Since the method of process identification employed (pulse testing) requires a steady state as starting and final condition, all tests had to be performed at different starting steady states.

Pulse tests were performed from the starting steady states shown in table 2. Initial tests indicated that varying feed temperature within the allowed range had a negligible effect. This is to be expected considering the relative magnitude of the sensible and latent heat changes. All tests were performed at a feed temperature of 328,5 K. Table 2 covers different composition profiles, liquid flowrates and vapour flowrates (and therefore pressure profiles). Different pressure and composition profiles correspond to different temperature profiles. All these conditions were investigated at both maximum and minimum allowed sump hold-up.

Table 2: *Starting steady states used for pulse testing*

No	F_{feed} (kg/s)	X_{feed} (m/m)	T_{feed} (K)	V_{st} (kg/s)	$F_{p,1}$ (kg/s)	$F_{p,2}$ (kg/s)	$F_{p,3}$ (kg/s)	$X_{p,2}$ (m/m)	h_1 (m)	h_2 (m)	h_3 (m)
1	4,4157	0,100	328,75	0,7271	1,6703	0,7981	3,6461	0,5533	0,50	0,54	0,54
2	4,4157	0,100	328,75	0,7271	1,6703	0,7981	3,6461	0,5533	0,20	0,24	0,24
3	4,4157	0,100	328,75	0,6340	1,8848	1,1191	3,7545	0,3946	0,50	0,54	0,54
4	4,4157	0,100	328,75	0,6340	1,8848	1,1191	3,7545	0,3946	0,20	0,24	0,24
5	2,3777	0,100	328,75	0,2487	0,7232	0,4275	2,1386	0,5562	0,50	0,54	0,54
6	2,3777	0,100	328,75	0,2487	0,7232	0,4275	2,1386	0,5562	0,20	0,24	0,24
7	2,3777	0,100	328,75	0,2009	0,8345	0,5941	2,1930	0,4002	0,50	0,54	0,54
8	2,3777	0,100	328,75	0,2009	0,8345	0,5941	2,1930	0,4002	0,20	0,24	0,24
9	4,4157	0,075	328,75	0,7797	1,5409	0,6040	3,5821	0,5483	0,50	0,54	0,54
10	4,4157	0,075	328,75	0,7797	1,5409	0,6040	3,5821	0,5483	0,20	0,24	0,24
11	4,4157	0,075	328,75	0,7031	1,7087	0,8548	3,6670	0,3874	0,50	0,54	0,54
12	4,4157	0,075	328,75	0,7031	1,7087	0,8548	3,6670	0,3874	0,20	0,24	0,24
13	2,3777	0,075	328,75	0,2750	0,6536	0,3232	2,1023	0,5518	0,50	0,54	0,54
14	2,3777	0,075	328,75	0,2750	0,6536	0,3232	2,1023	0,5518	0,20	0,24	0,24
15	2,3777	0,075	328,75	0,2344	0,7463	0,4620	2,1492	0,3860	0,50	0,54	0,54
16	2,3777	0,075	328,75	0,2344	0,7463	0,4620	2,1492	0,3860	0,20	0,24	0,24

The entire possible manipulated variable range in the case of liquid flowrates ($F_{p,1}$, $F_{p,2}$ and $F_{p,3}$) has not been covered. This is a result of the inability to find a steady state condition within the allowed operating feed range corresponding to these flowrates. This can to some extent be justified by considering the following:

- the transfer function between $F_{p,2}$ and h_2 and $F_{p,3}$ and h_3 is a simple, pure integrator; no uncertainty exists since the response is linear
- the effect of varying flowrate on film thickness (and as a consequence film hold-up and heat transfer coefficient) is reduced in all cases by recycle flow as discussed above

In experiments 9 and 10 the maximum allowed steam feed rate had to be exceeded in order to obtain a steady state. This is the result of the maximum possible evaporator loading (the minimum feed concentration has to be concentrated to the maximum outlet concentration at the maximum flowrate). This condition can not occur in practice.

2.1.2.2 TESTS PERFORMED

The desk-top nature of the study made it a simple matter to vary the manipulated variables one at a time, while keeping the others constant. For this reason the multivariable process identification reduces to a number of single loop identifications.

At each of the above steady state starting conditions the pulse tests listed in table 3 were performed and the time response of all output variables ($X_{p,2}$, h_1, h_2 and h_3) logged. Rectangular pulses were used

Table 3: *Pulses performed at each steady state*

Pulsed variable	Pulse height (kg/s)	Pulse duration (s)
V_{st}	0,05	2
$F_{p,1}$	0,5	2
$F_{p,3}$	0,5	2

The duration of the above pulses implies that the frequency response of the process becomes unbounded at a frequency of π rad/s (Chapter 1, paragraph 2.2.2). In order to achieve measurable output responses to pulses, the pulse height in case of $F_{p,1}$ and $F_{p,3}$ had to be a substantial fraction of the total operating range. Positive and negative pulses were performed of the height and duration indicated above, around a single operating point in the middle of the operating range. This was done to check that pulse size was not too big and forced the process away from a linearised model around the operating point (Luyben, 1990). The resulting outputs were close to mirror images, indicating a favourable result.

Initial tests indicated that $F_{p,2}$ only affects h_2. The transfer function is a simple, pure integrator with constant parameter. For this reason $F_{p,2}$ was not included in the above testing.

Each test was allowed to run until steady state was again reached. The duration of the tests are indicated in table 4.

Table 4: *Duration of pulse tests*

Pulsed variable	Output variable	Test duration (s)
$F_{p,1}$, $F_{p,3}$	h_1, h_2, h_3	50
$F_{p,1}$, $F_{p,3}$	$X_{p,2}$	10 000
V_{st}	$X_{p,2}$, h_1, h_2, h_3	10 000

The tests lasting 50 s was sampled at an interval of 0,1 s. The tests lasting for a total of 10 000 s was sampled as listed in table 5.

Table 5: *Sample times for 10 000 s test*

Time (s)	Sample time (s)
1 to 100	0,2
100 to 500	1
500 to 4000	4
4000 to 10 000	10

The short initial sample times are needed to accurately capture the fast initial process response. 10 000 s was sufficient time to again reach steady state operation. During the final portion of logging the process response was slow and therefore the increased sample times.

2.1.3 FREQUENCY RESPONSE

The frequency response was now calculated using the algorithm in paragraph 2.2.1, chapter 2, over a logarithmicaly spaced discrete frequency domain of 10^{-4} to $10^{0,5}$ rad/s. In the case of transfer functions relating to sump-heights as outputs, the response included pure integrators and the approach outlined in paragraph 2.1, chapter 2, was employed. Prior to computing the frequency response the logged data were written as deviation variables by subtracting the initial steady state values.

2.1.4 METHOD OF NOMINAL MODEL DEFINITION AND UNCERTAINTY DESCRIPTION

The uncertainty description used was independent norm-bounded additive uncertainty in the transfer function elements. This results in disk-shaped uncertainty regions. In order to obtain the least conservative uncertainty description it is necessary to have the smallest possible norm-bound (radius). Since the description is additive, the different transfer function matrix elements can be considered separately. At each of the discrete frequency points for each of the transfer function matrix elements the following operations were completed:

- determine the circle with smallest possible radius that includes all the responses at the given frequency
- the centre of the circle is defined as the nominal plant model, g_0
- the radius of the circle is the norm-bound on $\tilde{\delta}$, $\hat{\delta}$

The smallest possible circle was determined using the following novel algorithm

- all possible combinations of two points from the set of responses were selected in turn
- the two points yielding the largest distance between them was retained
- a circle was now constructed using the 2 points as end-points of a diameter
- if all points are included in the circle, stop
- else
    - select all possible combinations of three points

- construct a circle passing through the three points
- check that all points are included in the circle
- select the smallest circle containing all points
- stop

(To construct a circle passing through three given points a result from elementary geometry regarding central lead lines can be used. See appendix B.)

The nominal plant and uncertainty description was now normalised by employing the scaling given in paragraph 1.2. In practice this was achieved by pre-multiplying with

$$diag\left\{\frac{1}{0,0844}; \frac{1}{0,15}; \frac{1}{0,15}; \frac{1}{0,15}\right\}$$

and post-multiplying with

$$diag\{0,28;\ 1;\ 0,5;\ 2\}$$

2.1.5 MATLAB SOFTWARE

Matlab software was written for the purpose of streamlining the above process (see appendix D). Given an initial steady state the various pulse tests were performed, responses differentiated (where applicable), frequency responses calculated and stored. After all tests had been completed further programs determined the nominal plant model and uncertainty description using the algorithm described in paragraph 2.1.4.

2.2 CONTROLLER DESIGN

As shown above the identification procedures used directly yielded the frequency response of the process. A design method which directly utilises the frequency response removes any possible conservatism that may be introduced due to imperfect fitting of this response to a transfer function model.

Two controller design methods were employed, namely the Characteristic Locus method and the Inverse Nyquist Array method. These methods were briefly reviewed in paragraph 3 of chapter 2.

Matlab software was again written to facilitate the design task (see appendix D).

The control structure, i.e. the pairing of manipulated and controlled variables, was designed by using the relative gain array approach (Stephanopoulos, 1984).

2.3 ROBUST ANALYSIS

The process identification and controller design results were now combined to investigate the robust characteristics of the system applying the method presented in paragraph 1,chapter 2. In order to apply these methods the problem was first cast into the standard MΔ-structure (where Δ is a block-diagonal matrix with known structure and bounds of one on the magnitudes of the individual blocks).

In (Agamennoni et al, 1989) a controller is designed and then detuned in order to meet robustness requirements. This detuning is done by multiplying the controller with a scalar constant, q. In this study nominal stability, robust stability, nominal performance and robust performance were investigated over a range of controller detuning values. The values of detuning, q, investigated are indicated in table 6:

Table 6: *Values of controller detuning, q, investigated*

q:	0,1	0,25	0,5	0,75	1	1,25

At each q four tests were performed, namely: nominal stability, robust stability, nominal performance and robust performance.

The structured singular value (SSV) is of course calculated at a finite number of discrete values. It is however so that the SSV as a function of frequency has pronounced peaks in the crossover region (Agamennoni et al, 1989). For this reason a number of further discrete frequency values were added to the relevant matrix (M_{22} or M) in the region where peaks occur. This addition was done by performing a cubic spline interpolation on each of the individual matrix entries of the frequency response of M_{22} or M . Since the numbers are complex, a cubic spline was performed separately on the real and imaginary parts.

Matlab software was written to aid in the analysis (see appendix D).

In order to set meaningful performance objectives pulse tests were performed on the expected load disturbances. These tests were performed around the steady state starting condition in table 7. (This operating condition corresponds to the middle of the operating range)

Table 7: *Steady state starting condition for performance objective identification*

F_{feed} (kg/s)	X_{feed} (m/m)	T_{feed} (K)	V_{st} (kg/s)	$F_{p,1}$ (kg/s)	$F_{p,2}$ (kg/s)	$F_{p,3}$ (kg/s)	$X_{p,2}$ (m/m)	h_1 (m)	h_2 (m)	h_3 (m)
3,3967	0,087	328,75	0,4783	1,1978	0,6151	2,8931	0,4804	0,35	0,35	0,35

The pulses listed in table 8 were performed:

Table 8: *Pulses for performance objective identification*

Pulsed variable	Pulse height (kg/s)	Pulse duration (s)
F_{feed}	0,5	2
X_{feed}	0,01	2

Each test was allowed to run until steady state was again reached. The duration of the tests are indicated in table 9:

Table 9: *Duration of pulse tests for performance objective identification*

Pulsed variable	Output variable	Test duration (s)
F_{feed}, X_{feed}	h_1, h_2, h_3	50
F_{feed}, X_{feed}	$X_{p,2}$	10 000

Sample times were the same as used in paragraph 2.1.2.2. Scaling was done as previously discussed and the scaling factors listed in table 1 used.

CHAPTER 4: RESULTS AND DISCUSSION

1. PROCESS IDENTIFICATION AND UNCERTAINTY DESCRIPTION

The aim of process identification is to find a linear nominal plant, coupled with a norm-bounded, independent element by element, additive uncertainty description which describes the entire range of possible plant operating conditions. Such a description can be represented as:

$$\begin{pmatrix} X_2 \\ h_1 \\ h_2 \\ h_3 \end{pmatrix} = G_0 \begin{pmatrix} V_{st} \\ F_{p,1} \\ F_{p,2} \\ F_{p,3} \end{pmatrix} + \tilde{\Delta} \begin{pmatrix} V_{st} \\ F_{p,1} \\ F_{p,2} \\ F_{p,3} \end{pmatrix}$$

where

$$G_0 = \begin{pmatrix} g_{011} & g_{012} & g_{013} & g_{014} \\ g_{021} & g_{022} & g_{023} & g_{024} \\ g_{031} & g_{032} & g_{033} & g_{034} \\ g_{041} & g_{042} & g_{043} & g_{044} \end{pmatrix}$$

and

$$\tilde{\Delta} = \begin{pmatrix} \tilde{\delta}_{11} & \tilde{\delta}_{12} & \tilde{\delta}_{13} & \tilde{\delta}_{14} \\ \tilde{\delta}_{21} & \tilde{\delta}_{22} & \tilde{\delta}_{23} & \tilde{\delta}_{24} \\ \tilde{\delta}_{31} & \tilde{\delta}_{32} & \tilde{\delta}_{33} & \tilde{\delta}_{34} \\ \tilde{\delta}_{41} & \tilde{\delta}_{42} & \tilde{\delta}_{43} & \tilde{\delta}_{44} \end{pmatrix}$$

1.1 NOMINAL PLANT- AND UNCERTAINTY DESCRIPTION

The plant and uncertainty description is as shown in figures 1 to 13 (Appendix C). Figure a in each case is the Bode magnitude plot of the nominal transfer function, while figure b is its Bode phase plot. Figure c represents the magnitude of the norm-bounded uncertainty (no phase plot is required since the elements are pure real). The following transfer functions are equal to zero and not shown:

$$g_{13} = g_{23} = g_{33} = 0$$

The results are discussed in detail in paragraph 1.3.

1.2 SAMPLE CALCULATION

This section illustrates the method used in deriving the above nominal plant and uncertainty description. For this purpose a single transfer function matrix element is considered and thereafter a single frequency point of this transfer function.

1.2.1 FAMILY OF POSSIBLE PLANTS

Consider the transfer function

$$g_{11} = \frac{X_{p,2}}{V_{st}}$$

The 16 pulse tests needed to cover the range of possible plant operating conditions have been listed in table 2, chapter 3. Converting each of these pulses to the frequency domain is a trivial application of the algorithm described in paragraph 2.2.1, chapter 2. This algorithm was applied to 50 discrete, logarithmically spaced frequency points between 10^{-4} and $10^{0,5}$ rad/s. The 16 frequency responses obtained in this manner are shown in figure 1.

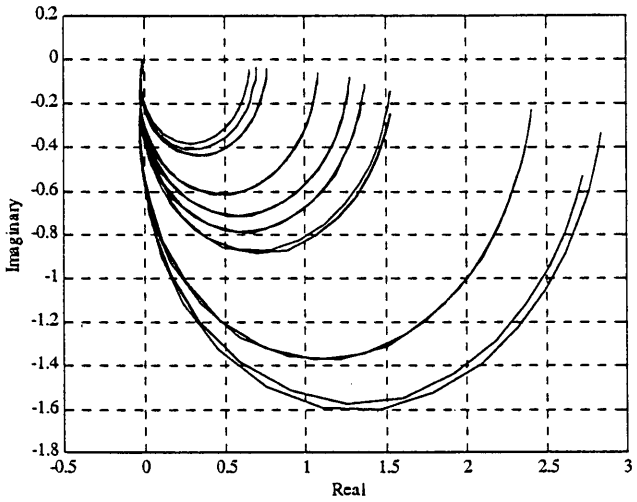

Figure 1: *Family of possible plant for* g_{11}

The frequency range is the same for all 16 plots, namely 10^{-5} to $10^{0,5}$ rad/s. The variation is self-evident.

1.2.2 DETERMINING THE LEAST CONSERVATIVE NORM-BOUNDED UNCERTAINTY REGION

Consider now the single frequency point $\omega = 6{,}707 \times 10^{-4}$ rad/s. The 16 frequency responses are as shown by the ×'s in figure 2.

Finding the least conservative norm-bound on the above 16 points in the complex plane is accomplished by finding the smallest disk-shaped region which includes all 16 points. Direct application of the algorithm described in paragraph 2.1.4, chapter 3, results in the disk-shaped region shown in figure 2. The centre of the circle corresponds to the nominal plant and its radius to the uncertainty bound. It should be clear that all possible plants are included as the uncertainty is allowed to vary to this maximum bound.

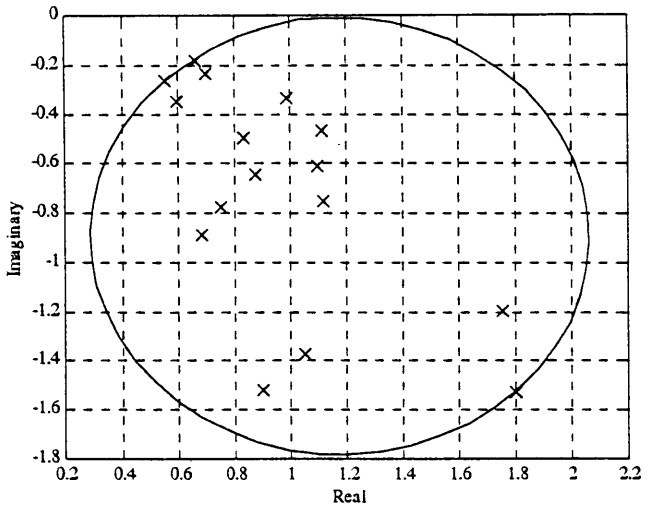

Figure 2: *Family of possible plants and least conservative norm-bound for* $g_{11}(j\cdot 6,707\times 10^{-4})$

It is not always the case that the smallest disk-shaped region passes through 3 points. As an example of this consider the frequency point ω = 0,016 rad/s of g_{11}. The least conservative norm-bound is shown in figure 3.

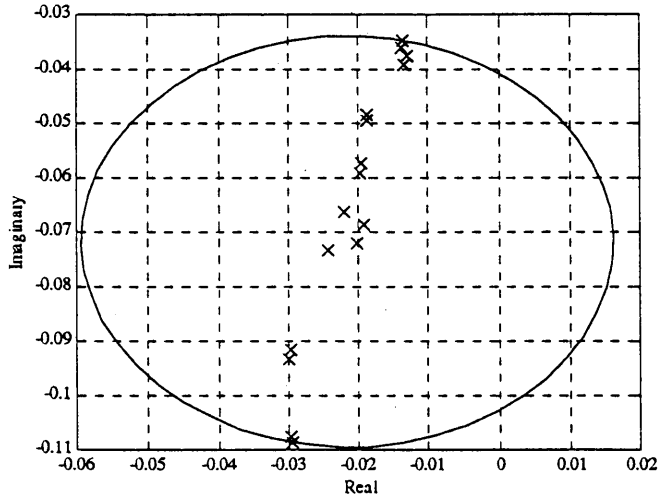

Figure 3: *Family of possible plants and least conservative norm-bound for* $g_{11}(j\cdot 0,016)$

1.2.3 FURTHER REMARKS

This calculation is now repeated at each frequency point. The result obtained is then scaled (in this case by multiplying with 0,28/0,0844). Application of this technique to all transfer function matrix elements at the 50 discrete frequency points considered yields the results in Appendix C. In the case of transfer functions including pure integrators the initial frequency response calculation is varied slightly as described in paragraph 2.1, chapter 2.

1.3 DISCUSSION

It is possible to derive a description encompassing the entire range of possible plant operating conditions using a linear nominal plant model with associated bounded perturbation for the system

under study. The uncertainty description used, independent norm-bounded additive uncertainty in the transfer function matrix elements, reduces the uncertainty evaluation to a number of single input single output problems.

The fact that results could be obtained at all using the identification procedure outlined above, is an indication that the plant is open-loop stable, containing at most pure integrators. As is evident from the graphs in appendix C all transfer functions with levels as outputs, contain pure integrators. (This is to be expected since hold-up does not influence outflow.) Recalling that a negative steady state gain corresponds to a 180° change in phase makes it a simple matter to determine which transfer functions have direct or indirect response.

The following can be said regarding the manipulated variables:

- The steam flow, V_{st}, affects all outputs.
- $F_{p,1}$ affects all outputs except for h_3.
- $F_{p,2}$ affects only h_2.
- $F_{p,3}$ affects all outputs except for h_2.

In the above, transfer functions with small values compared to others in the same row (that is relating to the same output) have been neglected. It is apparent that significant interaction is present in 11 of the 16 transfer functions describing the system. This is in other words a multivariable system and it can be expected that simple single loop controllers may find it difficult to achieve performance and stability objectives.

The magnitude of uncertainty in the elements: g_{11}, g_{21}, g_{31}, g_{41}, g_{12}, g_{32} and g_{14} exceeds at least 10% of the magnitude of the nominal plant value somewhere in the frequency region considered, with values around 70% not uncommon for certain transfer functions. This serves as motivation for application of robust analysis techniques. It is apparent that uncertainty in all transfer function elements relating level and liquid flow rate, excluding g_{32}, do not exceed 10% of the nominal value. This is confirmation of the mitigating effect of the recycle flow rate on these transfer functions postulated in paragraph 2.1.1, chapter 3.

Considering figures 2 and 3 in paragraph 1.2 it is evident that a considerable amount of conservatism is introduced by considering only norm-bounds and neglecting phase information. A tighter description of the uncertainty region is possible by employing a description containing magnitude and phase information. Techniques (paragraph 1.3.3, chapter 2) are available to do this. Such a description suffers in that the boundaries to be used for this less conservative uncertainty description are not unambiguous. Boundaries could probably be chosen by drawing some sort of polygon with vertices given by the different frequency responses, or by considering elliptical uncertainty regions.

The exact uncertainty region can only be determined by performing an infinite amount of tests at every possible operating point. Only the extremes of operation were considered here.

It is however so that a significant portion of the uncertainty stems from the fact that a linear plant model and uncertainty description is used for an inherently non-linear process. This implies that even when employing an uncertainty description using both magnitude and phase information, part of the known plant characteristics (its non-linearity), are treated as uncertainty. Surely a non-linear plant description will yield the least conservative uncertainty description.

It is also known (Morari&Zafiriou, 1989) that uncertainty descriptions considering independent uncertainty in the transfer function matrix elements yield conservative results, because possible coupling between uncertainty in various elements is ignored. A description accounting for this interaction would require a considerably more complex analysis of the process identification results.

The fact that the uncertainty description is conservative is comforting in that errors made during robust analysis will occur on the safe side of stability and performance.

The results obtained in this study are typical of real chemical engineering processes in that a triple-effect evaporator is a typical chemical engineering process for the reasons outlined in the introduction. The results are however different in that sensor and final control element dynamics have been ignored. It is expected that the dynamics of these units will start having an effect at higher frequencies. Uncertainty introduced by the dynamics of these elements can be incorporated in the form of output multiplicative uncertainty (for sensors) and input multiplicative uncertainty (for final control elements).

The identification procedures used here are applicable to open-loop stable processes; typical of chemical engineering applications. The following constraints should however be borne in mind:

- Performing this number of pulse tests on real plants would be extremely time consuming and expensive.
- The test procedure requires steady state starting conditions spanning the entire range of plant operating conditions. This shortcoming was satisfied in most cases and its effect mitigated by recycle flowrates in others, for this case study. This will not always be the case.
- Describing the entire range of plant operation may involve a considerable number of different combinations of operating variables for more complex plants.

It should however be said that in general the engineer will not approach the plant as a "black box", but will have some plant model and uncertainty description based on rigorous modelling. From this point of view, what has been done up to now in this study, may be viewed as the derivation of a plant model and uncertainty description based on rigorous modelling.

2. CONTROLLER DESIGN

The Inverse Nyquist Array and Characteristic Locus design methods were now used to design controllers for the nominal plant defined above.

The control structure was decided by employing the relative gain array approach (Stephanopoulos, 1984). The control structure in table 1 was used.

Table 1: *Pairing of controlled and manipulated variables*

Controlled variable	Manipulated variable
$X_{p,2}$	V_{st}
h_1	$F_{p,1}$
h_2	$F_{p,2}$
h_3	$F_{p,3}$

The absolute value of the relative gain array of this control structure at low, medium and high frequencies are presented in table 2:

Table 2: *RGA of the control structure*

Frequency (rad/s)	RGA
10^{-4}	$\begin{pmatrix} 0,58 & 0,31 & 0 & 0,11 \\ 0,15 & 0,68 & 0 & 0,17 \\ 0 & 0 & 1 & 0 \\ 0,27 & 0,007 & 0 & 0,72 \end{pmatrix}$
$5,56\times10^{-3}$	$\begin{pmatrix} 0,49 & 0,47 & 0 & 0,07 \\ 0,23 & 0,54 & 0 & 0,24 \\ 0 & 0 & 1 & 0 \\ 0,29 & 0,007 & 0 & 0,71 \end{pmatrix}$
$3,82\times10^{-1}$	$\begin{pmatrix} 0,77 & 0,27 & 0 & 0,005 \\ 0,39 & 0,77 & 0 & 0,12 \\ 0 & 0 & 1 & 0 \\ 0,13 & 0,002 & 0 & 1,13 \end{pmatrix}$

It is evident that the control structure used results in diagonal elements closest to 1, and it is therefore the most favourable structure.

2.1 INVERSE NYQUIST ARRAY

2.1.1 DECOUPLING

Recall that the first step in this design approach is to decouple the system. The extent to which a plant is decoupled can be characterised by evaluating either its row or column dominance. When applying the inverse approach row dominance is preserved when implementing the controller, and therefore achieving row dominance is the objective (Maciejowski, 1989). The row dominance of row i of matrix A is defined as (Ford, Maciejowski & Boyle, 1990):

$$\text{row dominance} = \frac{\sum_{j=1, j\neq i}^{n} |A_{i,j}|}{|A_{i,i}|}$$

It follows that the smaller the row dominance, the more decoupled the system. The row dominance of all four rows of the uncompensated nominal plant inverse, G_0^{-1}, is shown in figure 4.

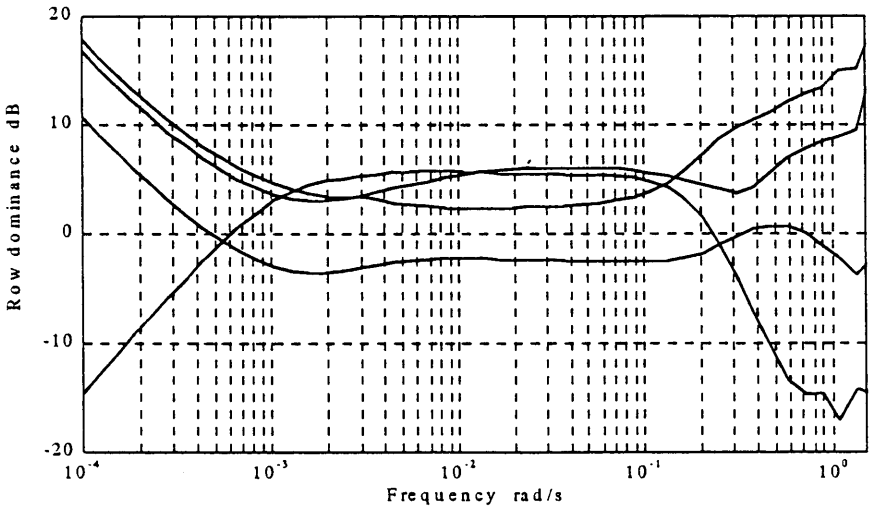

Figure 4: *Row dominance of G_0^{-1} prior to decoupling*

Table 3: *Elimination functions used for decoupling*

Element (i,j)	Elimination function ($m_{i,j}$)
2,1	$\frac{-2{,}1838s - 0{,}60201}{11{,}818s + 1}$
3,1	$\frac{-1{,}6857}{23{,}829s^2 + 13{,}37s + 1}$
4,1	$\frac{-0{,}15083}{26{,}915s^2 + 13{,}96s + 1}$

3,2	$\frac{-2{,}4183s + 1{,}8449}{4{,}3745s + 1}$
4,2	$\frac{0{,}14189s^2 + 0{,}044123s - 0{,}0072871}{22{,}027s^2 + 2{,}1925s + 1}$
4,3	$\frac{0}{1}$
3,4	$\frac{-0{,}80925s + 0{,}067302}{5{,}6071s^2 + 1{,}328s + 1}$
2,4	$\frac{1{,}2636s + 1{,}9924}{1{,}0475s + 1}$
1,4	$\frac{17{,}827s + 1{,}7643}{12{,}293s^2 + 4{,}2821s + 1}$
2,3	$\frac{0}{1}$
1,3	$\frac{0}{1}$
1,2	$\frac{167{,}42s + 0{,}51508}{20{,}755s^2 + 176{,}14s + 1}$

The elimination functions shown in table 3 were now applied to the nominal process model obtained in paragraph 1. The order of application of the elimination functions is the order in which they appear in table 3. Note that low order transfer functions are employed as stated in paragraph 3.1.1, chapter 2. These functions were obtained by the method described there.

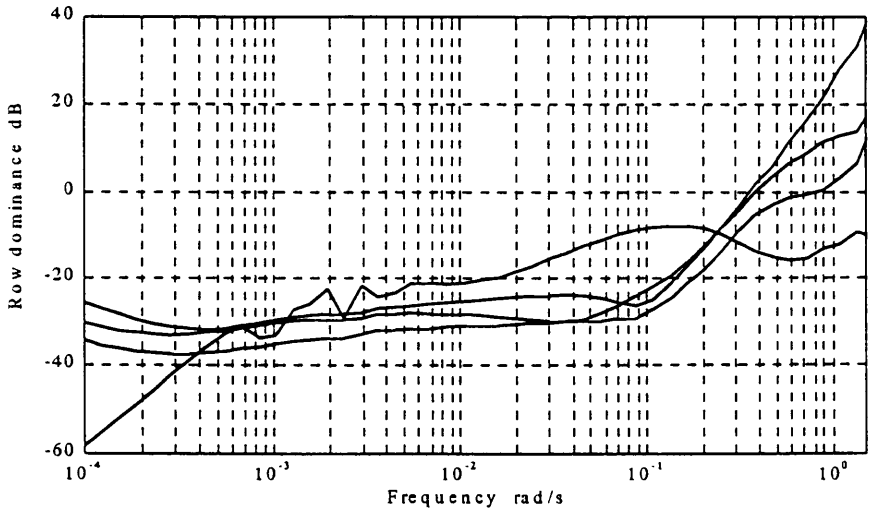

Figure 5: *Row dominance of G_0^{-1} after decoupling*

The resulting row-dominance of all four rows of the inverse nominal plant and decoupler, $(G_0K_a)^{-1}$ are shown in figure 5. Comparison with figure 4 clearly indicates that the row dominance has been significantly reduced. A typical value of row dominance from figure 5 is -30 dB = 0,03.

2.1.2 DIAGONAL CONTROLLER DESIGN

Diagonal controller design proceeded as a number of single loop designs using PI-controllers and the resulting controller, K_b, is a diagonal matrix with entries listed in table 4.

Table 4: *Diagonal controller transfer functions*

element (i,j)	Controller ($K_{bi,j}$)
1,1	$\frac{5{,}6\cdot(15s+1)}{15s}$
2,2	-18
3,3	-32
4,4	-10

2.1.3 CONTROLLER IMPLEMENTATION

The controller can now be implemented as:

$$K = K_{a,1}K_{a,2}K_b$$

where $K_{a,1}$ is an identity matrix with all elements below the diagonal replaced with $-m_{i,j}$ in table 1 and $K_{a,2}$ is an identity matrix with all elements above the diagonal replaced with $-m_{i,j}$ in table 1. This simplification in the controller implementation follows from (Burden&Faires, 1993).

The Nyquist plot of G_0K is shown in figures 6. Figure 6a is the Nyquist plot over the frequency domain 10^{-4} to 1 rad/s. (There are 3 loci located close to the negative imaginary axis.) Figure 6b is a magnification of the region surrounding the critical point.

It is clear that no encirclements of the critical point occurs. Since the system is open-loop stable, it follows directly from the Nyquist stability criterion (paragraph 1.1.1, chapter 2) that no encirclements correspond to closed-loop stability of the nominal plant and controller.

The maximum and minimum singular values of the nominal complimentary sensitivity (T_0) and nominal sensitivity (S_0) are depicted in figures 7 and 8 respectively. The results are discussed in paragraph 2.3.

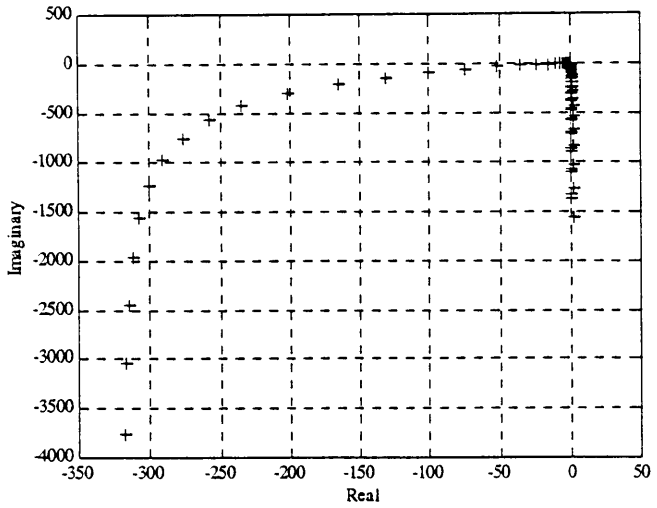

Figure 6a: *Nyquist plot of G_0K for INA controller (10^{-4} to 1 rad/s)*

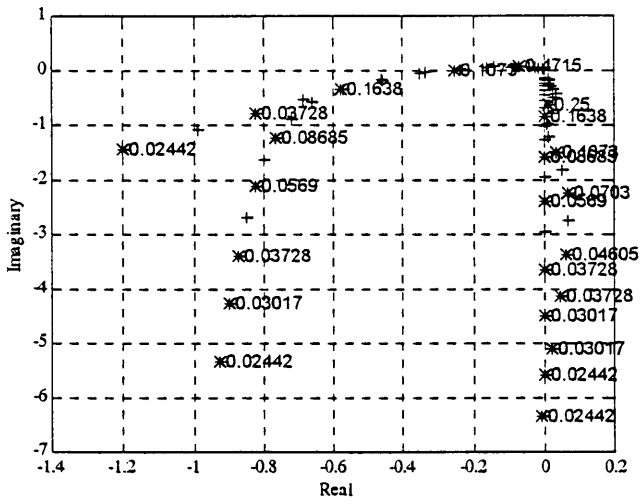

Figure 6b: *Nyquist plot of G_0K for INA controller (0,02442 to 1 rad/s)*

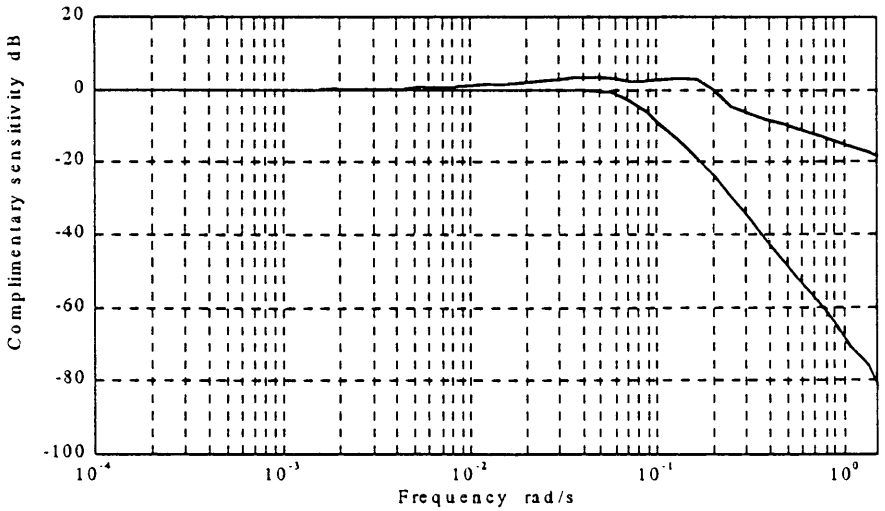

Figure 7: *Singular values of nominal complimentary sensitivity (T_0), INA controller*

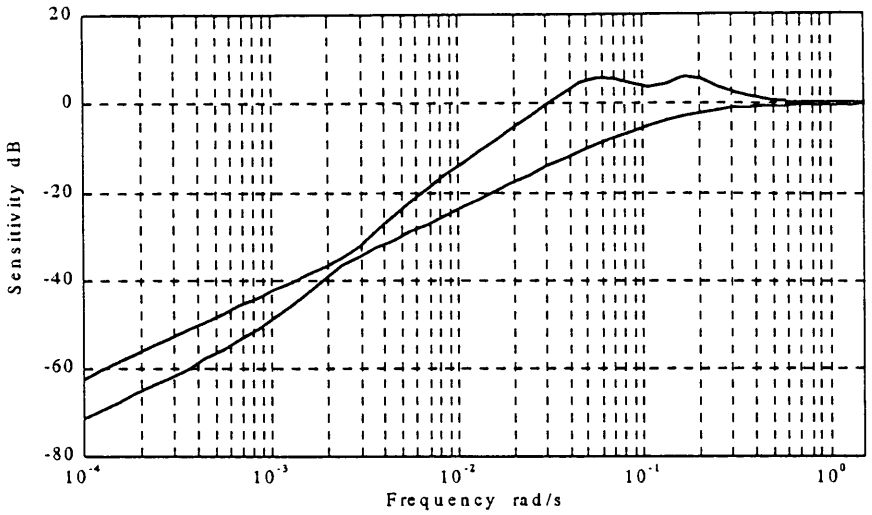

Figure 8: *Singular values of nominal sensitivity (S_0), INA controller*

2.2 CHARACTERISTIC LOCUS

2.2.1 HIGH FREQUENCY

The high frequency design was performed at a frequency of 0,16379 rad/s. Some trial and error was needed to find that the high frequency compensator designed at this point, resulted in decoupling over the widest frequency range at high frequencies. The constant controller obtained is:

$$K_h = \begin{pmatrix} -29{,}314 & 34{,}336 & 0 & 35{,}894 \\ 6{,}6704 & 12{,}536 & 0 & 10{,}478 \\ 8{,}5119 & 11{,}452 & -38{,}539 & 9{,}3323 \\ 0.0991 & -1{,}2393 & 0 & 9{,}5433 \end{pmatrix}$$

Post-multiplication of G_0 with this controller results in the misalignment shown in figure 9a. It is clear that the plant has been suitably decoupled at high frequencies (where the magnitude of the loci become small, figure 9b).

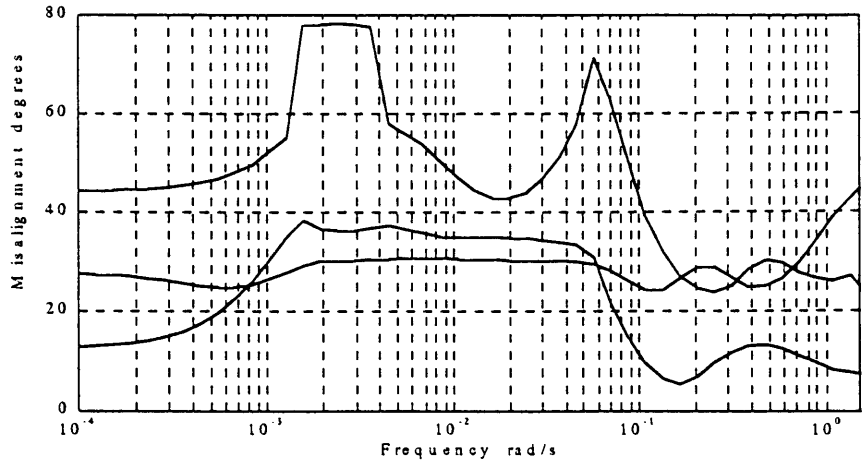

Figure 9a: *Misalignment of loci after high frequency decoupling*

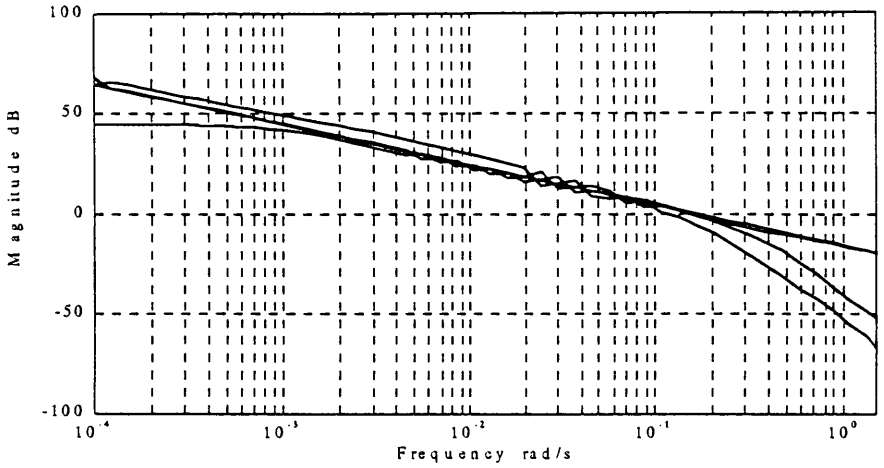

Figure 9b: *Magnitude of loci after high frequency decoupling*

Post-multiplying further with diag{-1;-1;1;-1} results in the characteristic loci shown in figure 10. It is clear that the required encirclements of the critical point (namely zero), is achievable during medium and low frequency design. There are 2 loci located close to the negative imaginary axis.

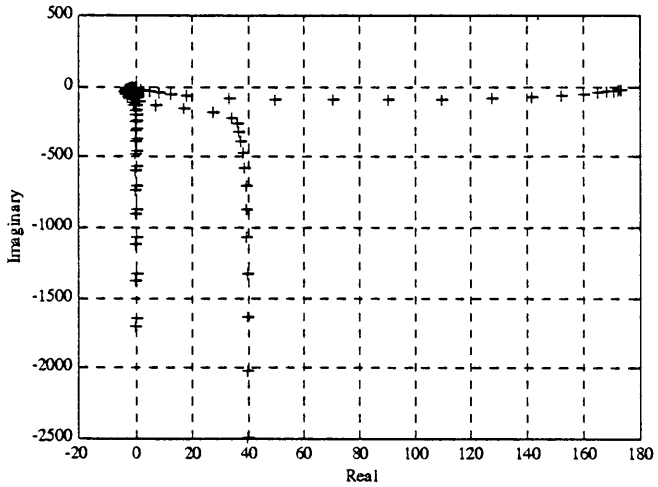

Figure 10: *Characteristic loci after manipulation (10^{-4} to 1 rad/s)*

2.2.2 MEDIUM FREQUENCY

Medium frequency design was done at a frequency of 0,0869 rad/s and the phase lead listed in table 5 were added to the loci.

Table 5: *Medium frequency loci manipulation*

Locus no	Phase lead (degrees)
1	20
2	15
3	-15
4	0

Some trial and error was required to find a frequency point and phase lead to be added to the controller that resulted in the desired behaviour. This is a result of the fact that the compensator is only commutative over a small frequency range. The resulting commutative controller is given by

$$K_m = \frac{1}{s^4 + 0{,}39072s^3 + 5{,}624 \times 10^{-2}s^2 + 3{,}528 \times 10^{-3}s + 8{,}126 \times 10^{-5}} \begin{pmatrix} C_1 & C_2 & C_3 & C_4 \end{pmatrix}$$

with

$$C_1 = \begin{pmatrix} 1{,}1106s^4 + 0{,}36393s^3 + 4{,}3802 \times 10^{-2}s^2 + 2{,}2987 \times 10^{-3}s + 4{,}447 \times 10^{-5} \\ 0{,}29786s^4 + 9{,}9886 \times 10^{-2}s^3 + 1{,}2355 \times 10^{-2}s^2 + 6{,}7056 \times 10^{-4}s + 1{,}3537 \times 10^{-5} \\ 2{,}7876 \times 10^{-2}s^4 + 1{,}419 \times 10^{-2}s^3 + 2{,}4109 \times 10^{-3}s^2 + 1{,}6747 \times 10^{-4}s + 4{,}0693 \times 10^{-6} \\ -3{,}3132 \times 10^{-2}s^4 - 1{,}6729 \times 10^{-2}s^3 - 3{,}0455 \times 10^{-3}s^2 - 2{,}3838 \times 10^{-4}s - 6{,}8058 \times 10^{-6} \end{pmatrix}$$

$$C_2 = \begin{pmatrix} 0{,}5105s^4 + 0{,}16781s^3 + 2{,}0344 \times 10^{-2}s^2 + 1{,}0813 \times 10^{-3}s + 2{,}1346 \times 10^{-5} \\ 1{,}1017s^4 + 0{,}38394 \times 10^{-2}s^3 + 4{,}9285 \times 10^{-2}s^2 + 2{,}7769 \times 10^{-3}s + 5{,}8259 \times 10^{-5} \\ -0{,}10142s^4 - 4{,}163 \times 10^{-2}s^3 - 6{,}4559 \times 10^{-3}s^2 - 4{,}4762 \times 10^{-4}s - 1{,}1682 \times 10^{-5} \\ 0{,}14662s^4 + 1{,}8141 \times 10^{-2}s^3 - 3{,}3745 \times 10^{-3}s^2 - 6{,}1392 \times 10^{-4}s - 2{,}4323 \times 10^{-5} \end{pmatrix}$$

$$C_3 = \begin{pmatrix} 0 \\ 0 \\ s^4 + 0{,}39072s^3 + 5{,}624 \times 10^{-2}s^2 + 3{,}528 \times 10^{-3}s + 8{,}126 \times 10^{-5} \\ 0 \end{pmatrix}$$

$$C_4 = \begin{pmatrix} -5{,}0161 \times 10^{-2}s^4 - 1{,}8507 \times 10^{-2}s^3 - 2{,}5755 \times 10^{-3}s^2 - 1{,}6094 \times 10^{-4}s - 3{,}8208 \times 10^{-6} \\ -1{,}3296 \times 10^{-2}s^4 - 1{,}2251 \times 10^{-2}s^3 - 2{,}8904 \times 10^{-3}s^2 - 2{,}6076 \times 10^{-4}s - 8{,}1141 \times 10^{-6} \\ -2{,}399 \times 10^{-1}s^4 - 8{,}949 \times 10^{-2}s^3 - 1{,}211 \times 10^{-2}s^2 - 6{,}9808 \times 10^{-4}s - 1{,}4256 \times 10^{-5} \\ 0{,}44653s^4 + 0{,}19141s^3 + 3{,}0693 \times 10^{-2}s^2 + 2{,}1812 \times 10^{-3}s + 5{,}7908 \times 10^{-5} \end{pmatrix}$$

The resulting Bode and Nyquist diagrams of the loci are shown in figures 11 and 12.

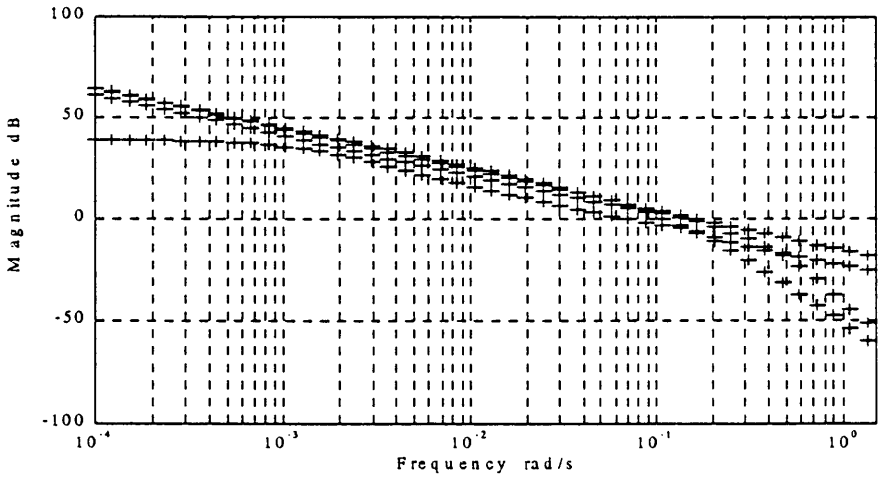

Figure 11: *Magnitude of characteristic loci after medium frequency compensation*

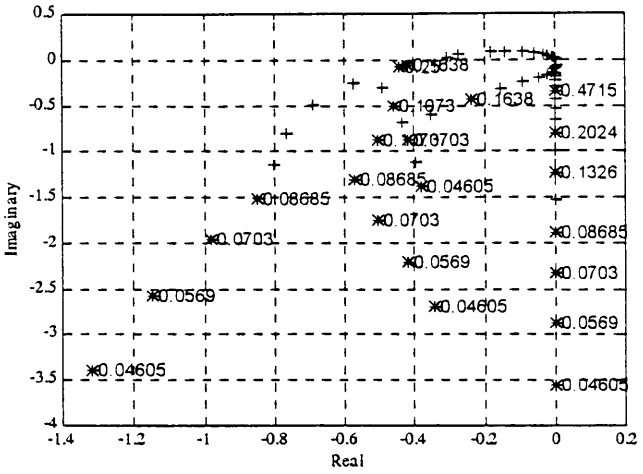

Figure 12: *Nyquist plot of characteristic loci after medium frequency design*

Note that it has been attempted to balance the magnitude of the loci and shape it in the region of the critical point, in the medium frequency range.

2.2.3 LOW FREQUENCY

Designing the low frequency compensator at a frequency of $1{,}024\times10^{-3}$ rad/s yielded satisfactory results. Integral action was added to the first locus and a value of $\alpha = 0{,}1$ used. The resulting controller is

$$K_l = \frac{1}{s}\begin{pmatrix} C_{12} & C_{34} \end{pmatrix}$$

where

$$C_{12} = \begin{pmatrix} 1{,}005s + 5{,}6799\times10^{-3} & -2{,}3769\times10^{-3}s - 1{,}7537\times10^{-3} \\ 1{,}5104\times10^{-4}s - 9{,}2966\times10^{-4} & 1{,}0069s - 2{,}8703\times10^{-4} \\ -5{,}3957\times10^{-3}s + 1{,}5048\times10^{-3} & 6{,}3846\times10^{-3}s + 4{,}6461\times10^{-4} \\ -3{,}6442\times10^{-3}s + 1{,}8348\times10^{-3} & 1{,}1698\times10^{-2}s + 5{,}6649\times10^{-4} \end{pmatrix}$$

$$C_{34} = \begin{pmatrix} 0 & -1{,}1452\times10^{-3}s - 2{,}7484\times10^{-4} \\ 0 & -2{,}1952\times10^{-3}s + 4{,}4984\times10^{-5} \\ 1{,}0164s & 4{,}7036\times10^{-3}s - 7{,}2814\times10^{-5} \\ 0 & 1{,}0102s - 8{,}878\times10^{-5} \end{pmatrix}$$

Balancing of the loci around the low frequency point is illustrated in figure 13.

2.2.4 CONTROLLER IMPLEMENTATION

The final controller is now realised as

$$K = K_h \cdot diag\{-1;-1;1;-1\} \cdot K_m K_l$$

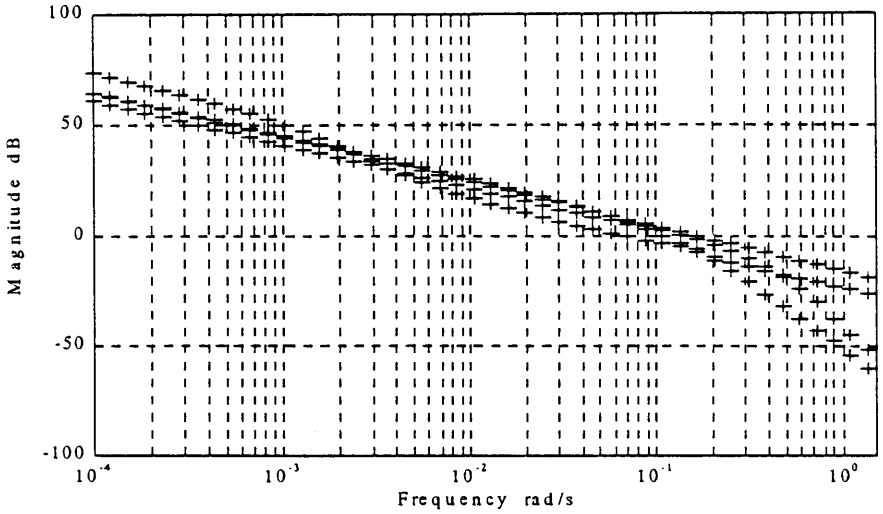

Figure 13: *Magnitude of characteristic loci after low frequency design*

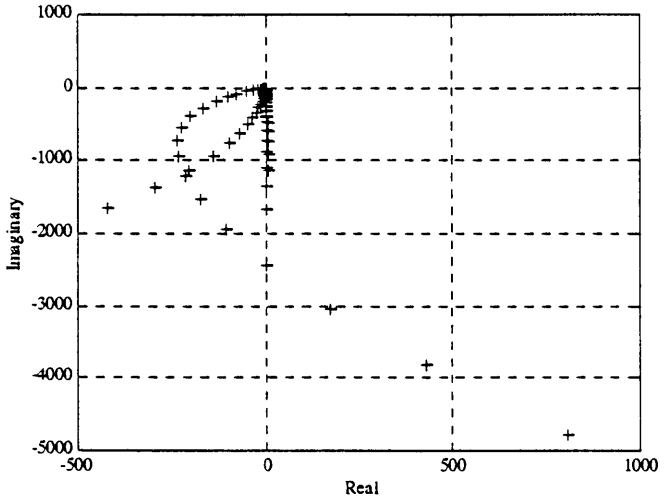

Figure 14a: *Nyquist plot of G_0K for CL controller (10^{-4} to 1 rad/s)*

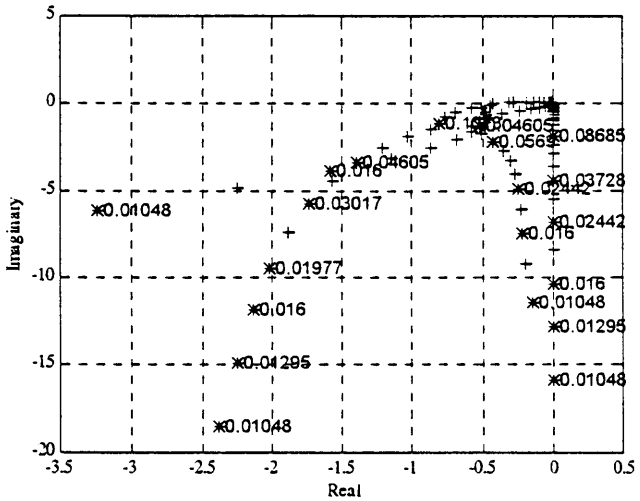

Figure 14b: *Nyquist plot of G_0K for CL controller (0,0105 to 1 rad/s)*

The resulting Nyquist plot of G_0K is shown in figures 14. There are 2 loci located close to the imaginary axis in figure 14a. No encirclements of the critical point occur and by similar reasoning to that in paragraph 2.1.3, the nominal plant and controller is closed-loop stable.

The maximum and minimum singular values of the nominal complimentary sensitivity (T_0) and nominal sensitivity (S_0) are depicted in figures 15 and 16 respectively.

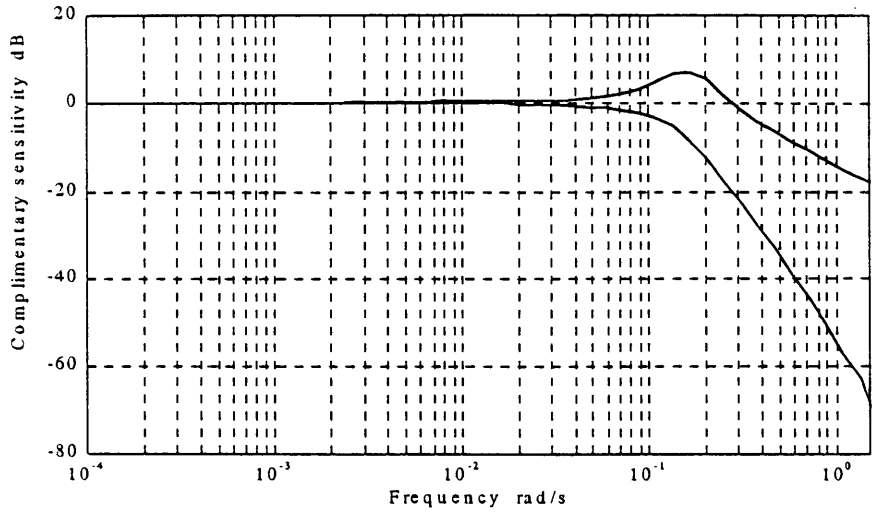

Figure 15: *Singular values of nominal complimentary sensitivity (T_0), CL controller*

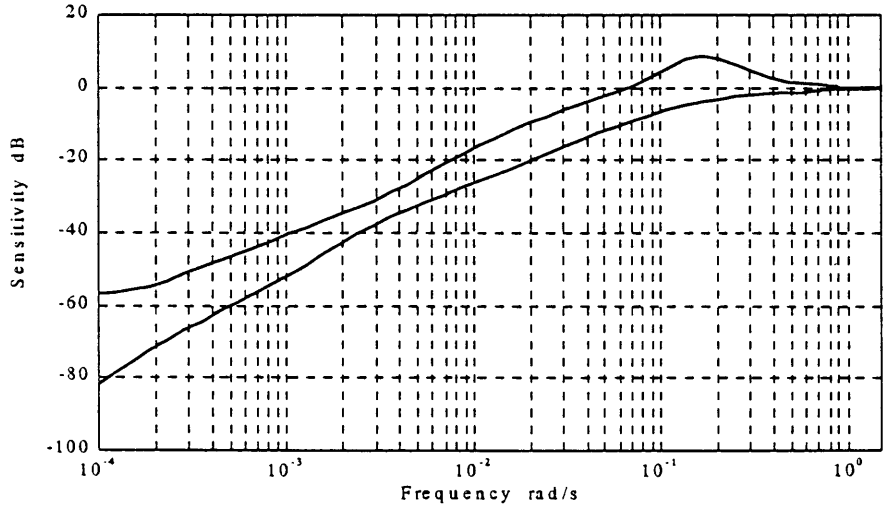

Figure 16: *Singular values of nominal sensitivity (S_0), CL controller*

2.3 DISCUSSION

Both controller design approaches yielded nominally stable closed loop systems, as indicated by application of the Nyquist stability criterion.

The equation in paragraph 1.1, (chapter 1) relating system output to external disturbances, noise and reference signals is now relevant. The sensitivity of the controller to external disturbances is partly characterised by the value of frequency at which $\sigma^*(S_0)$ crosses 0,707 from below (the higher the

better). The ability for setpoint tracking and noise rejection is partly characterised by considering the value of frequency where $\sigma^*(T_0)$ crosses 0,707 from above (the higher the better, up to the frequency range where noise becomes a problem). These frequencies (where 0,707 is crossed) are the bandwidths of the system. In the frequency region between the two bandwidths controller performance is poor, since both noise and external disturbances are amplified (both S_0 and T_0 are large). The height of the peaks correspond to the amount in which the response is underdamped, i.e. oscillatory. A high rate of decrease in $\sigma^*(T_0)$ above its bandwidth is desirable, since it limits noise propagation. (Skogestad&Postlethwaite, 1996; Maciejowski, 1989)

The following discussion refers to figures 7, 8, 15 and 16. The low frequency asymptotes of complimentary sensitivity (T_0) equal to 1, indicate error-free tracking of reference signals. The Inverse Nyquist Array controller (figures 7 and 8) has a $\sigma^*(S_0)$ bandwidth of 0,03 rad/s and a $\sigma^*(T_0)$ bandwidth of 0,2 rad/s. The peak value in $S_0 \approx 1,9$ and in $T_0 \approx 1,5$. $\sigma^*(T)$ decreases at high frequencies at a rate of -1/decade. The peaks are broad and exhibits two humps. The broad peaks imply that amplification of signals occur over a wide frequency region; this is undesirable.

The Characteristic Locus controller (figures 15 and 16) has a $\sigma^*(S)$ bandwidth of 0,07 rad/s and a $\sigma^*(T)$ bandwidth of 0,3 rad/s. The peak value in $S \approx 2,6$ and in $T \approx 2,21$. $\sigma^*(T)$ decreases at high frequencies at a rate of -1/decade.

From the above it is apparent that the characteristic locus design yields a faster response (higher bandwidth), but more oscillatory behaviour (higher peaks). It may be necessary to detune the controller somewhat to reduce the amount of oscillation, but this will in turn decrease the speed (move the bandwidth to the left). The region between S and T crossover for the CL controller is smaller than the INA-controller. Both controllers have a similar decay ratio of T at higher frequencies.

Both controller design methods were fairly easy to implement in this case. A bit of trial and error was required to determine elimination functions for the INA-controller. It is possible that a more advanced single-loop design approach during the diagonal controller design step, than simple PI-control, would have balanced the system out more and resulted in narrower peaks.

The method of INA-controller design employed (Quasi-Gauss elimination), results in a very high order controller. Some method of controller order reduction would probably need to be employed before actual implementation. This reduction will of course result in reduced performance. This is idea is explored further in (Figueroa et al, 1993).

The Characteristic Locus controller has the disadvantage that the commutative compensators yielded by the ALIGN algorithm, are commutative over a very small frequency range. This necessitated

considerable trial and error in order to find the desired frequencies (low, medium and high) and loci manipulation to yield the desired results.

Other controller design approaches, such as H_∞ and μ-synthesis, could also have been used (Skogestad&Postlethwaite, 1996). These approaches are superior in that the desired loop-shape is explicitly optimised for in the controller design step. μ-Synthesis even allows for the incorporation of uncertainty descriptions during the design stage. The resulting controllers are high order and controller order reduction techniques are in general required. These design techniques however require a state space plant model. State space models are unable to handle deadtime and approximations (e.g. the Padé approximation) have to be used.

3. ROBUST ANALYSIS

The process identification step led to the conclusion that uncertainty in each of the transfer function matrix elements: g_{11}, g_{21}, g_{31}, g_{41}, g_{12}, g_{32} and g_{14}, exceeds the nominal plant value by at least 10% somewhere in the frequency region considered. These are the uncertainties which will be considered during robust analysis. In more detail, these transfer functions are:

$$\frac{X_{p,2}}{V_{st}} = g_{11} \qquad \frac{X_{p,2}}{F_{p,1}} = g_{12} \qquad \frac{X_{p,2}}{F_{p,3}} = g_{14} \qquad \frac{h_1}{V_{st}} = g_{21}$$

$$\frac{h_2}{V_{st}} = g_{31} \qquad \frac{h_3}{V_{st}} = g_{41} \qquad \frac{h_2}{F_{p,1}} = g_{32}$$

3.1 NOMINAL STABILITY

The robust analysis method detects possible instability by checking for a change in the number of encirclements of the critical point. Before applying these techniques, it is therefore first required to confirm nominal stability. Applying the standard Nyquist test indicated that both controllers were nominally stable over the entire range of controller detuning.

The Nyquist test was applied in a similar fashion to that described in paragraphs 2.1.3 and 2.1.4; i.e. no encirclements of the critical point by the characteristic loci of $G_0(qK)$, where q is the controller detuning. No encirclements of the critical point is required since the plant is open-loop stable.

3.2 ROBUST STABILITY

As indicated above, 2 of the 7 elements with significant uncertainty have h_2 as output. It is however known that $F_{p,2}$, the manipulated variable associated with h_2, does not affect any other process output. Uncertainty in g_{31} and g_{32} can therefore not lead to instability and must be left out of the stability analysis. Attempts to include uncertainty in these 2 elements result in singular matrices. Intuitively this fact can be explained by considering that there is no mechanism whereby uncertainty in these 2 elements can be fed back into the system.

3.2.1 *MΔ-STRUCTURE*

The approach to casting the stability problem with independent uncertainty in the transfer function matrix elements into block-diagonal form used here and subsequently, follows (Morari&Zafiriou, 1989). The standard MΔ-structure for this problem is represented in figure 17.

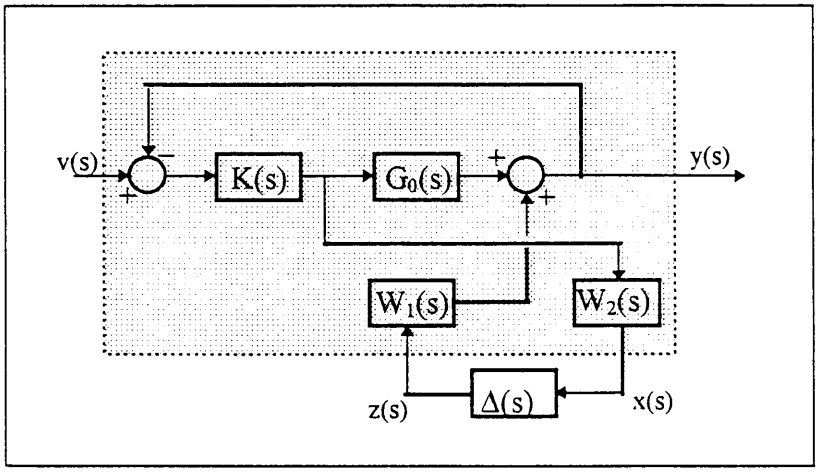

Figure 17: *MΔ-structure for additive uncertainty*

In the above figure M is represented by the shaded region, W_1 and W_2 are scaling matrices which make $\Delta(s)$ a block-diagonal matrix, with unit norm-bounds on the magnitude of the individual blocks. The blocks are all 1×1. Δ, W_1 and W_2 are given by:

$$\Delta(s) = diag\{\delta_1(s);\delta_2(s),\ldots,\delta_5(s)\} \quad , \quad |\delta_i| \le 1$$

$$W_1 = \begin{pmatrix} 1 & 0 & 0 & 1 & 1 \\ 0 & 1 & 0 & 0 & 0 \\ 0 & 0 & 0 & 0 & 0 \\ 0 & 0 & 1 & 0 & 0 \end{pmatrix}$$

$$W_2(s) = \begin{pmatrix} \hat{\delta}_{11}(s) & 0 & 0 & 0 \\ \hat{\delta}_{21}(s) & 0 & 0 & 0 \\ \hat{\delta}_{41}(s) & 0 & 0 & 0 \\ 0 & \hat{\delta}_{12}(s) & 0 & 0 \\ 0 & 0 & 0 & \hat{\delta}_{14}(s) \end{pmatrix}$$

Notice that the resulting Δ, after transforming the system to standard format, is 5×5 (it contains 5 blocks). This is a result of the fact that independent uncertainty in 5 transfer function matrix elements are considered. Also the bounds calculated will be conservative, and not exact, since $5>3$.

The transfer function of which the structured singular value (SSV) is to be calculated with respect to Δ, is:

$$M_{22}(s) = \frac{x(s)}{z(s)}$$
$$= -W_2\left(I + KG_0\right)^{-1} KW_1$$

3.2.2 STRUCTURED SINGULAR VALUE

The calculated SSV for the robust stability analysis is presented in figure 18, for the Inverse Nyquist controller, and figure 19 for the Characteristic Locus controller.

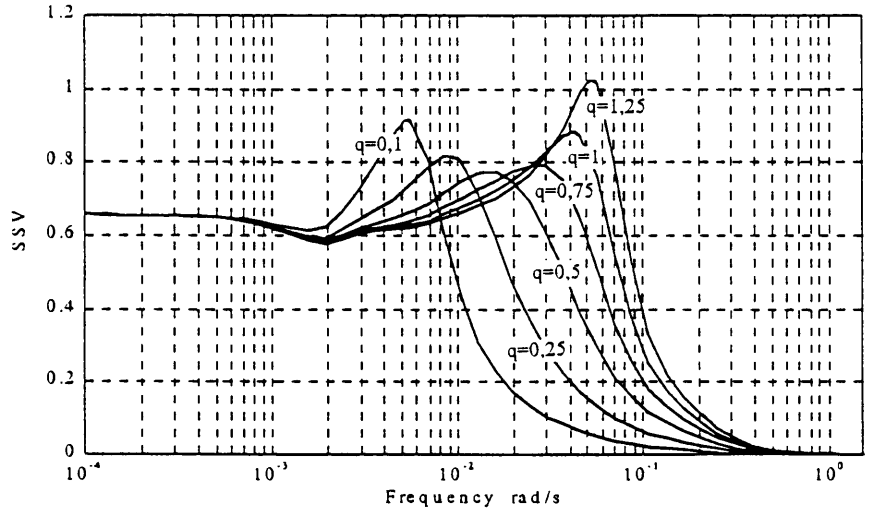

Figure 18: *Robust stability for INA controller*

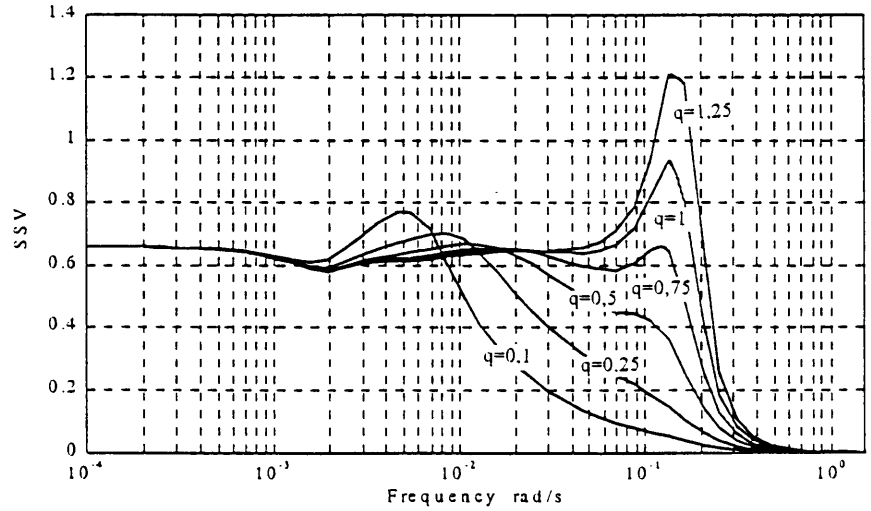

Figure 19: *Robust stability for CL controller*

The interpretation of these results are discussed in paragraph 3.4. For the moment it suffices to remind the reader that values of $\|M_{22}\|_\mu$ < 1 correspond to robust stability in this case. The smaller the value of $\|M_{22}\|_\mu$, the greater the margin of safety.

3.3 PERFORMANCE

For robust stability analysis uncertainty in transfer functions relating to h_2 as output had to be excluded. In the case of robust performance this uncertainty must be included. A feedback path between this output and the system is here provided by the performance specification.

3.3.1 PERFORMANCE SPECIFICATION

Process identification in order to determine the required performance specification yielded the following results after scaling.

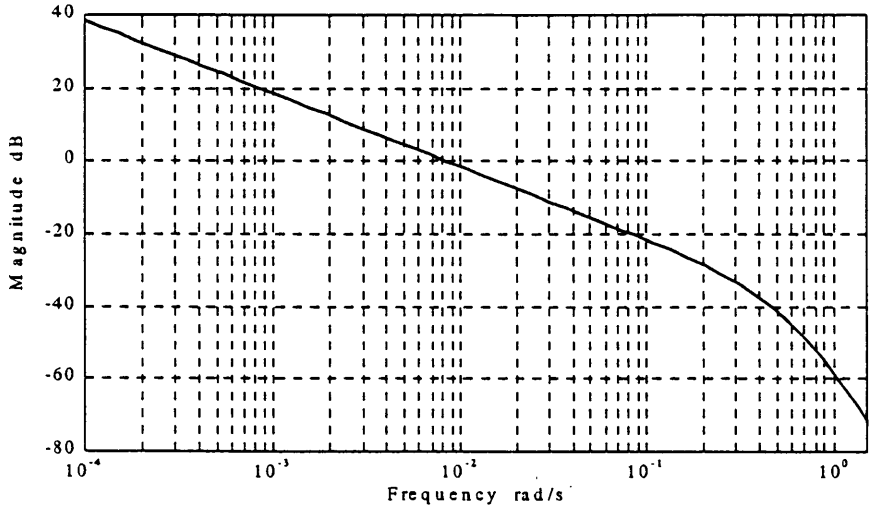

Figure 20: h_3/F_{feed}

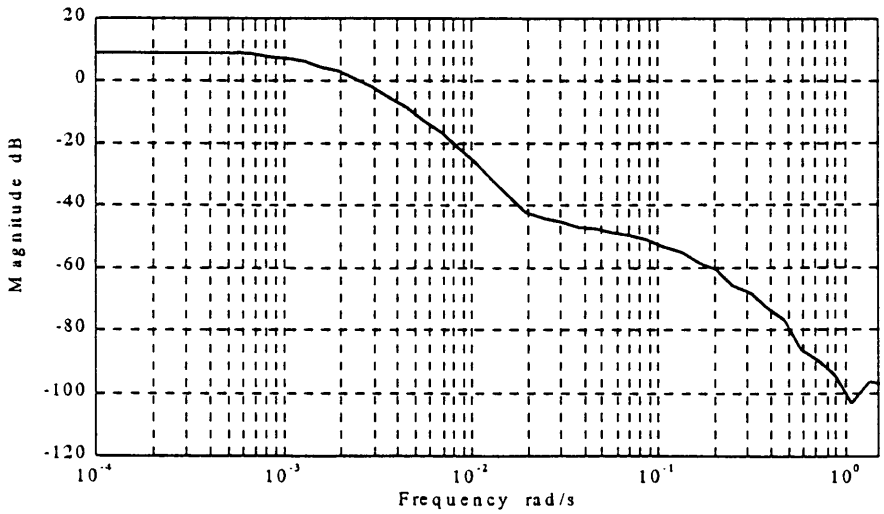

Figure 21: $8 \times X_{P,2}/F_{feed}$

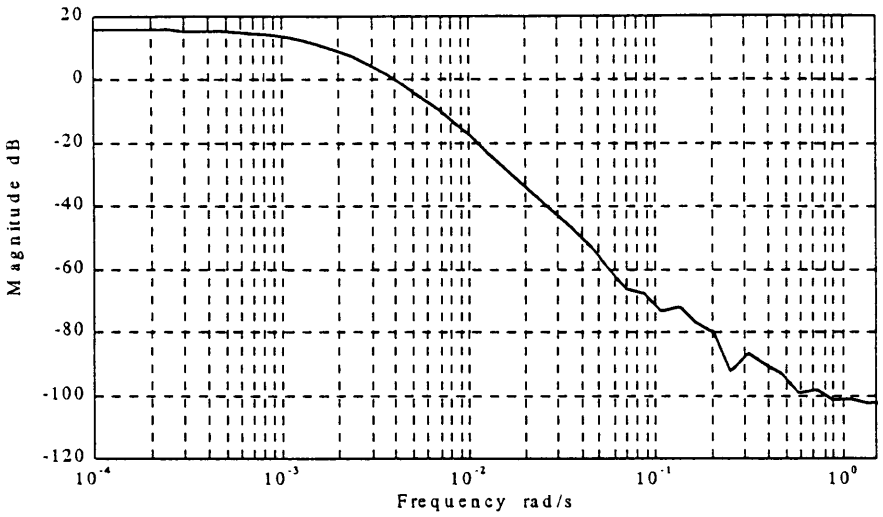

Figure 22: $8 \times X_{P,2}/X_{feed}$

$$\frac{h_1}{F_{feed}} = \frac{h_2}{F_{feed}} = \frac{h_1}{X_{feed}} = \frac{h_2}{X_{feed}} = \frac{h_3}{X_{feed}} = 0$$

Shown in figures 21 and 22 is 8× the actual magnitude. The reason for this is that it corresponds to an allowed variation of 0,01 in the output $X_{P,2}$, which is acceptable. Variation of output h_3 over its entire range is acceptable.

From the above the following conclusions regarding the required sensitivity bandwidth (where the magnitude crosses 0,707) can be drawn:

- $X_{p,2}$ requires 0,005 rad/s; X_{feed} (figure 22) places a stronger requirement than F_{feed} (figure 21)
- h_3 requires 0,01 rad/s from figure 20; a value of 0,03 rad/s was used
- h_1 and h_2 are not affected directly by external disturbances and a bandwidth of 0,001 rad/s was chosen

3.3.2 NOMINAL PERFORMANCE

Performance of the nominal system, i.e. uncertainty equal to zero, could as well have been analysed using singular value techniques, since the resulting Δ-matrix consists of only one block. For the purpose of illustration and comparison, use is made of the standard MΔ-structure. Performance is evaluated by considering the robust stability of a perturbed system.

3.3.2.1 MΔ-STRUCTURE

The standard MΔ-structure for this analysis can be represented as in figure 23. $\Delta_P(s)$ is a single 4×4 block with $\sigma^*(\Delta_P) \leq 1$ and $W_P(s)$ is given by

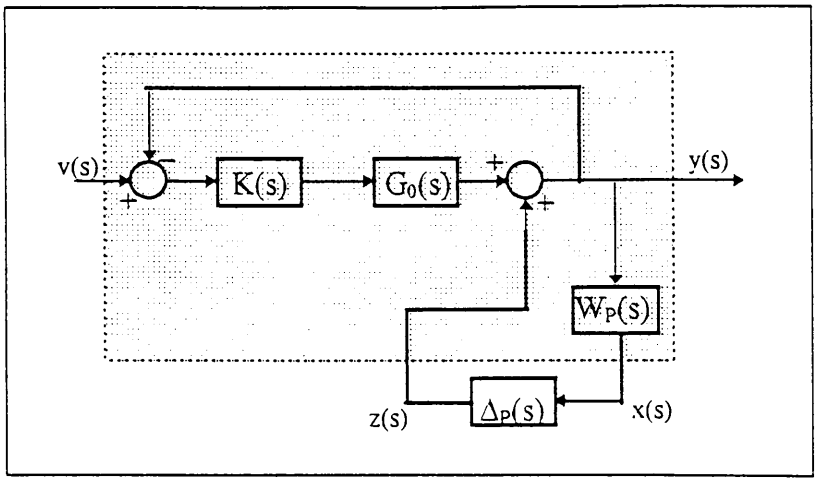

Figure 23: *MΔ-structure for nominal performance*

$$W_P(s) = diag\left\{\frac{s/2+0{,}005}{s+0{,}005\times 0{,}03};\frac{s/2+0{,}001}{s+0{,}001\times 0{,}03};\frac{s/2+0{,}001}{s+0{,}001\times 0{,}03};\frac{s/2+0{,}03}{s+0{,}03\times 0{,}03}\right\}$$

Since 1 < 3 the bounds calculated are exact. The transfer function of which the structured singular value (SSV) is to be calculated with respect to Δ_P, is:

$$M_{22}(s) = \frac{x}{z} = W_P\left(I + G_0K\right)^{-1}$$

3.3.2.2 STRUCTURED SINGULAR VALUE

The calculated SSV for the nominal performance analysis is presented in figure 24, for the Inverse Nyquist controller, and figure 25 for the Characteristic Locus controller. The interpretation of these results are discussed in paragraph 3.4. For the moment it suffices to remind the reader that values of $\|M_{22}\|_\mu$ < 1 correspond to nominal performance in this case. The smaller the value of $\|M_{22}\|_\mu$, the greater the margin of safety.

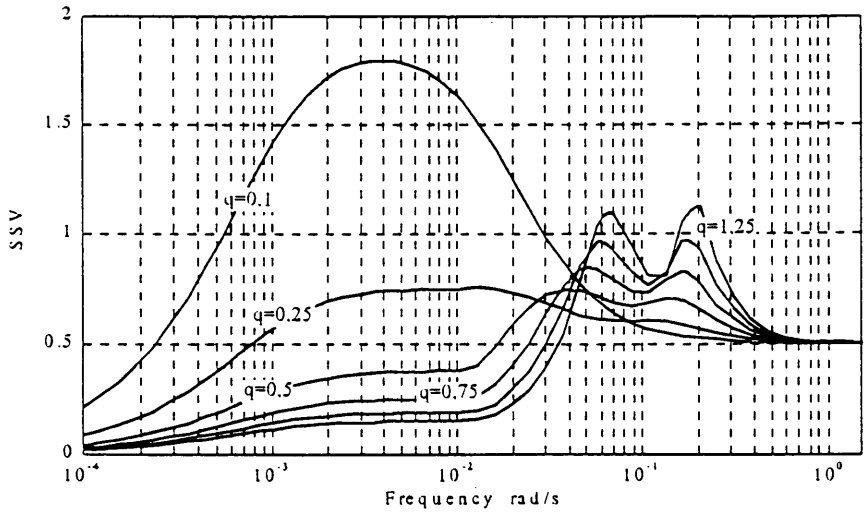

Figure 24: *Nominal performance for INA controller*

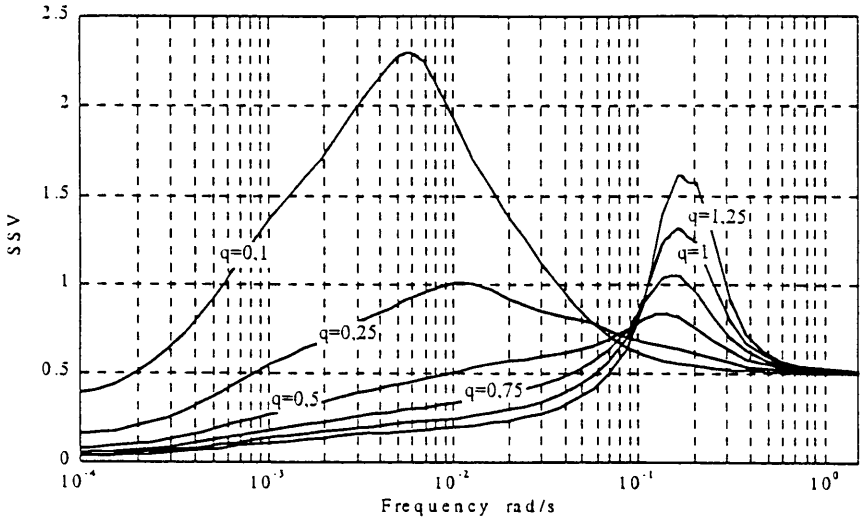

Figure 25: *Nominal performance for CL controller*

3.3.3 ROBUST PERFORMANCE

3.3.3.1 MΔ-STRUCTURE

For robust performance analysis the robust stability of the worst case combination of the perturbations for robust stability and nominal performance have to be evaluated. The standard MΔ-structure for this analysis is shown in figure 26.

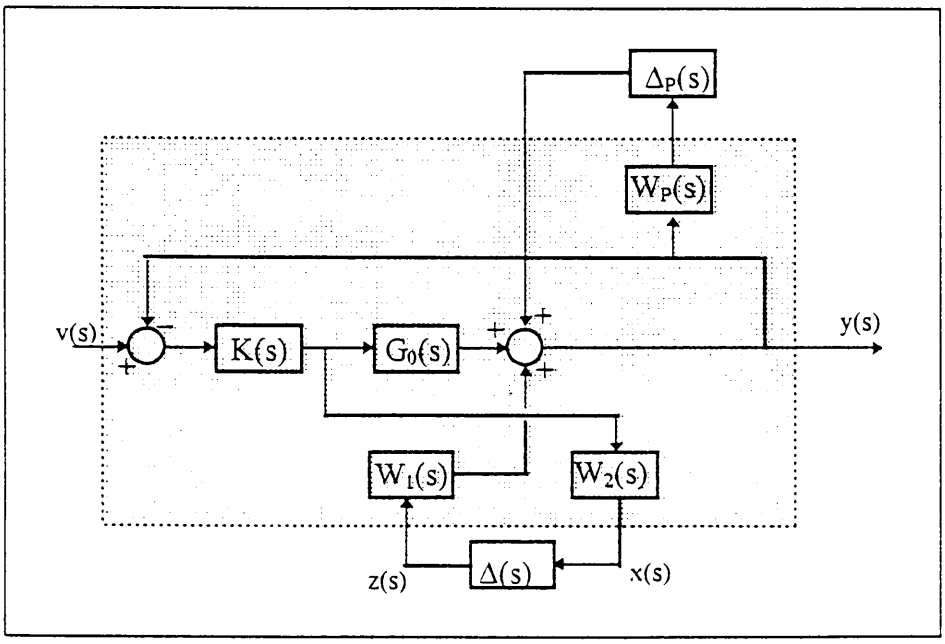

Figure 26: *MΔ-structure for robust performance with additive uncertainty*

where $\Delta_P(s)$ is a single 4×4 block with $\sigma^*(\Delta_P) \leq 1$ and $\Delta(s)$ is a block diagonal matrix consisting of 7 1×1 blocks, i.e.

$$\Delta(s) = diag\{\delta_1(s), \delta_2(s), \ldots, \delta_7(s)\} \quad , \quad |\delta_i| \leq 1$$

W_P, W_1 and W_2 are weighting matrices and are given by

$$W_P(s) = diag\left\{\frac{s/5+0{,}005}{s+0{,}005\times 0{,}03};\frac{s/5+0{,}001}{s+0{,}001\times 0{,}03};\frac{s/5+0{,}001}{s+0{,}001\times 0{,}03};\frac{s/5+0{,}03}{s+0{,}03\times 0{,}03}\right\}$$

$$W_1 = \begin{pmatrix} 1 & 0 & 0 & 0 & 1 & 0 & 1 \\ 0 & 1 & 0 & 0 & 0 & 0 & 0 \\ 0 & 0 & 1 & 0 & 0 & 1 & 0 \\ 0 & 0 & 0 & 1 & 0 & 0 & 0 \end{pmatrix}$$

$$W_2(s) = \begin{pmatrix} \hat{\delta}_{11}(s) & 0 & 0 & 0 \\ \hat{\delta}_{21}(s) & 0 & 0 & 0 \\ \hat{\delta}_{31}(s) & 0 & 0 & 0 \\ \hat{\delta}_{41}(s) & 0 & 0 & 0 \\ 0 & \hat{\delta}_{12}(s) & 0 & 0 \\ 0 & \hat{\delta}_{32}(s) & 0 & 0 \\ 0 & 0 & 0 & \hat{\delta}_{14}(s) \end{pmatrix}$$

Note that a different performance specification was used than in the nominal case. The restriction on peak height, namely 5, is higher than the typical value of 2 used for nominal performance evaluation. This corresponds to more oscillatory behaviour.

The transfer function of which the structured singular value (SSV) is to be calculated with respect to $\{\Delta_P,\Delta\}$, is:

$$M(s) = \begin{pmatrix} W_P(I+G_0K)^{-1} & W_P(I+G_0K)^{-1}W_1 \\ -W_2(I+KG_0)^{-1}K & -W_2(I+KG_0)^{-1}KW_1 \end{pmatrix}$$

Since the problem has an 8-block uncertainty description (the 7 uncertainty blocks and Δ_P), the calculated bounds are conservative.

3.3.3.2 STRUCTURED SINGULAR VALUE

The calculated SSV for the robust performance analysis is presented in figure 27, for the Inverse Nyquist controller, and figure 28 for the Characteristic Locus controller.

The interpretation of these results are discussed in paragraph 3.4. For the moment it suffices to remind the reader that values of $\|M_{22}\|_\mu < 1$ correspond to robust performance in this case. The

smaller the value of $\|M_{22}\|_{\mu}$, the greater the margin of safety. Of course robust performance implies robust stability.

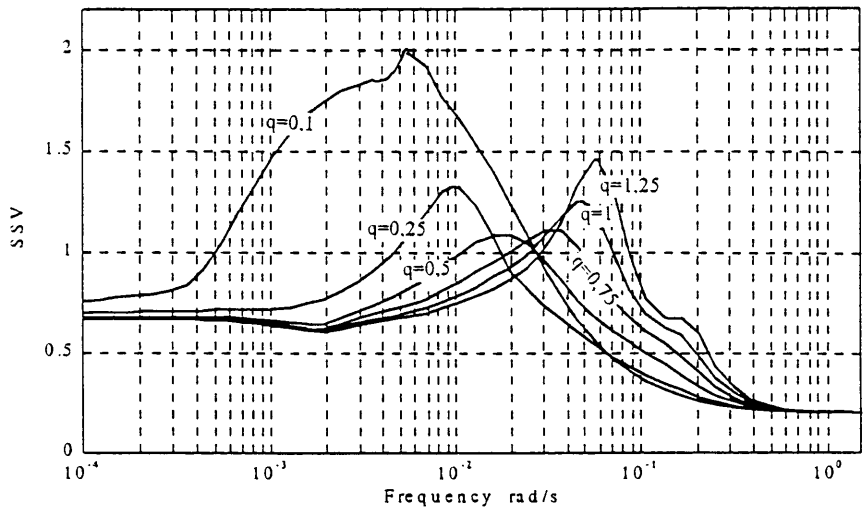

Figure 27: *Robust performance for INA controller*

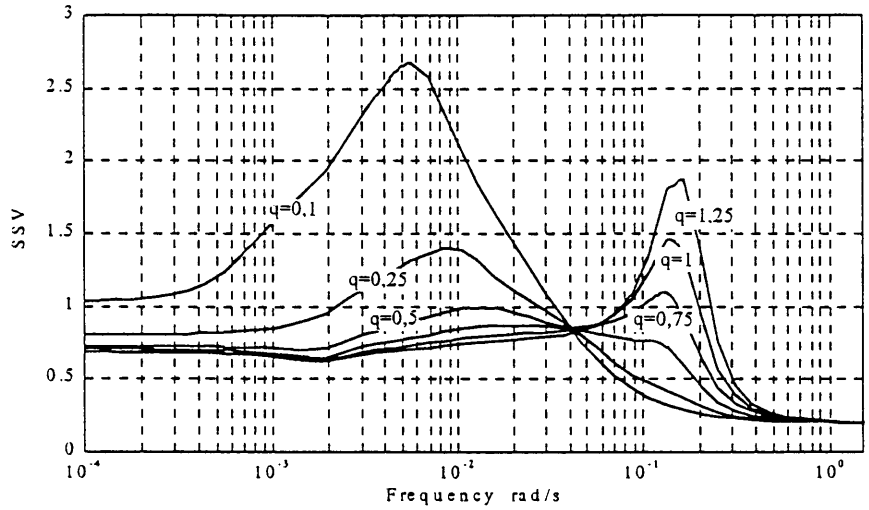

Figure 28: *Robust performance for CL controller*

3.4 DISCUSSION

3.4.1 GENERAL REMARKS

Application of the standard Nyquist stability criterion indicated that both controllers are nominally stable over the entire range of detuning investigated. Robust analysis could therefore be applied over the entire range. Failure to establish that nominal stability has been achieved renders results obtained from robust analysis invalid. The reason is that the robust analysis techniques pick up on a change in the number of encirclements of the critical point by the characteristic loci. If the number of encirclements of the nominal system is incorrect, it is obvious that the results are meaningless.

Application of the robust analysis techniques are straightforward, once the basic principles and manipulation required to obtain the standard MΔ-structure are understood. As illustrated here the MΔ-structure can be used to test robust stability, nominal performance and robust performance. Performance is tested by considering the robust stability of an MΔ-structure with the performance specification included as uncertainty. The performance bounds used were easy to determine and the frequency-domain characteristics can be extended to time-domain characteristics in a fairly straight-forward manner.

Values of $\|M_{22}\|_\mu < 1$ (or $\|M\|_\mu < 1$) correspond to satisfaction of the condition set in the standard MΔ-structure. The smaller the value of $\|M_{22}\|_\mu$ (or $\|M\|_\mu$), the greater the margin of safety. The utility of robust analysis to a controller designer should be obvious. Use is made of a plot of SSV against frequency. Checking whether robustness bounds are met is done by simply investigating the peak value of the SSV. A more ambitious step would be to try and maximise the safety margin (i.e. minimising the peak value of SSV). It also gives the designer an indication of the frequency ranges where problems are likely to arise and additional loop-shaping is required. Alternatively the best possible performance from the controller can be obtained by adjusting the performance specification until a peak value of 1 is obtained.

The work done here (detuning the controller by multiplication with a scalar) is a simple application of the above ideas. Surveying all the robust analysis graphs it is apparent that it would be possible in each case to find a value of detuning, q, such that the overall stability or performance margin of the process is maximised as put forward in (Agamennoni et al, 1989).

It would also be possible to incorporate robust analysis techniques as the final step in an iterative controller design loop. One would redesign the controller until satisfactory robust behaviour is obtained. The most advanced application of these techniques corresponds to μ-synthesis; the so called DK-iteration (Skogestad&Postlethwaite, 1996). Here robustness is considered explicitly during the actual controller design step.

It is unfortunately so that the utility of the results obtained is limited by the accuracy and appropriateness of the uncertainty description. These techniques are also insensitive to constraints. Manipulated variable saturation can therefore not be taken into account.

3.4.2 ROBUST STABILITY

Considering figures 18 and 19 it is apparent that both controllers are robustly stable for all controller detunings except q = 1,25.

Both controllers have the feature that as q is increased the maximum value of the SSV first decreases and then increases, while the peak itself occurs at higher frequency. Recall from appendix C that the magnitude of uncertainty in all transfer function matrix elements decreases with frequency for the system considered. As q is increased the low frequency region, $\omega \approx 0{,}005$ rad/s, (and its uncertainty) is moved sufficiently away from the critical point to prevent encirclements. It however forces the higher frequency region, $\omega \approx 0{,}1$ rad/s for the CL controller and $\omega \approx 0{,}06$ rad/s for the INA controller, closer to the critical point, leading to peaks in this area. It is apparent that an optimum value for q can be found which would balance out the two peaks leading to a maximum stability margin. This optimum value for the INA controller is ≈0,5 and ≈0,75 for the CL controller.

A peculiar feature of figures 18 and 19 is that both controllers over the entire detuning range have identical SSV's of ≈0,65 in the low frequency range. This can be explained by considering the following:

$$\begin{aligned} M_{22}(s) &= -W_2\left(I + KG_0\right)^{-1} KW_1 \\ &\approx -W_2\left(KG_0\right)^{-1} KW_1 \qquad \text{at low frequencies} \\ &= -W_2 G_0^{-1} W_1 \end{aligned}$$

i.e. M_{22} is independent of K at low frequencies.

3.4.3 NOMINAL PERFORMANCE

Considering the nominal performance results (figures 24 and 25) it is apparent that two peaks are again evident. The lower frequency peak is caused by bandwidth requirements, while the higher frequency peak is caused by sensitivity peak height requirements. It is obvious that detuning the controller results in a lower sensitivity peak height, but also lower bandwidth, i.e. slower response. The undesirable broadness of the peak in the sensitivity function for the INA-controller can not be diminished by varying the detuning factor, unless detuning is done to such an extent that the higher frequency peak disappears.

In the case of the INA controller, nominal performance is satisfied for detunings of 0,25 to 1. For the CL controller nominal performance is satisfied for detunings 0,25 and 0,5, with 0,75 just failing.

3.4.4 ROBUST PERFORMANCE

Robust performance (figures 27 and 28) yields similar results to the robust stability and nominal performance combined. Even though the allowed peak height has been increased from 2 (nominal performance) to 5 (robust performance), the performance objective is only achieved for a narrow range of detunings of the CL controller ($q \approx 0{,}5$). This performance deterioration is to be expected,

since the worst case from the entire range of plants allowed by the uncertainty description, is effectively pointed out. Again it is evident that an optimum value for controller detuning exists that will lead to maximum robust performance margins. This optimum value corresponds to $\approx 0,6$ for both controllers.

CHAPTER 5: CONCLUSIONS

Process identification indicated significant interaction in 11 of the 16 transfer function matrix elements for the triple-effect evaporator. Furthermore, sizeable interaction (more than 10% of the nominal plant magnitudes) were present in 7 of the 16 transfer function matrix elements. As already motivated, the system is typical of chemical engineering systems. It can therefore be said that meaningful conclusions can be drawn regarding the utility of the robust analysis methods considered in this study.

It was found that the robust analysis techniques provide a useful source of information: the traditional use of stability margins based on rules of thumb (e.g. the Doyle-Stein criterion (Luyben, 1991)) can be replaced by precise values. This allows one to accurately assess trade-offs between performance and robustness. Conversion of robust analysis problems to the standard MΔ-structure needed by the calculation algorithm is a straightforward matter. Robustness with regard to stability and performance is now evaluated by considering an upper bound on a scalar-valued function of frequency, namely the structured singular value.

The techniques can be used to analyse previously designed controllers. As an example of this a simple method of controller adjustment was investigated. By simply detuning the controller by a constant scalar it is possible to optimise the robust performance of the controller (its worst case performance), or to maximise the process's robust stability margins. Although it was not investigated in this work, design techniques (e.g. μ-synthesis) exist which even allow for the explicit consideration of robustness bounds during the controller synthesis step.

The analysis techniques make use of the frequency domain. Frequency domain conditions for stability of feedback systems, e.g. the Nyquist stability criterion, are central to the derivation of these techniques. Robust performance is evaluated by considering the robust stability of a particular uncertainty structure. Included in this structure is a frequency dependent bound on performance.

It is possible to derive a description encompassing the entire range of possible plant operating conditions using a linear nominal plant model with associated bounded perturbation for the system under study. The uncertainty description used, independent norm-bounded additive uncertainty in the transfer function matrix elements, reduces the problem to a number of single input single output problems. Using simple pulse tests, linear plant models were derived in the frequency domain at the extremes of plant operation. A novel algorithm was now used to determine the least conservative nominal plant model and norm-bounded uncertainty which contain all possible plants. This procedure was repeated for each transfer function matrix element. These calculations were performed in the frequency domain.

The uncertainty description suffers from the following defects:

- Since only norm-bounds were considered, available phase information was neglected and unnecessary conservatism introduced. Techniques (paragraph 1.3.3, chapter 2) are available to reduce this conservatism.
- Considering the uncertainty in the transfer function matrix elements to be independent significantly simplifies the difficulty associated with obtaining an uncertainty description. It is however conservative in that coupling exists between transfer function matrix elements. An approach accounting for this coupling would necessitate a considerably more complicated analysis.
- A significant proportion of the uncertainty results from the fact that a linear model is used to describe a non-linear plant. What is treated as uncertainty is in fact well known non-linearity.

The uncertainty description obtained using the simple approach as was done in this work, however yields conservative results. One is therefore erring on the safe side.

The identification procedure used here is applicable to open-loop stable processes; typical of chemical engineering plants. It is however so that as the number of variables needed to describe the operating condition increases, a sizeable amount of pulse tests would have to be performed to characterise the entire range of operating conditions (tests at each extreme). To conduct this amount of tests on real equipment would result in a very lengthy and expensive exercise. It is however possible to limit these tests by use of rigorous modelling as a source of information regarding uncertainty, particularly associated with non-linearity.

The multivariable controller design methods employed, namely the Inverse Nyquist Array and Characteristic Locus methods, yielded satisfactory results. Robust analysis is not included in the actual design step, and can only be applied in an iterative manner. (Designing a controller, checking its robust characteristics and then redesigning.) Controller design techniques such as μ-analysis, which incorporates the uncertainty directly in the controller design step, should provide even greater benefits.

The disadvantage of robust analysis techniques is that they are heavily dependent on the validity and tightness of the uncertainty description. Furthermore a lot of conservatism is introduced due to the linear models used to describe what is inherently (known) non-linear processes. It is believed that these techniques provide a significant aid to the control engineer, but that what is needed in reality is an approach which allows for non-linear descriptions. This needs to be investigated further.

Although more powerful linear techniques are available than were applied in this study (e.g. incorporating phase information in the uncertainty description), they should be seen in the light of the above paragraph. They provide more accurate answers to the wrong questions.

REFERENCE LIST

Agamennoni, O., Rotstein, H., Desages, A., and Romagnoli, J. A. (1989). "Robust controller design methodology for multivariable chemical processes: structured perturbations." *Chemical engineering science*, 44(11), 2597-2605.

Baker, W.M., and Bourne, A.A. (1920). *Elementary geometry*, G. Bell and Sons, London.

Burden, R.L., and Faires, J.D. (1993). *Numerical analysis*, PWS Publishing, Boston.

Chun, K. R., and Seban, R. A. (1971). "Heat transfer to evaporating liquid films." *Journal of heat transfer, Transactions of the ASME, Series C*, 93(4), 391-396.

Doyle, J. (1982). "Analysis of feedback systems with structured uncertainties." *Proceedings of the IEE Part D*, 129(6), 242-250.

Doyle, J. C., and Stein, G. (1981). "Multivariable feedback design: concepts for a classical/modern synthesis." *IEEE transactions on automatic control*, AC-26(1), 4-16.

Figueroa, J. L., Desages, A. C., Palazoglu, A., and Romagnoli, J. A. (1993). "Trade-offs in robust controller design." *International journal of control*, 58(6), 1265-1278.

Figueroa, J. L., Desages, A. C., Romagnoli, J. A., and Palazoglu, A. (1991). "Highly structured stability margins for process control systems. A case study of decoupling control in distillation." *Computers and chemical engineering*, 15(7), 493-502.

Ford, M. P., Maciejowski, J. M., and Boyle, J. M. (1990). *Multivariable frequency domain toolbox for use with MATLAB, User's guide*, Cambridge Control Ltd.

Hulbert, D. G., and Braae, M. (1982). "Software for the design of multivariable control systems by use of the Inverse Nyquist Array." *M31*, Mintek, Randburg.

Khambanonda, T., and Palazoglu, A. (1990). "Robustness studies for multivariable feedback systems using refined eigenvalue inclusion regions (REIR)." *Computers and chemical engineering*, 14(4/5), 391-400.

Kouvaritakis, B., and Latchman, H. (1985b). "Necessary and sufficient stability criterion for systems with structured uncertainties: the major principal direction alignment principle." *International journal of control*, 42(3), 575-598.

Kouvaritakis, B., and Latchman, H. (1985a). "Singular-value and eigenvalue techniques in the analysis of systems with structured perturbations." *International journal of control*, 41(6), 1381-1412.

Kouvaritakis, B., Rossiter, J. A., and Wang, J. (1991). "Generalised Nyquist bands for structured and highly structured uncertainty." *International journal of control*, 53(6), 1295-1309.

Kyle, B. G. (1992). *Chemical and process thermodynamics*, Prentice Hall, Englewood Cliffs.

Luyben, W. L. (1990). *Process modeling, simulation and control for chemical engineers*, McGraw-Hill, Singapore.

MacFarlane, A. G. J., and Belletrutti, J. J. (1973). "The characteristic locus design method." *Automatica*, 9, 575-588.

MacFarlane, A. G. J., and Kouvaritakis, B. (1977). "A design technique for linear multivariable feedback systems." *International Journal of Control*, 25(6), 837-874.

Maciejowski. (1989). *Multivariable feedback design*, Addison-Wesley Publishing Company.

Morari, M., and Zafiriou, E. (1989). *Robust process control*, Prentice Hall, Englewood Cliffs.

O'Neil, P. V. (1991). *Advanced engineering mathematics*, Wadsworth publishing company, Belmont.

Packard, A., and Doyle, J. (1992). "The complex structured singular value." *Automatica*, 29(1), 71-109.

Palazoglu, A., and Khambanonda, T. (1989). "On the use of the numerical range for the robust stability problem." *Chemical engineering science*, 44(11), 2483-2492.

Postlethwaite, I., Edmunds, J. M., and MacFarlane, A. G. J. (1981). "Principal gains and principal phases in the analysis of linear multivariable feedback systems." *IEEE transactions on automatic control*, AC-26(1), 32-46.

Rotstein, H., Desages, A., and Romagnoli, J. (1989). "Calculation of highly structured stability margins." *International journal of control*, 49(3), 1079-1092.

Sinnot, R. K. (1993). *Coulson and Richardson's chemical engineering volume 6*, Pergamon Press, Exeter.

Skogestad, S., and Morari, M. (1987). "Design of resilient processing plants-IX. Effect of model uncertainty on dynamic resilience." *Chemical engineering science*, 42(7), 1765-1780.

Skogestad, S., and Postlethwaite, I. (1996). *Multivariable feedback control, analysis and design*, John Wiley&Sons.

Stephanopoulos, G. (1984). *Chemical process control: an introduction to theory and practice*, Prentice Hall.

APPENDIX A: PROCESS MODELLING

Dynamic modelling in chemical engineering reduces to the setting up of differential equations describing the conservation of three fundamental properties, i.e. mass/moles (either total mass or mass of individual components), energy and momentum [Luyben, 1990; Stephanopoulos, 1984; Seborg, Edgar &Mellichamp, 1989)].

The fundamental quantities referred to in the above equations are in general not directly measurable, or from the modelling point of view, can be more conveniently described in terms of other properties, e.g. energy in terms of temperature and heat capacity. Furthermore, these quantities are not necessarily independent, e.g. multi-component phase equilibrium. These algebraic equations form an important part of the model and need to be solved at each iteration step during the simulation process. Simplifying assumptions are also generally made. This is done by consideration of the operating conditions and the purpose of the model.

1. EVAPORATORS IN GENERAL

According to Sinnot (1993), evaporation "is the removal of a solvent by vaporisation, from solids that are not volatile". Evaporators can be grouped into the following basic types (Green&Perry, 1984):

- **Direct-heated**: includes solar pans and submerged combustion units
- **Long-tube (LTV)**: liquid flows as a thin film on the walls of a long, vertical heated tube; falling and rising film types
- **Forced-circulation**: liquid is pumped through the tubes
- **Agitated thin-film**: a thin layer of solution is spread on heating surface by mechanical means
- **Short-tube, callandria**: used in the sugar industry
- **Horizontal tube**: the steam is inside the tubes and the process fluid outside

Different applications require different features.

In this study falling film LTV evaporators are considered. The liquid is fed to the top of long vertical tubes, and subsequently runs down the tubes as a thin film. Separation of vapour and liquid normally occurs at the bottom of the tubes. The pressure drop through the tubes is usually very small, and therefore the boiling-temperature throughout the tube is almost uniform with negligible overheating of product taking place. Evaporators of this type also feature a short hold-up time. Furthermore good heat-transfer coefficients can be achieved even at low boiling temperatures. Owing to the characteristics mentioned above these evaporators are commonly used for heat-sensitive materials.

Problems with these units are mostly related to feed distribution. It is required that all surfaces be wetted continually. This usually requires recirculation of the process liquid, which to a degree offsets the short hold-up time. A diagrammatic representation of a falling film LTV is shown in figure 1.

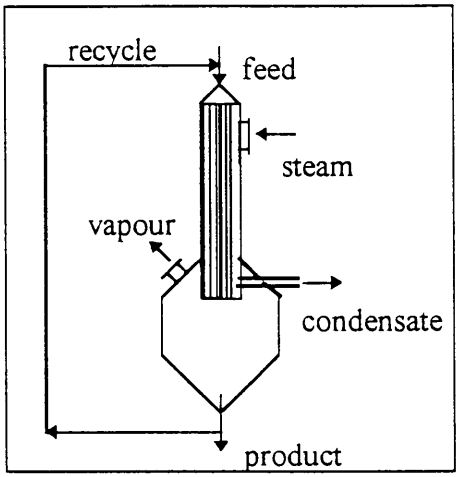

Figure 1: *Falling film LTV evaporator*

Increasing cost of energy and equipment has necessitated the development of technology to optimise energy input. In evaporators this has led to multiple-effect evaporators. In this operation the vapour generated in one effect is used as the energy source in adjacent effects. It should however be borne in mind that the temperature of the energy source must be higher than the liquid being evaporated. This can be done by operating effects at different pressures, by vapour recompression or by adding of fresh steam. The effect of boiling point rise as the concentration of solids increase must also be taken into account. In other words the boiling point of the mixture is higher than the saturation temperature at the same pressure of the pure vapour that is formed.

The above mentioned discussion leads to the term steam economy. It is defined as the mass of vapour produced per mass unit of steam supplied to the evaporator train. For a well designed system this is typically 10% smaller than the number of effects. It is customary to number effects in the direction of steam flow.

Multiple-effect evaporators can be divided into two main groups:

- **Cocurrent**: feed and steam follow parallel paths through the evaporator train
- **Countercurrent**: feed and steam enter the train at different ends

The application that is considered does not fit either of the above cases. Process flow is from 3rd to 1st to 2nd effect.

2. PROCESS DESCRIPTION

The process flowsheet is as shown in figure 2.

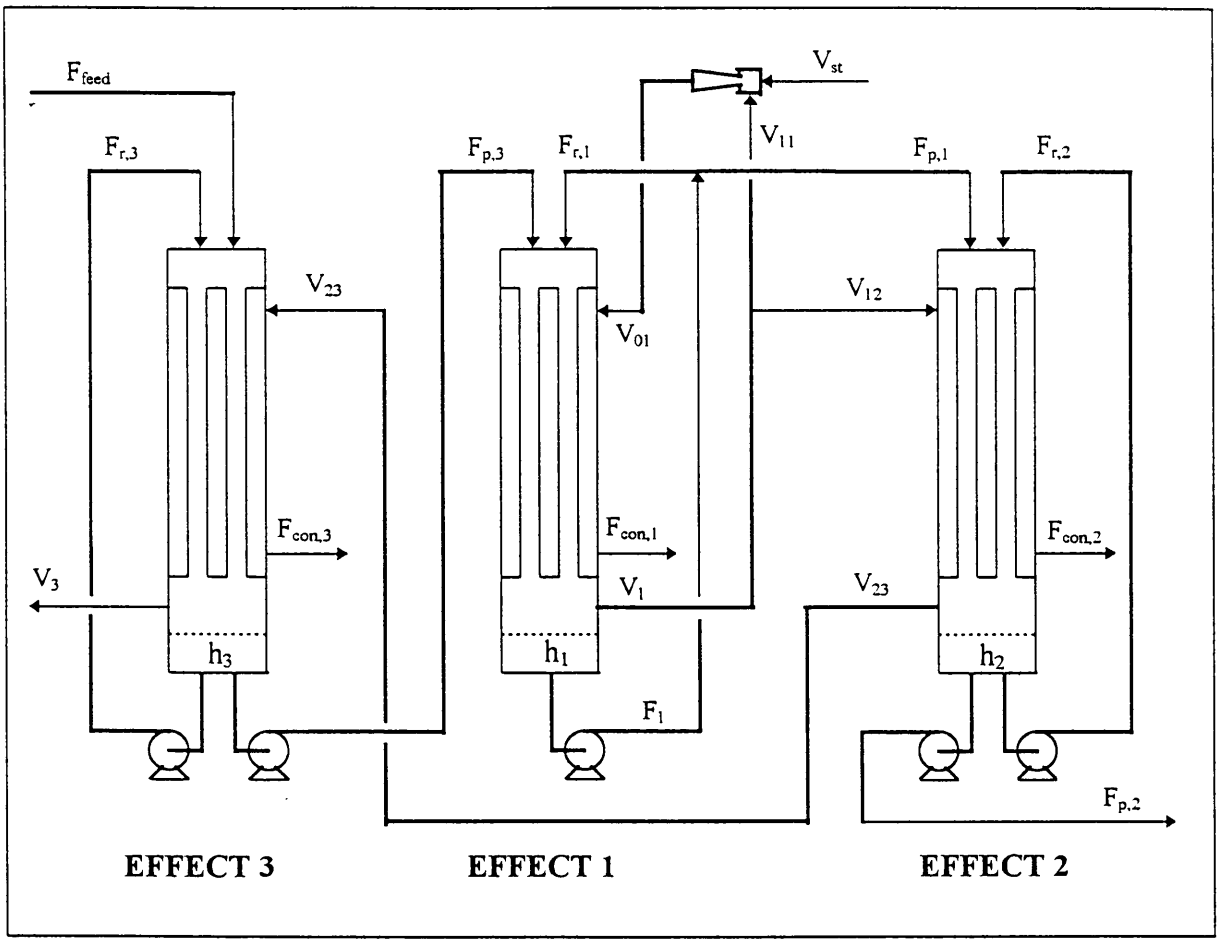

Figure 2: *Process flowsheet*

The process consists of a triple-effect falling film evaporator used for concentrating solutions of water and a non-volatile solute. The steam fed to the process is high pressure steam. Given that the solute is heat-sensitive operation is under vacuum. The nature of the upstream processing causes step changes in the overall load to the plant, i.e. F_{feed}, the most important disturbance to take cognisance of.

- *Controlled variables*
  - ⇒ final product composition, $X_{p,2}$
  - ⇒ heights in all the sumps: h_1, h_2 and h_3

The following variables are set externally:

- *External disturbances*
  - ⇒ feed flowrate, F_{feed}
  - ⇒ feed composition, X_{feed}

⇒ recycle flowrates, F_{r2}, F_{r3} and F_1

⇒ downstream pressure after the third effect, P_{down}

- *Manipulated variables*

⇒ V_{st}

⇒ F_{p1}

⇒ F_{p2}

⇒ F_{p3}

3. DERIVING A MATHEMATICAL MODEL

3.1 MODELLING A SINGLE EFFECT

For the purpose of modelling, a single effect is divided into the parts shown schematically in figure 3.

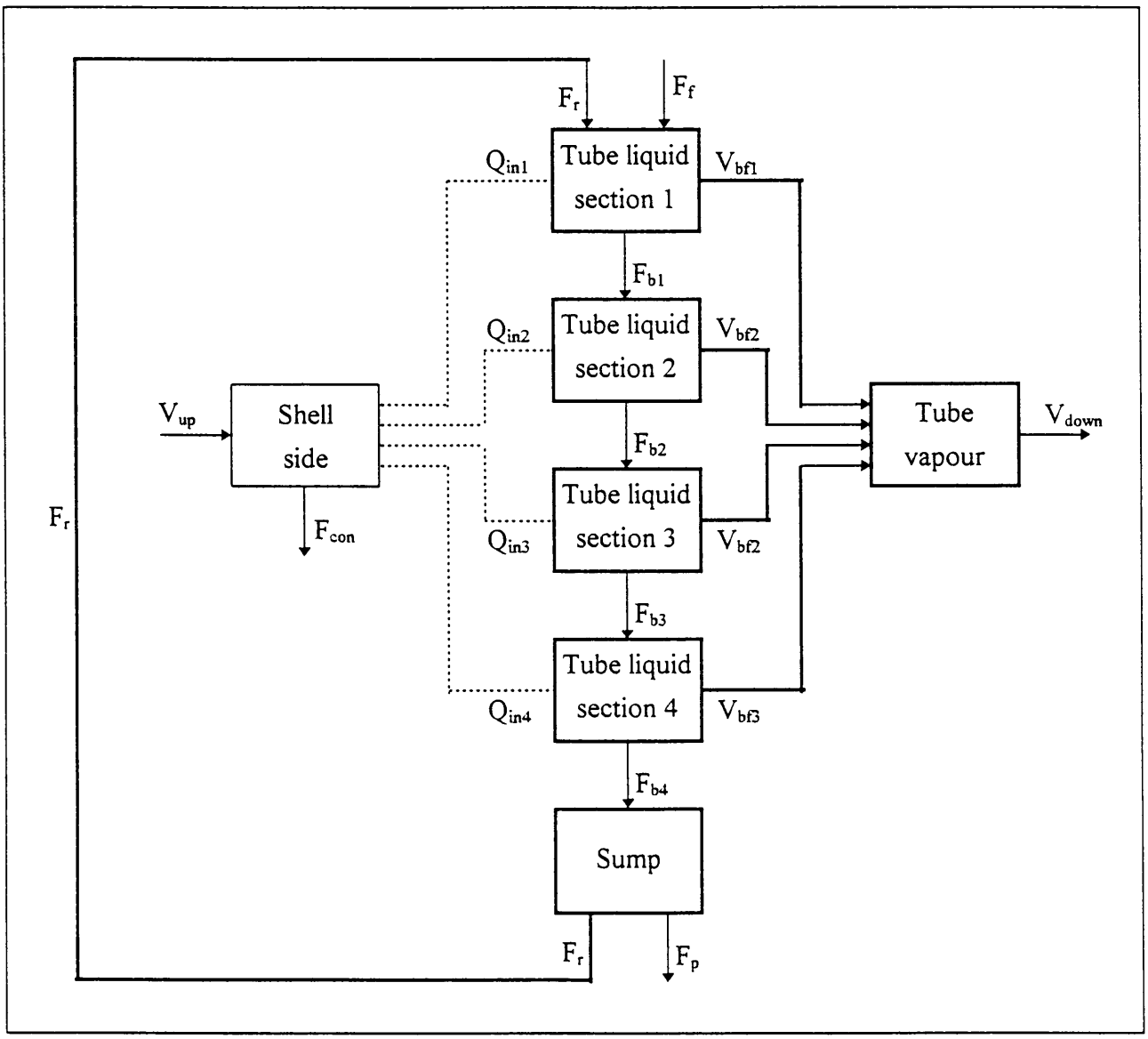

Figure 3: *A single effect*

Each of these sections are assumed to be infinitely well-mixed. Solid lines indicate material transfer whereas the dashed lines indicate heat transfer from the shell-side to the tube side liquid. Streams indicated with F are liquid flows, whereas streams indicated with V are vapour flows. The pressure is considered constant for the entire tube-length, i.e. the pressure in tube sections 1 and 4 is identical.

3.1.1 CONSERVATION EQUATIONS

3.1.1.1 TUBE LIQUID SECTION

For section j the balances are as follows:

Total mass:

$$F_{b,j-1} - F_{b,j} - V_{bf,j} = \frac{dW_{b,j}}{dt}$$

for section 1

$$F_{b,0} = F_f + F_r$$

Dissolved substance:

$$F_{b,j-1}X_{b,j-1} - F_{b,j}X_{b,j} = \frac{d(W_{b,j}X_{b,j})}{dt}$$

for section 1

$$F_{b,0}X_{b,0} = F_f X_f + F_r X_r$$

Energy:

$$Q_{in,j} + F_{b,j-1}H_{b,j-1} - F_b H_b - V_{bf,j}H_{bvf,j} = \frac{d(W_{b,j}H_{b,j})}{dt}$$

for section 1

$$F_{b,0}H_{b,0} = F_f H_f + F_r H_r$$

3.1.1.2 TUBE VAPOUR

Total mass:

$$\sum_{j=1}^{4} V_{bf,j} - V_{down} = \frac{dW_{bv}}{dt}$$

Energy

$$\sum_{j=1}^{4} V_{bf,j}H_{bvf,j} - V_{down}H_{bv} = \frac{d(W_{bv}H_{bv})}{dt}$$

3.1.1.3 SUMP

Total mass:

$$F_{b,4} - F_r - F_p = \frac{dW_s}{dt}$$

Dissolved substance:

$$F_{b,4}X_{b,4} - (F_r + F_p)X_s = \frac{d(W_s X_s)}{dt}$$

Energy:

$$F_{b,4}H_{b,4} - (F_r + F_p)H_s = \frac{d(W_s H_s)}{dt}$$

3.1.1.4 *Shell Side*

Total mass:

$$V_{up} - F_{con} = \frac{dW_{st}}{dt}$$

Energy:

$$V_{up}H_{vup} - F_{con}H_{con} - \sum_{j=1}^{4} Q_{in,j} = \frac{d(W_{st}H_{st})}{dt}$$

3.1.2 *Relating Model Parameters and Further Assumptions*

3.1.2.1 *Gas behaviour*

Ideal gas behaviour is assumed to hold. Given that operation is under vacuum, this is a meaningful assumption. This implies

$$PV = nRT$$

and also

$$\rho_v = \frac{MP}{RT}$$

and also that gas enthalpy is independent of pressure and only a function of temperature and composition.

3.1.2.2 *Equilibrium*

Use is made of Raoult's law to describe the boiling point elevation of the solution. Noting that the solute is involatile the condition necessary for phase equilibrium reduces to (Kyle, 1989)

$$x_w P_w^{vap}(T) = P$$

The vapour pressure of water is calculated using the Antoine equation (Sinnot, 1993). Equilibrium is assumed to hold between liquid phase and the vapour leaving the phase. With reference to figure 2 this means that V_{bf1} is in equilibrium with the liquid in tube section 1. Equilibrium is also assumed to hold on the shell-side.

3.1.2.3 ENTHALPY

Enthalpy of the liquid phase is calculated using a weighted average heat capacity

$$H_l = \left(x_w C_{p,w} + x_s C_{p,s}\right) \cdot \left(T - T_{ref}\right)$$

The enthalpy of steam is calculated by adding the latent heat of vaporisation of water to the enthalpy of pure water at the desired temperature.

3.1.2.4 HOLD-UP

The following relationship holds between the hold-up and film thickness in tube section of height z

$$W_b = \left(N_b \cdot \pi d_b \cdot z \cdot \delta\right)\rho_l$$

The following relates the vapour hold-up in volume V_{el} and the gas conditions

$$W_v = \rho_v V_{el} = \frac{MPV_{el}}{RT}$$

3.1.2.5 FILM-FLOW

The following relationship exists between film flow and film thickness in the laminar regime (Chun& Seban, 1971)

$$F_b = N_b \cdot \pi d_b \frac{\rho_l g \delta^3}{3\mu_l}$$

Operation is in the laminar regime.

3.1.2.6 HEAT-TRANSFER

The heat transfer coefficient through a falling laminar film is given by (Chun&Seban, 1971)

$$h = \frac{k}{\delta}$$

A typical heat transfer coefficient value for condensing steam of 8 kW/(m^2·°C) was used (Sinnot, 1993). The heat transfer over a tube section of length z is now determined with

$$Q_{in} = \frac{1}{1/h + 1/h_{cond}} N_b \cdot \pi d_b \cdot z \cdot \left(T_{st} - T_b\right)$$

3.1.2.7 PIPE-FLOW

All time delays associated with pipe-flow are neglected, i.e. the fluid entering and leaving a pipe at any particular instant in time is identical in magnitude and composition. For the above effect this implies

$$X_r = X_s$$

Vapour flow rate is given by

$$V = \frac{\sqrt{\Delta P}}{R}$$

3.2 MODELLING THE ENTIRE SYSTEM

Combining the entire process leads to the following equalities

3.2.1 EFFECT 1

$$F_f = F_{p,3}$$
$$F_p = F_{p,1}$$
$$V_{up} = V_{01}$$
$$V_{down} = V_1$$

The following relations can be derived from simple mass balances

$$V_{12} = V_1 - V_{11}$$
$$V_{01} = V_{11} + V_{st}$$
$$H_{01}V_{01} = H_{11}V_{11} + H_{st}V_{st}$$
$$F_{r,1} = F_1 - F_{p,1}$$

In the above relations V_{11} and F_1 are assumed constant. $F_{p,1}$ and V_{st} are manipulated variables. V_{12} is calculated from

$$V_{12} = \frac{\sqrt{P_{b,1} - P_{st,2}}}{R_1}$$

3.2.2 EFFECT 2

$$F_f = F_{p,1}$$
$$F_p = F_{p,2}$$
$$V_{up} = V_{12}$$
$$V_{down} = V_{23} = \frac{\sqrt{P_{b,2} - P_{st,3}}}{R_2}$$

3.2.3 EFFECT 3

$$F_f = F_{feed}$$
$$F_p = F_{p,3}$$
$$V_{up} = V_{23}$$
$$V_{down} = V_3 = \frac{\sqrt{P_{b,3} - P_{down}}}{R_3}$$

4. IMPLEMENTATION IN MATLAB/SIMULINK

Simulink is a dynamic simulation package that runs in the *Matlab* environment. It consists of a number of objects which are connected in order to create new objects. *Simulink* features a number of integrators including Runge-Kutta, Adams and Gear algorithms among others. During simulations the structure formed by connecting objects is flattened to a system of differential and algebraic equations which is then solved simultaneously. There is easy interchange of information between *Matlab* and *Simulink*, and all *Matlab* functions, including user-defined functions, retain their meaning.

The above model was realised in the *Matlab/Simulink* environment by employing the following strategy (see appendix D for a more detailed description of the approach followed):

- a number of new *Matlab* functions were defined in order to relate parameters, e.g. enthalpy in terms of pressure and temperature
- these functions were now included in a *Simulink* structure and grouped into rudimentary objects, e.g. tube liquid section mass balance, sump energy balance, etc.
- these objects were grouped together to create a single effect
- these effects were connected up in the appropriate manner to form the entire evaporator plant

4.1 RATE OF EVAPORATION AND CONDENSATION

These are determined using the following approach. Consider the energy balance

$$Q_{in,j} + F_{b,j-1}H_{b,j-1} - F_b H_b - V_{bf,j}H_{bvf,j} = \frac{d(W_{b,j}H_{b,j})}{dt}$$

At any particular time instant everything on the left of the above equation is known, except for V_{bf}, the rate of evaporation. Numerically approximating the derivative on the right of the equation, yields a simple algebraic equation to be solved for V_{bf}. The rate of condensation on the shell side is determined in a similar manner.

4.2 DETERMINATION OF STEADY STATE

A first approximation of the nominal steady state was made by directly solving the set of non-linear equations obtained by setting the derivatives equal to zero in the differential equations and using the algebraic relations above using Newton's method. To facilitate computation a constant heat transfer coefficient was assumed and an entire tube considered as a single, well-mixed entity.

Secondly, flow rates of all product streams, F_p, were set to a simple linear relationship with sump hold-up, W_s. Using the approximate answer as a starting point the system was run for a sufficient time to reach steady state. A relaxation method was in other words used to determine initial steady states. A number of steady states were determined covering the entire range of operating conditions.

5. MODEL VALIDATION

The model itself was not validated against any physical equipment. This is justifiable, since:

- material and energy balances over the system were achieved at all times
- in subsequent work the computer model is regarded as a "black box" and none of the information used thus far is utilised; the linear model and uncertainty description is derived using process identification techniques
- the model has features typical of chemical engineering processes
  - ⇒ capacious in the ability to store mass and energy
  - ⇒ non-linearity
  - ⇒ open loop stable
- the aim of the study is to implement robust analysis to a typical engineering system; this can now be accomplished in a fast and efficient manner

APPENDIX B: FITTING A CIRCLE THROUGH ANY THREE POINTS

The following theorem is used to determine the circle which passes through three arbitrary points (Baker&Bourne, 1920):

> The line drawn from the centre of a circle to bisect a chord is perpendicular to it: and the perpendicular drawn to a chord from the centre bisects the chord.

Given any three points one proceeds as follows:

- label the three points (A, B and C); the labelling is completely arbitrary
- find the point which bisects AB and draw a line through it perpendicular to AB
- find the point which bisects BC and draw a line through it perpendicular to BC
- the intersection of the lines drawn in steps 2 and 3 is the centre of the circle
- the radius is simply the distance from the centre to either of points A, B or C

APPENDIX C: NOMINAL PLANT AND UNCERTAINTY DESCRIPTION

The plant and uncertainty description is as shown in figures 1 to 13. Figure a in each case is the Bode magnitude plot of the nominal transfer function, while figure b is its Bode phase plot. Figure c represents the magnitude of the norm-bounded uncertainty (no phase plot is required since the elements are pure real). The following transfer functions are equal to zero and not shown:

$$g_{13} = g_{23} = g_{33} = 0$$

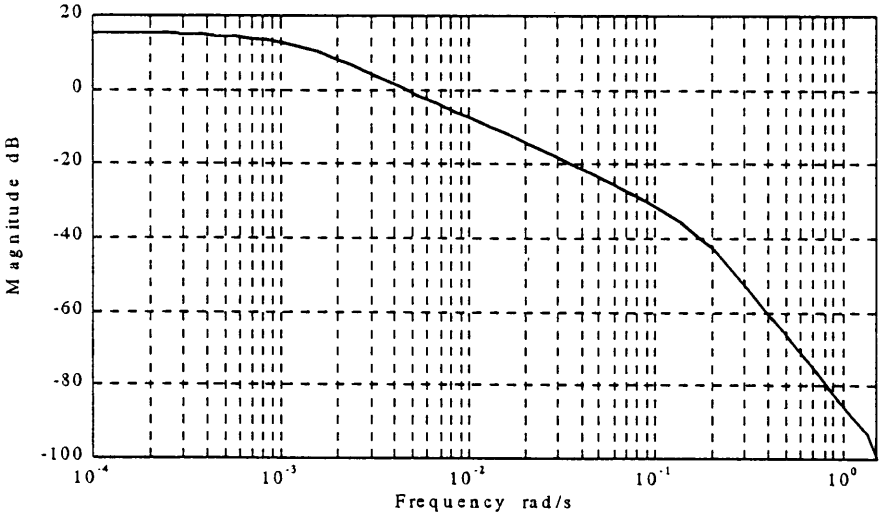

Figure 1a: g_{011} - *amplitude ratio*

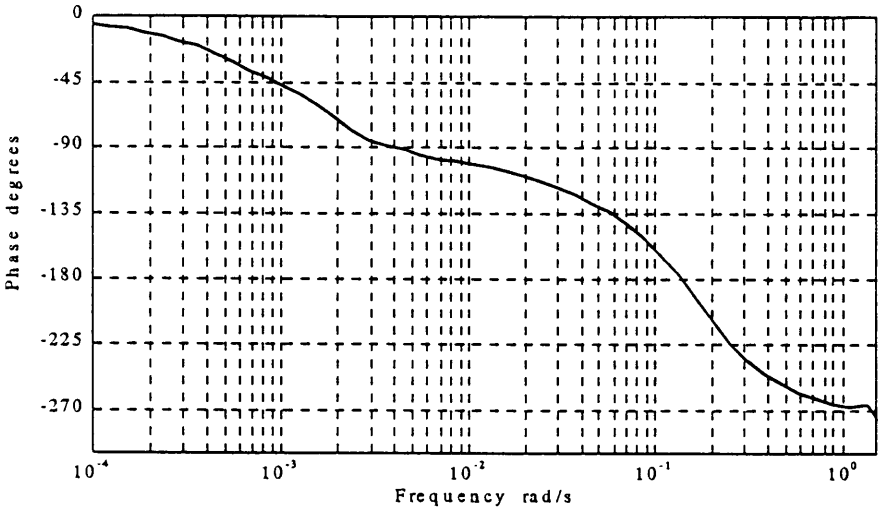

Figure 1b: g_{011} - *phase angle*

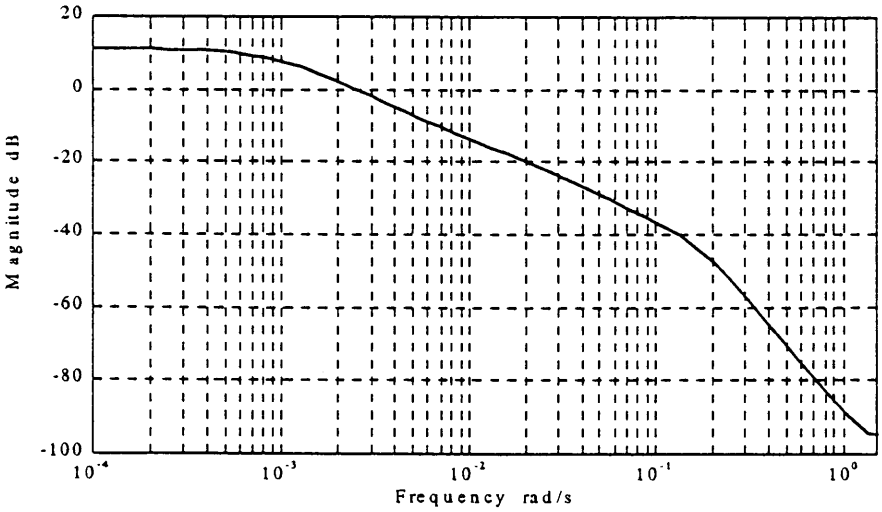

Figure 1c: $\hat{\delta}_{11}$ - *magnitude*

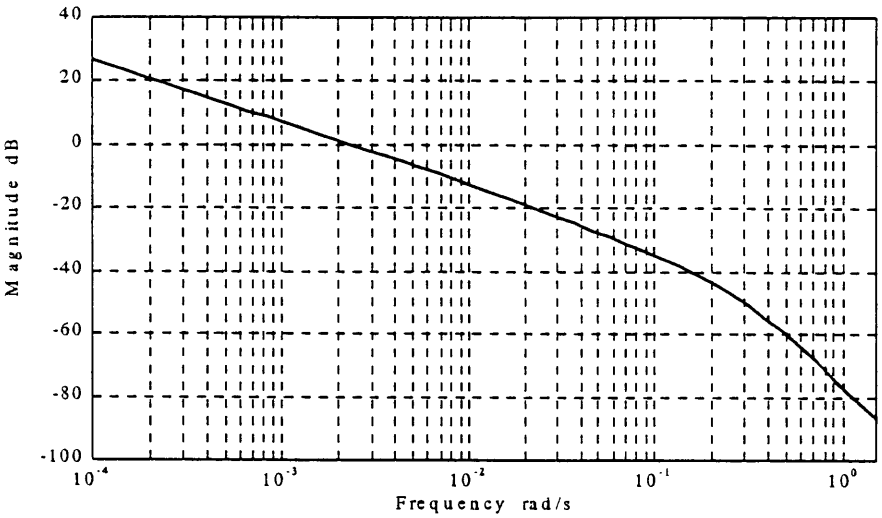

Figure 2a: g_{021} - *amplitude ratio*

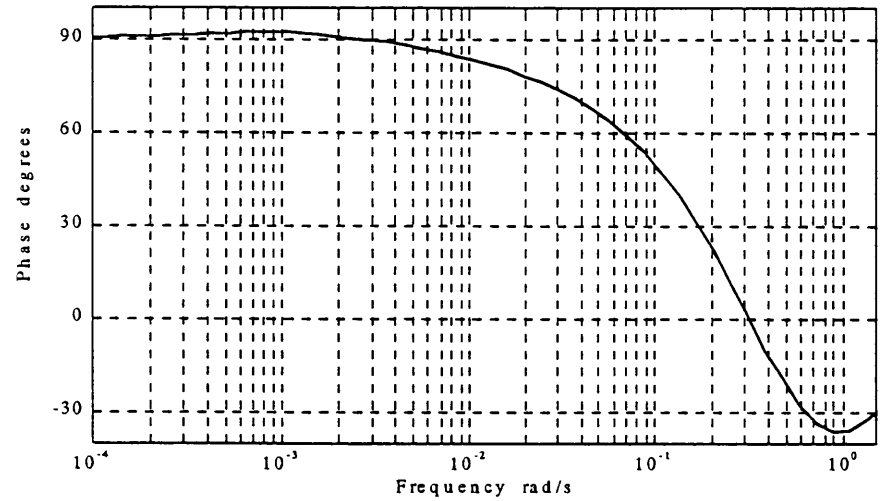

Figure 2b: g_{021} - *phase angle*

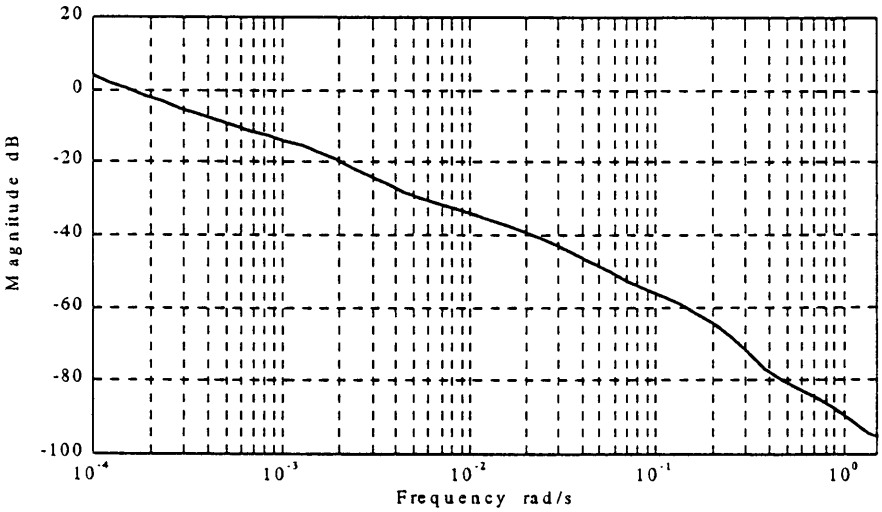

Figure 2c: $\hat{\delta}_{21}$ - *magnitude*

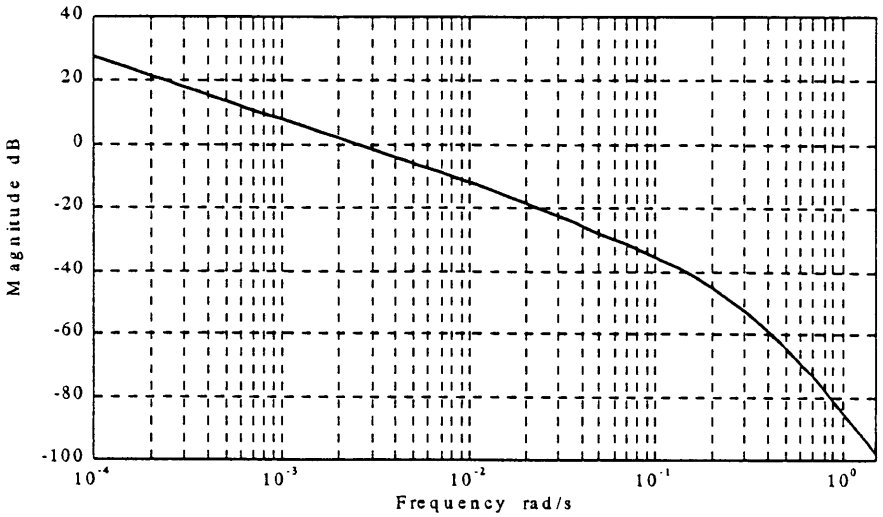

Figure 3a: g_{031} - *amplitude ratio*

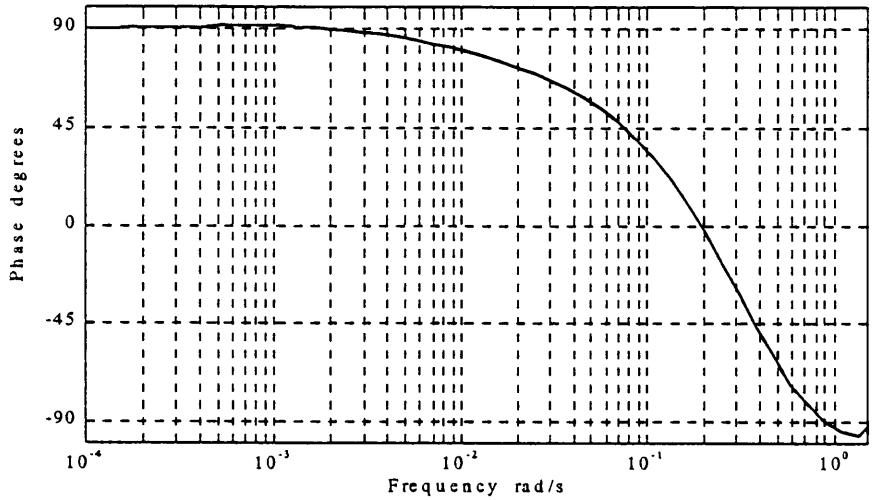

Figure 3b: g_{031} - *phase angle*

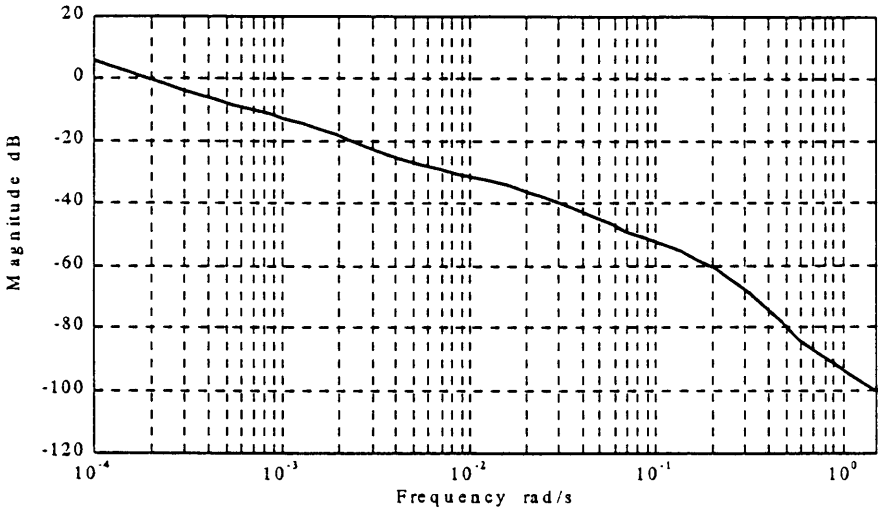

Figure 3c: $\hat{\delta}_{31}$ - *magnitude*

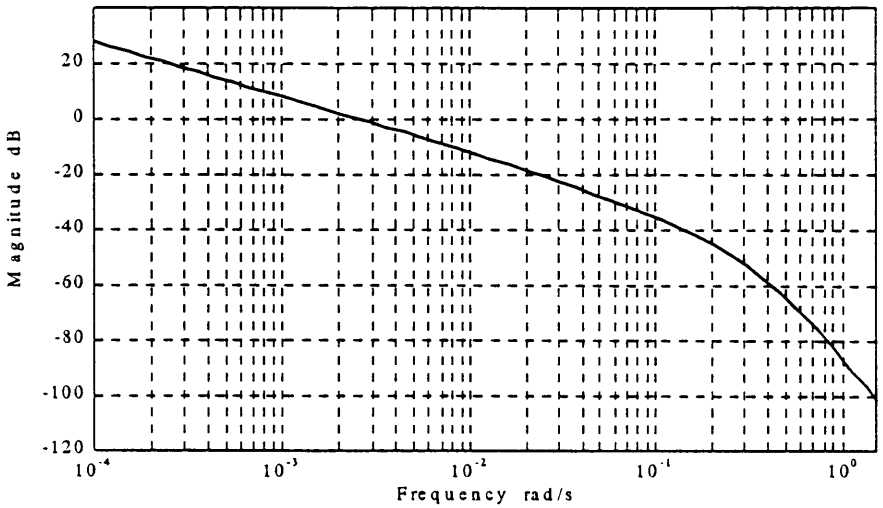

Figure 4a: g_{041} - *amplitude ratio*

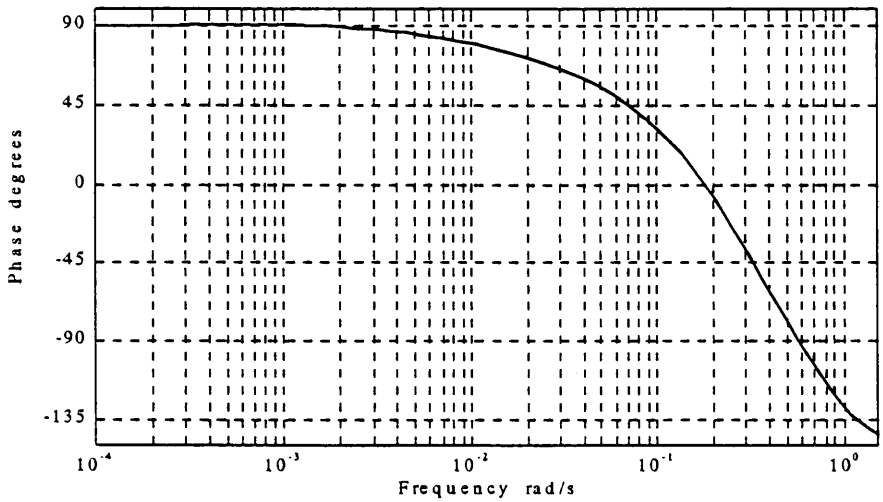

Figure 4b: g_{041} - *phase angle*

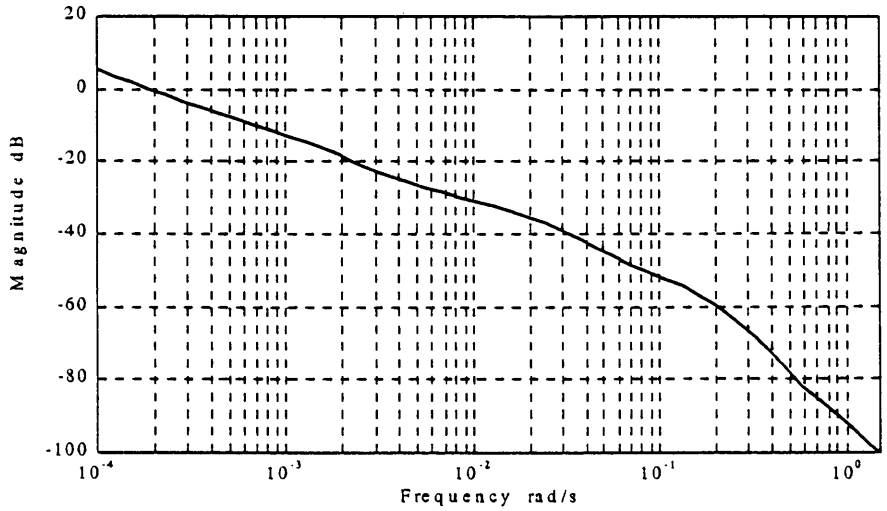

Figure 4c: $\hat{\delta}_{41}$ - *magnitude*

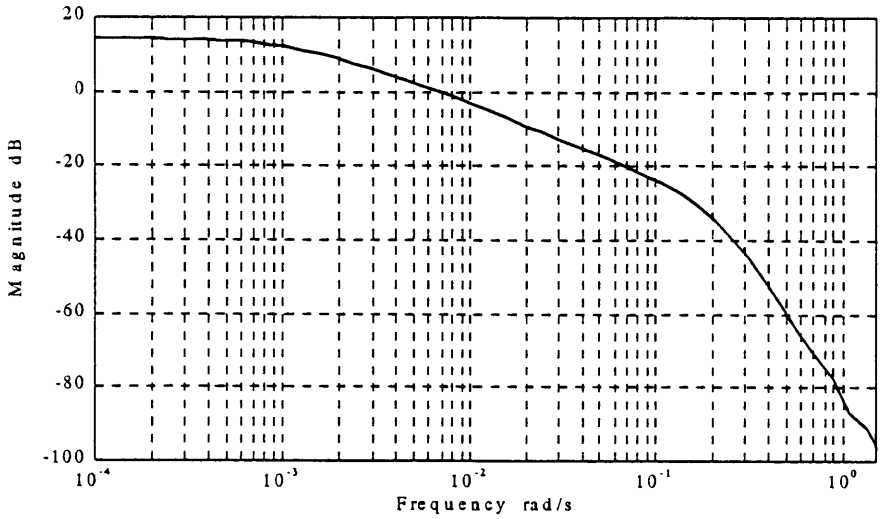

Figure 5a: g_{012} - *amplitude ratio*

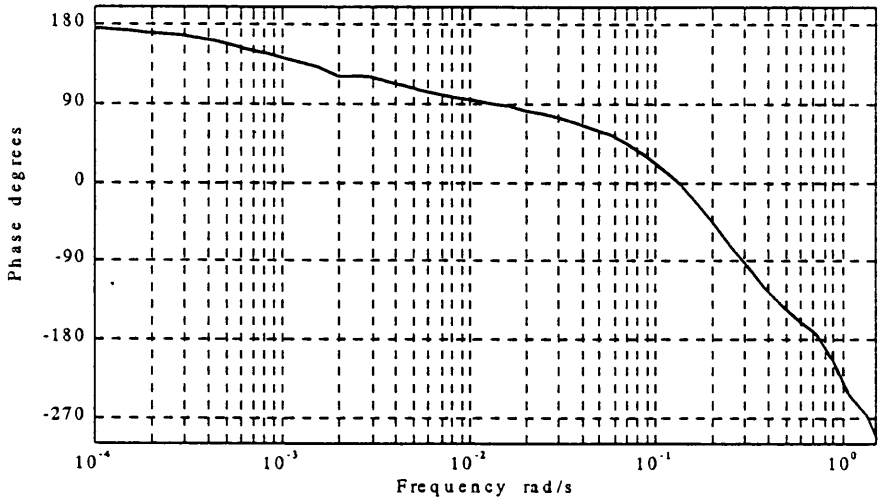

Figure 5b: g_{012} - *phase angle*

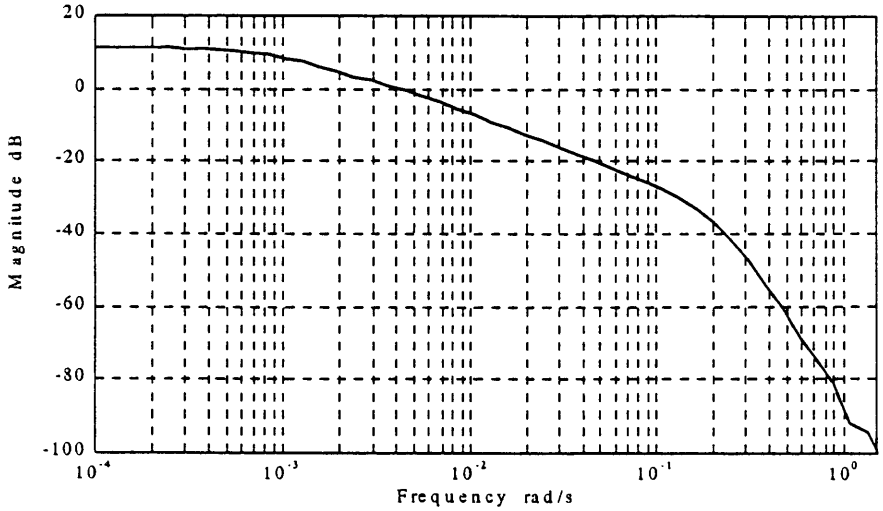

Figure 5c: $\hat{\delta}_{12}$ - *magnitude*

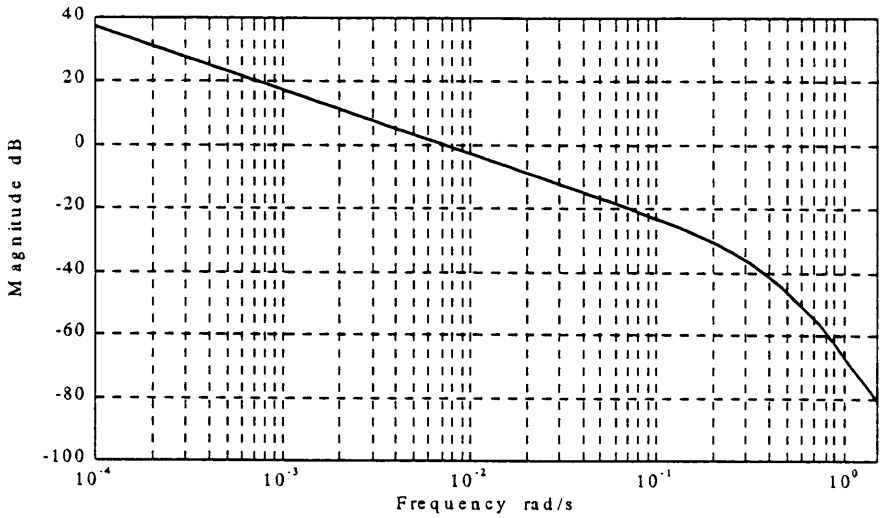

Figure 6a: g_{022} - *amplitude ratio*

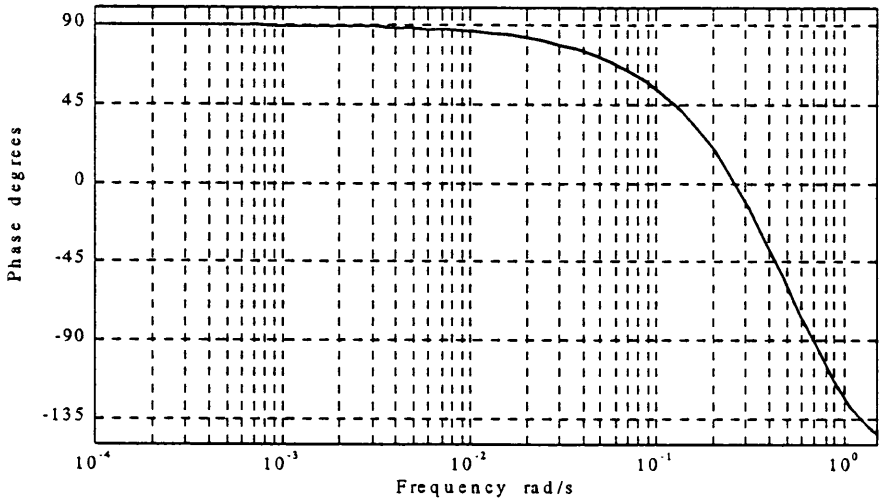

Figure 6b: g_{022} - *phase angle*

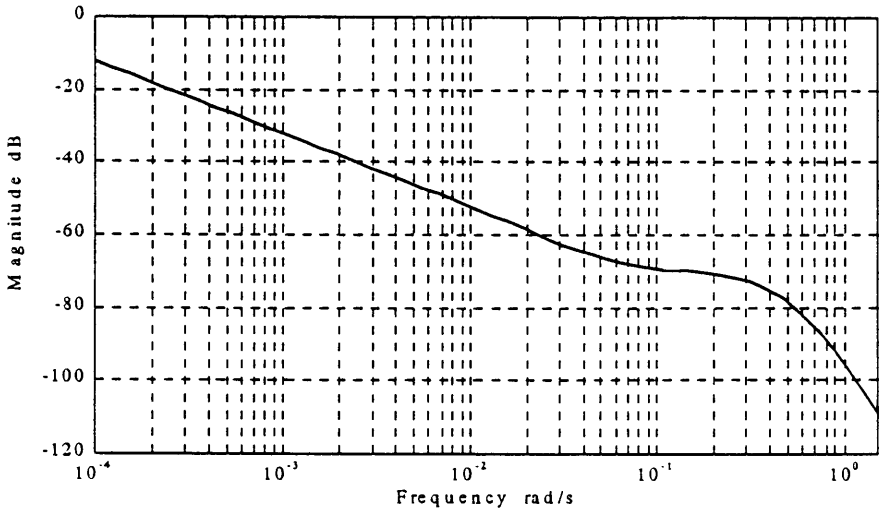

Figure 6c: $\hat{\delta}_{22}$ - *magnitude*

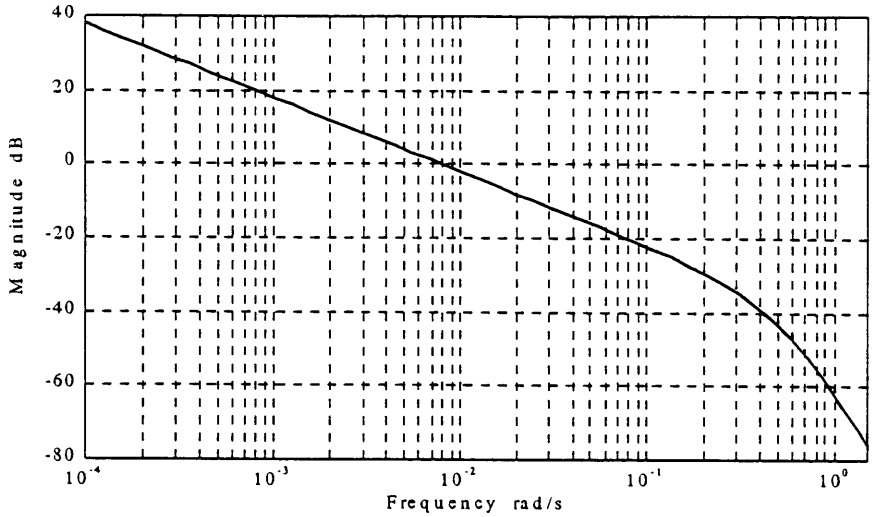

Figure 7a: g_{032} - *amplitude ratio*

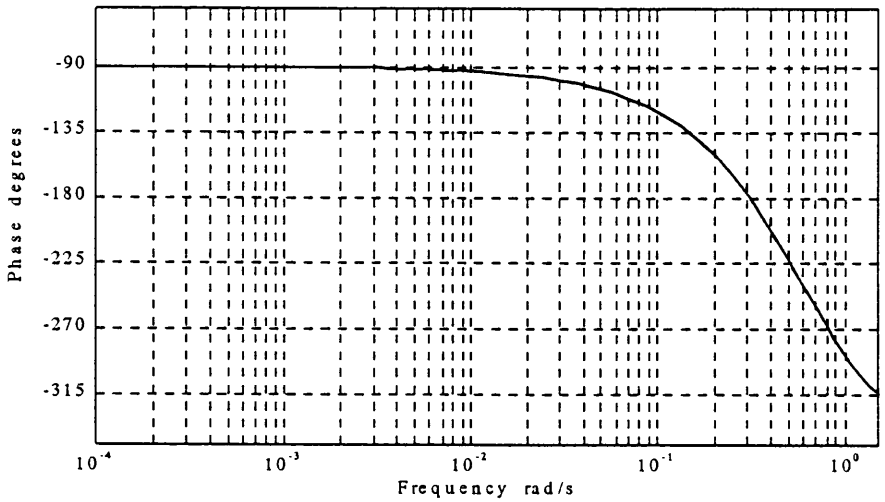

Figure 7b: g_{032} - *phase angle*

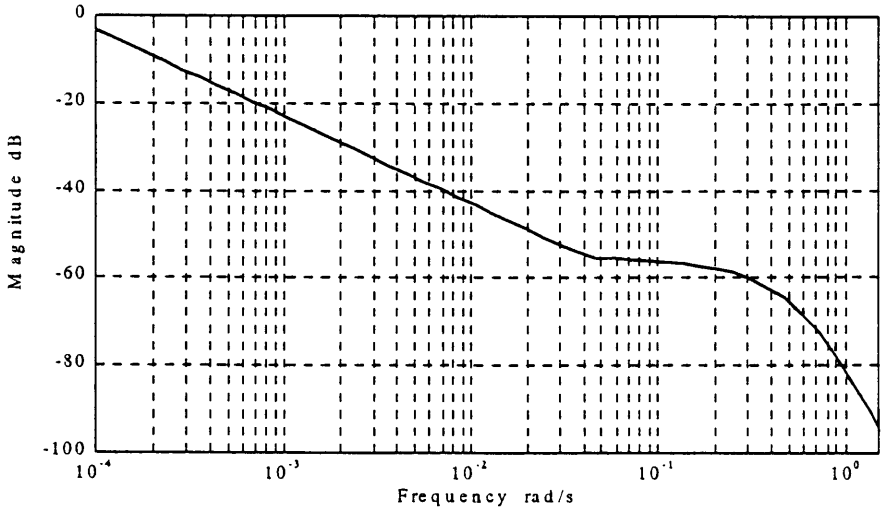

Figure 7c: $\hat{\delta}_{32}$ - *magnitude*

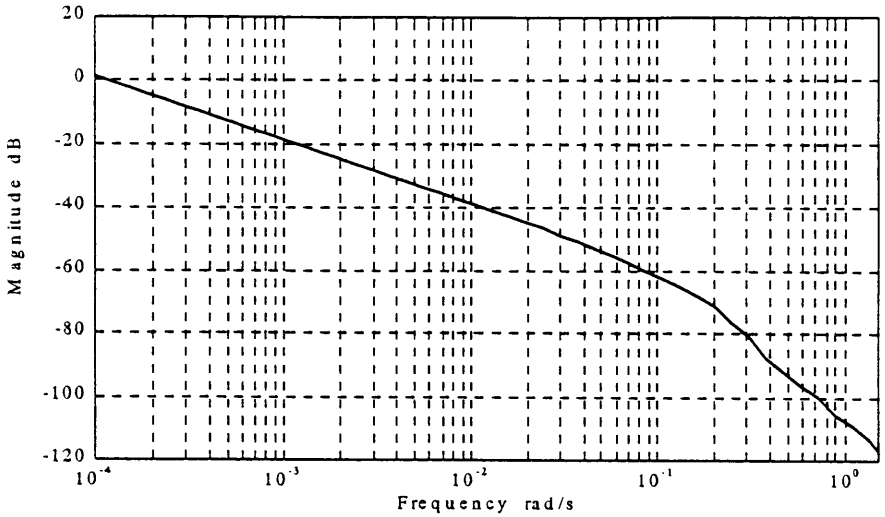

Figure 8a: g_{042} - *amplitude ratio*

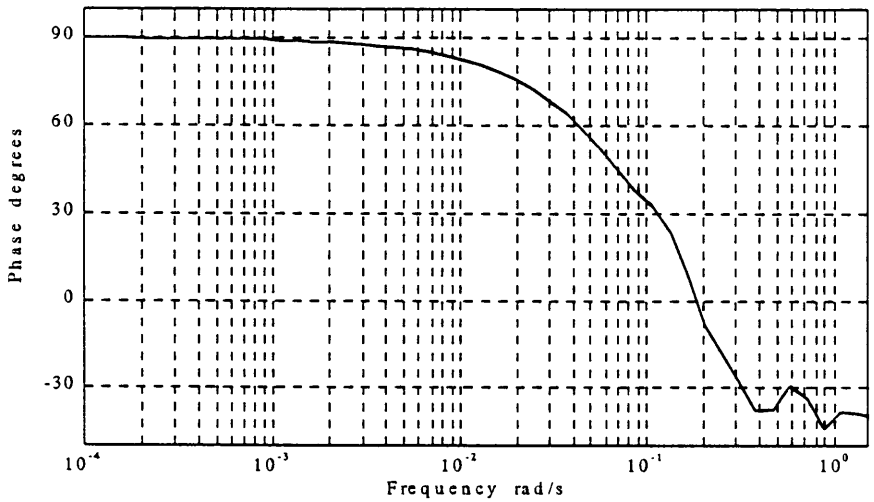

Figure 8b: g_{042} - *phase angle*

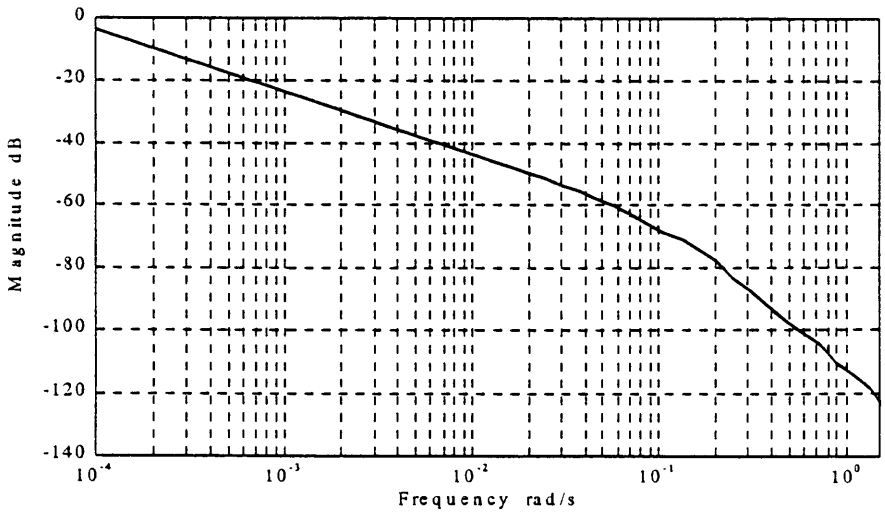

Figure 8c: $\hat{\delta}_{42}$ - *magnitude*

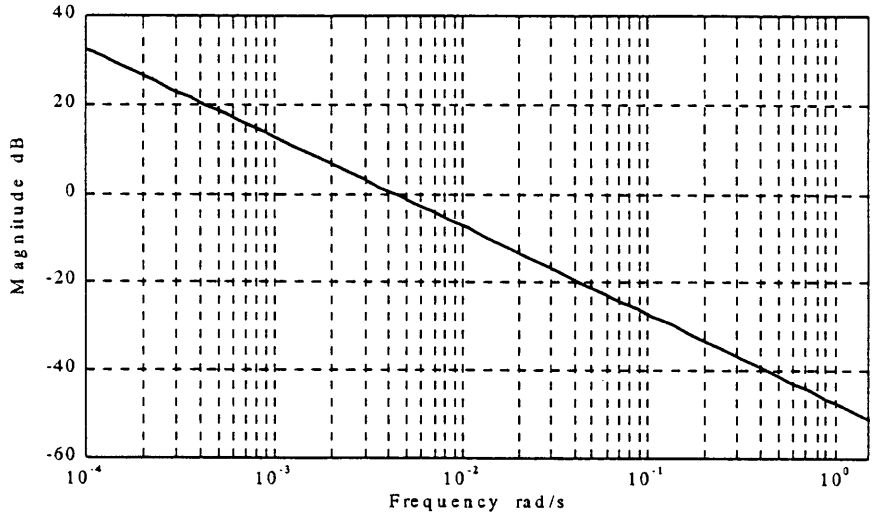

Figure 9a: g_{033} - *amplitude ratio*

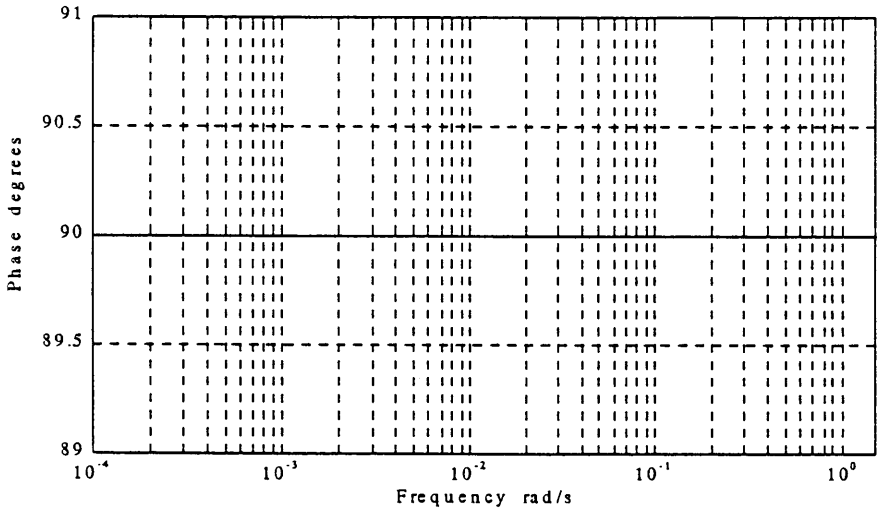

Figure 9b: g_{033} - *phase angle*

$$\tilde{\delta}_{33} = 0$$

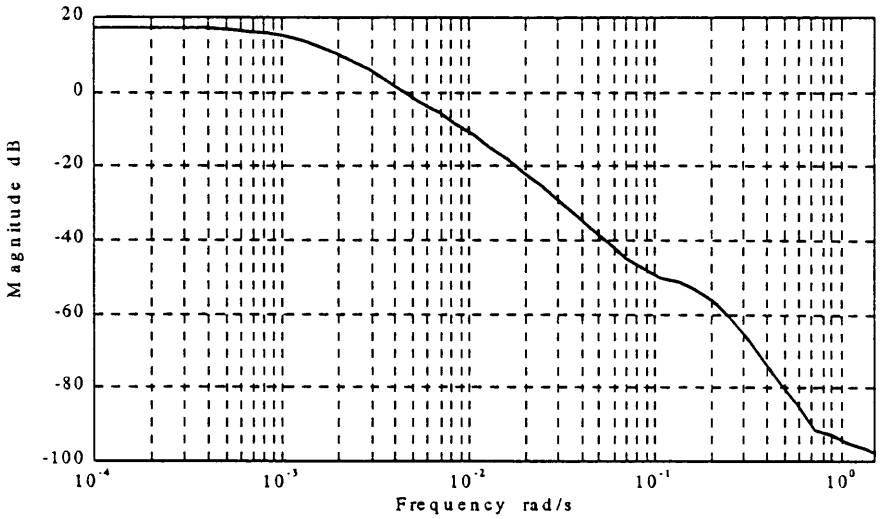

Figure 10a: g_{014} - *amplitude ratio*

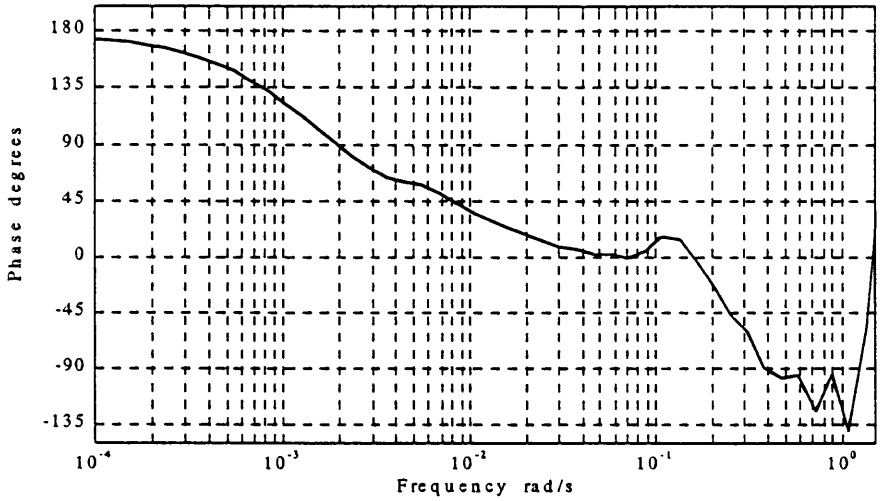

Figure 10b: g_{014} - *phase angle*

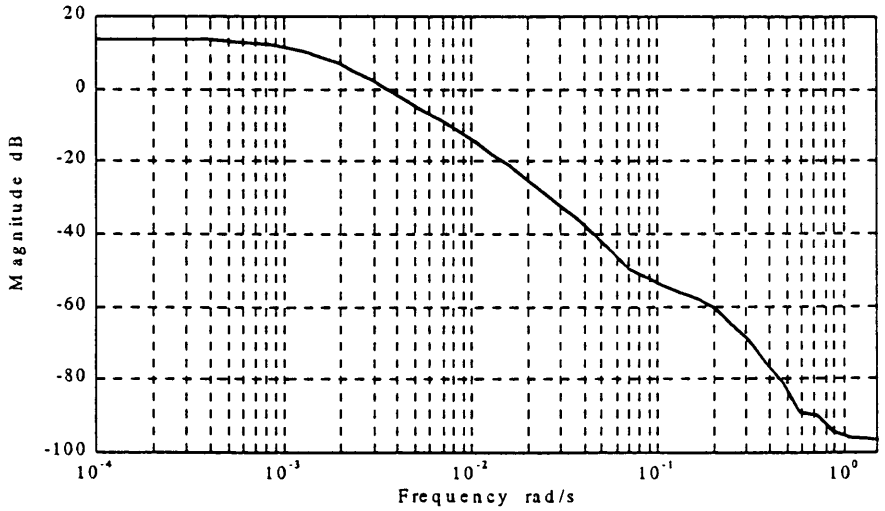

Figure 10c: $\hat{\delta}_{14}$ - *magnitude*

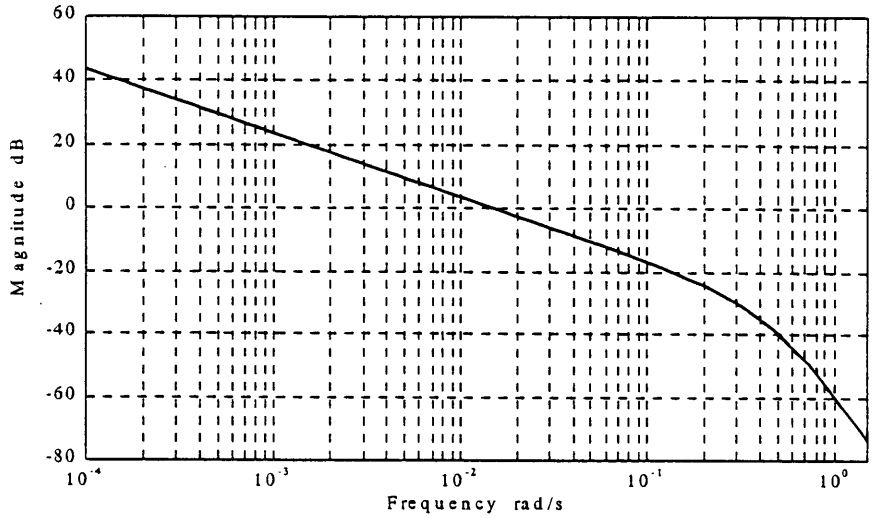

Figure 11a: g_{024} - *amplitude ratio*

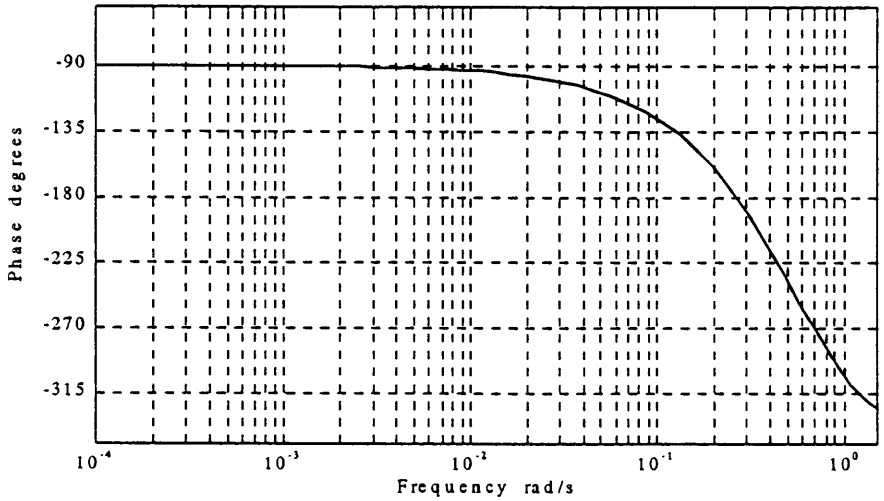

Figure 11b: g_{024} - *phase angle*

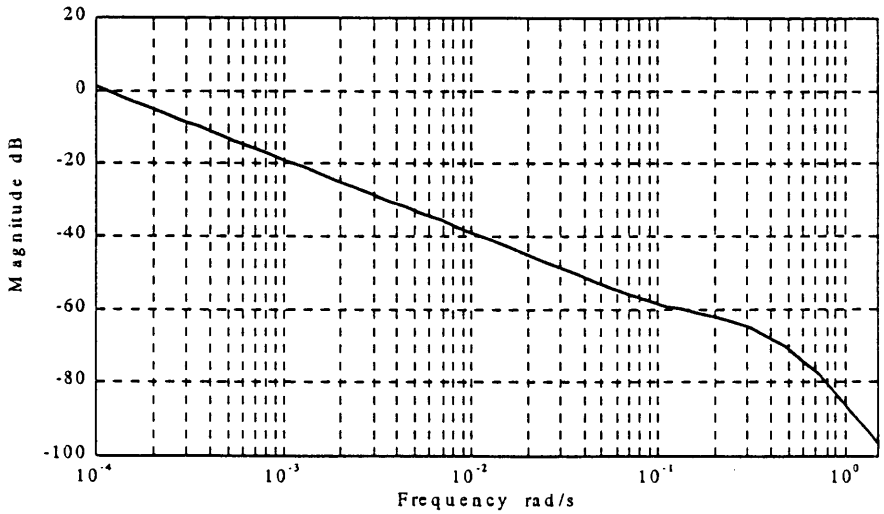

Figure 11c: $\hat{\delta}_{24}$ - *magnitude*

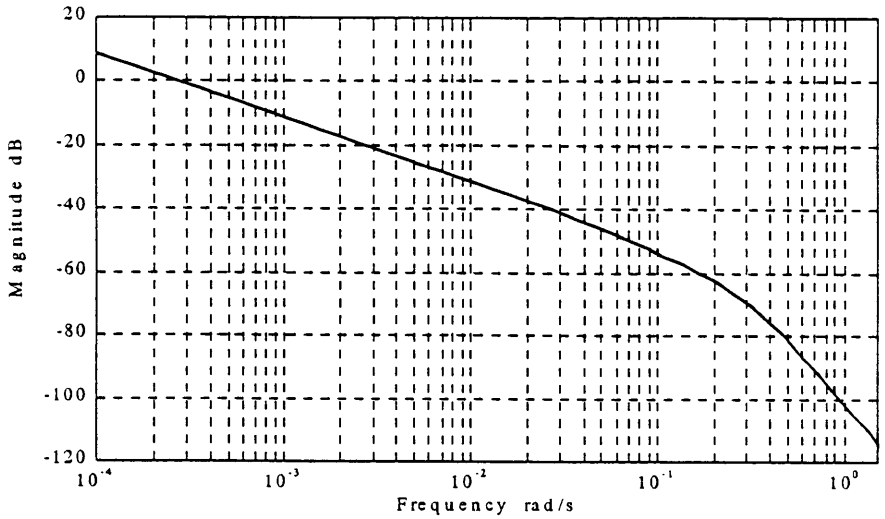

Figure 12a: g_{034} - *amplitude ratio*

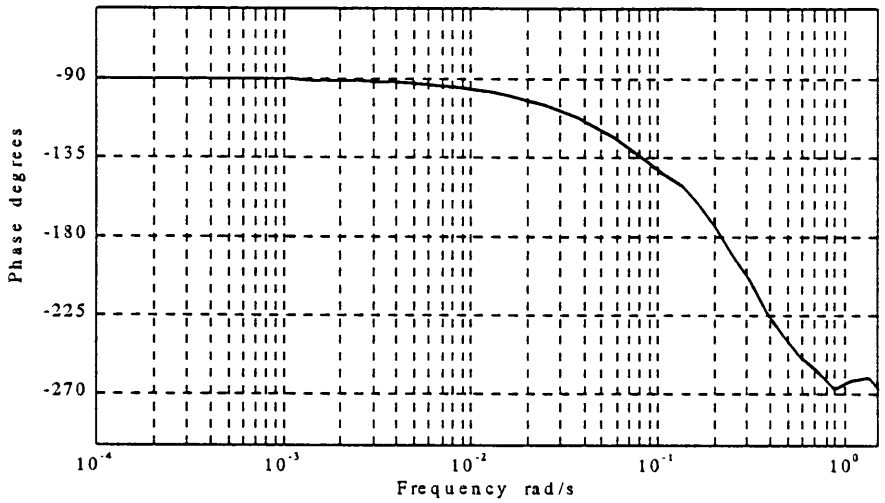

Figure 12b: g_{034} - *phase angle*

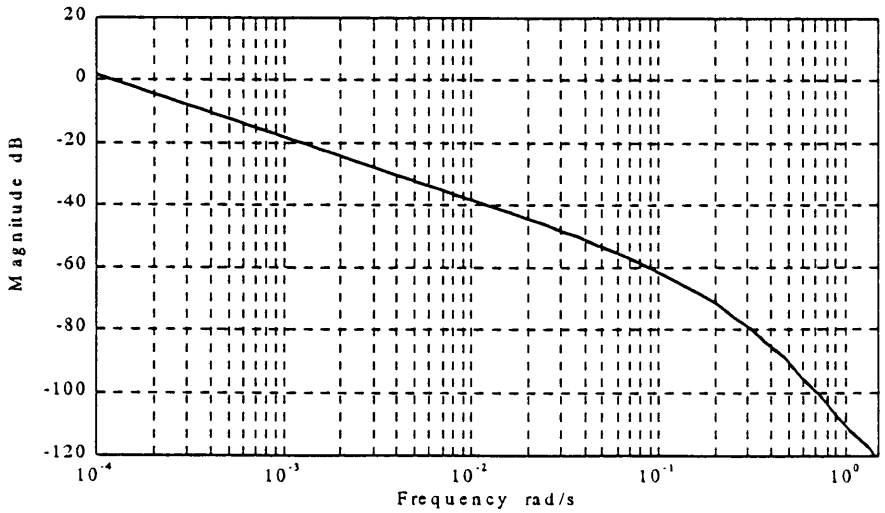

Figure 12c: $\hat{\delta}_{34}$ - *magnitude*

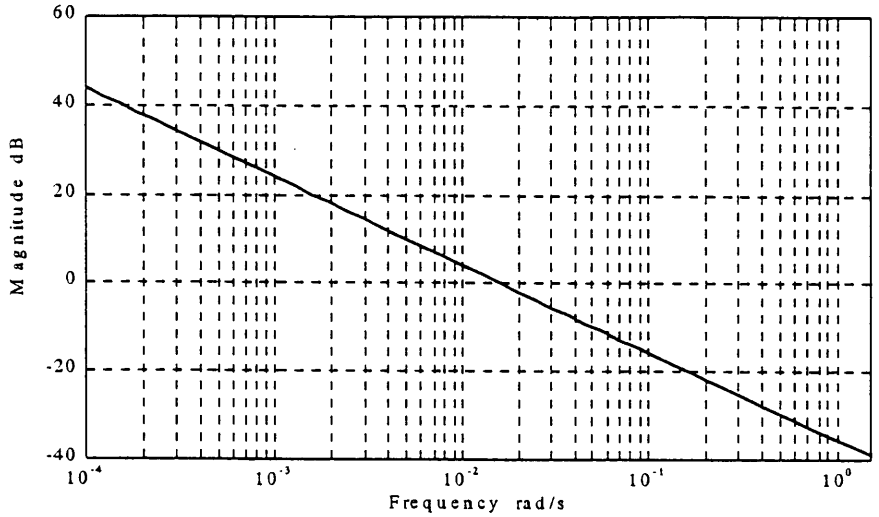

Figure 13a: g_{044} - *amplitude ratio*

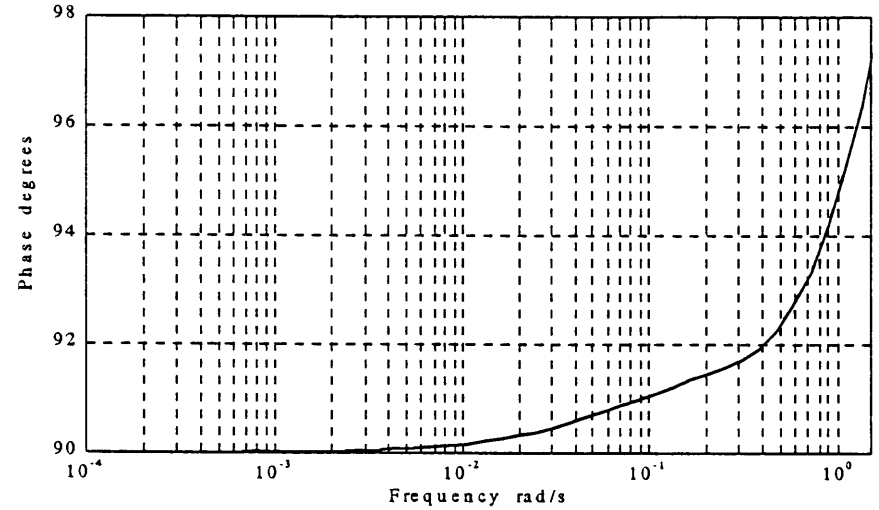

Figure 13b: g_{044} - *phase angle*

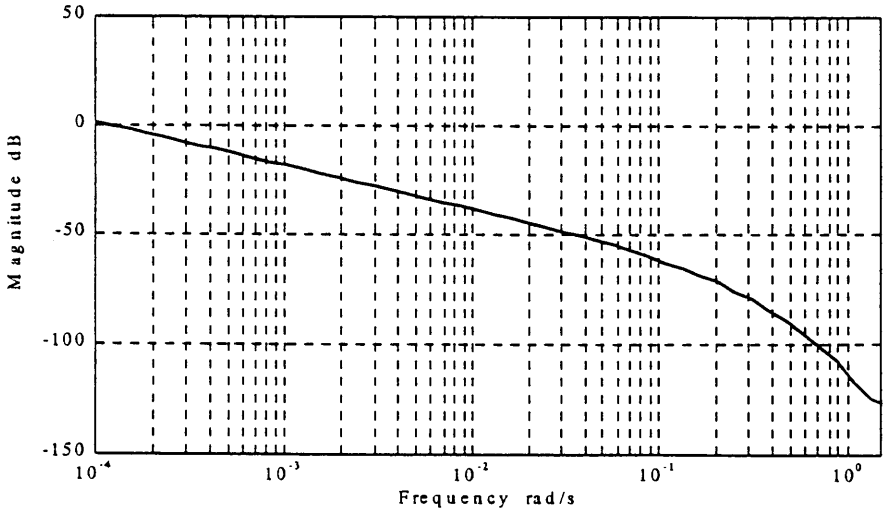

Figure 13c: $\hat{\delta}_{44}$ - *magnitude*

APPENDIX D: DESCRIPTION OF SOFTWARE

The aim of this appendix is to give an overview of the software that was used during this study. The existing features of the *Matlab/Simulink* environment were combined into a user-friendly interface to create a powerful modelling, process identification, controller design and robust analysis tool.

1. *MATLAB/SIMULINK* MODEL

The *Simulink* environment is ideally suited to an object-oriented approach. The rudimentary objects in the standard *Simulink* library were combined into simple objects pertaining to the evaporator plant, e.g. sump mass balance, tube liquid section energy balance etc. Included in these objects are calls to user-defined functions to perform calculations such as enthalpy, boiling point etc. As an example of a simple object the mass balance over a single tube section is shown in figure 1.

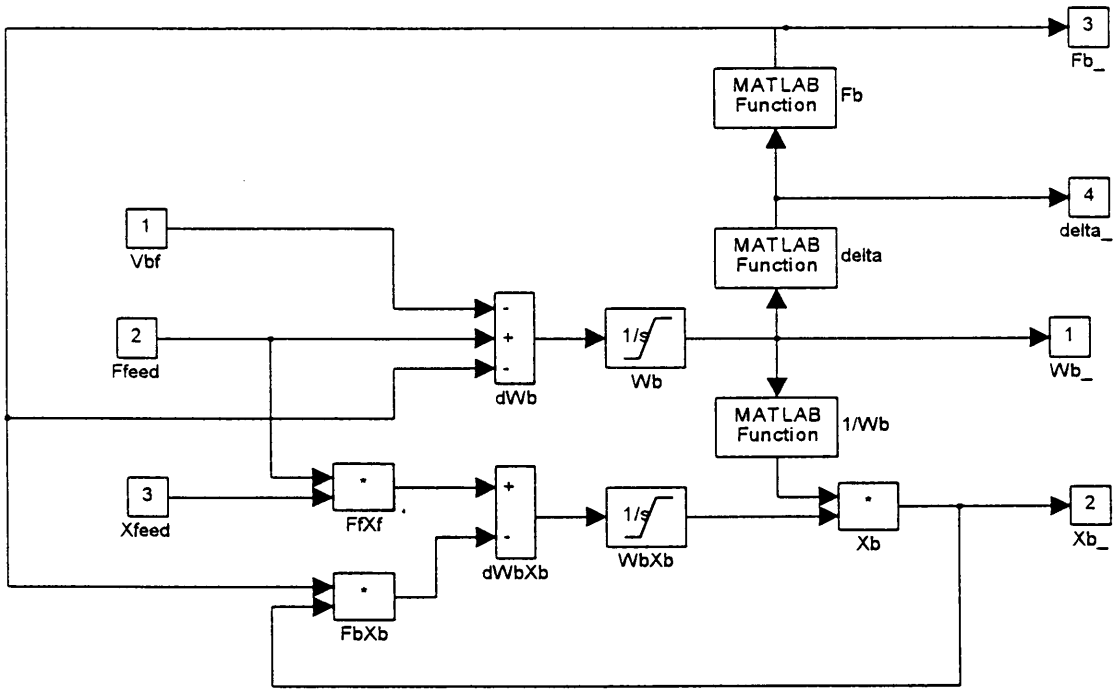

Figure 1: *Mass balance over the liquid in a single tube section*

The external inputs to the object are V_{bf} ($V_{bf,j}$ in the equations below), F_{feed} ($F_{b,j-1}$) and X_{feed} ($X_{b,j-1}$). The outputs from the object are W_b ($W_{b,j}$), X_b ($X_{b,j}$), F_b ($F_{b,j}$) and delta. A quick inspection will reveal that the object solves the following two differential equations (appendix A):

Total mass:

$$F_{b,j-1} - F_{b,j} - V_{bf,j} = \frac{dW_{b,j}}{dt}$$

Dissolved substance:

$$F_{b,j-1}X_{b,j-1} - F_{b,j}X_{b,j} = \frac{d(W_{b,j}X_{b,j})}{dt}$$

The blocks W_b and W_bX_b are integrators. The signal fed into these blocks are the left hand sides of the above equations.

In this object there are three calls to *Matlab*-functions (refer to appendix A for the detailed equations):

- F_b calculates the liquid flow rate from the tube section given the film thickness, δ
- delta calculates the film thickness given the total hold-up of liquid, W_b (the number of tubes and tube diameter is also required and is set in the function call)
- $1/W_b$ simply calculates the inverse of W_b

The structure shown in figure 1 can be grouped into a single object with input and output ports in the order in which they are numbered. This new user-defined object (tube liquid mass balance) is now combined with a similar object which calculates the energy balance over a tube liquid section (tube liquid energy balance). This is shown in figure 2. The input P_b is the pressure in the tube, H_{feed} is the enthalpy of the liquid from the above tube section and Q_{in} is the heat transferred to the tube section from the shell-side. The output T_b is the temperature of the liquid (its boiling point), H_b is its enthalpy and V_{bf} the rate of vapour formation in the tube section.

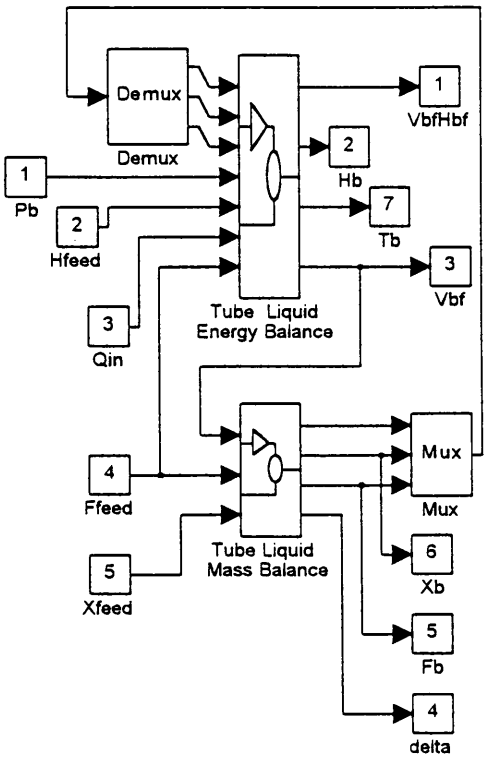

Figure 2: *Balances over the liquid in a single tube section*

The object formed by grouping figure 2 into a single object (tube liquid section balance), are now combined with three identical tube liquid section balances to model the total balance over the liquid in a single tube (tube liquid balance main). This object is now combined with objects describing mass and energy balances over the vapour phase (tube vapour balance) and sump (sump balances) to model the process side of a single effect. This object is shown in figure 3.

The object formed by grouping figure 3 (process side) is now combined with a similar object modelling the mass and energy balances on the shell-side of the same effect (shell side) in order to model a total effect. This is shown in figure 4.

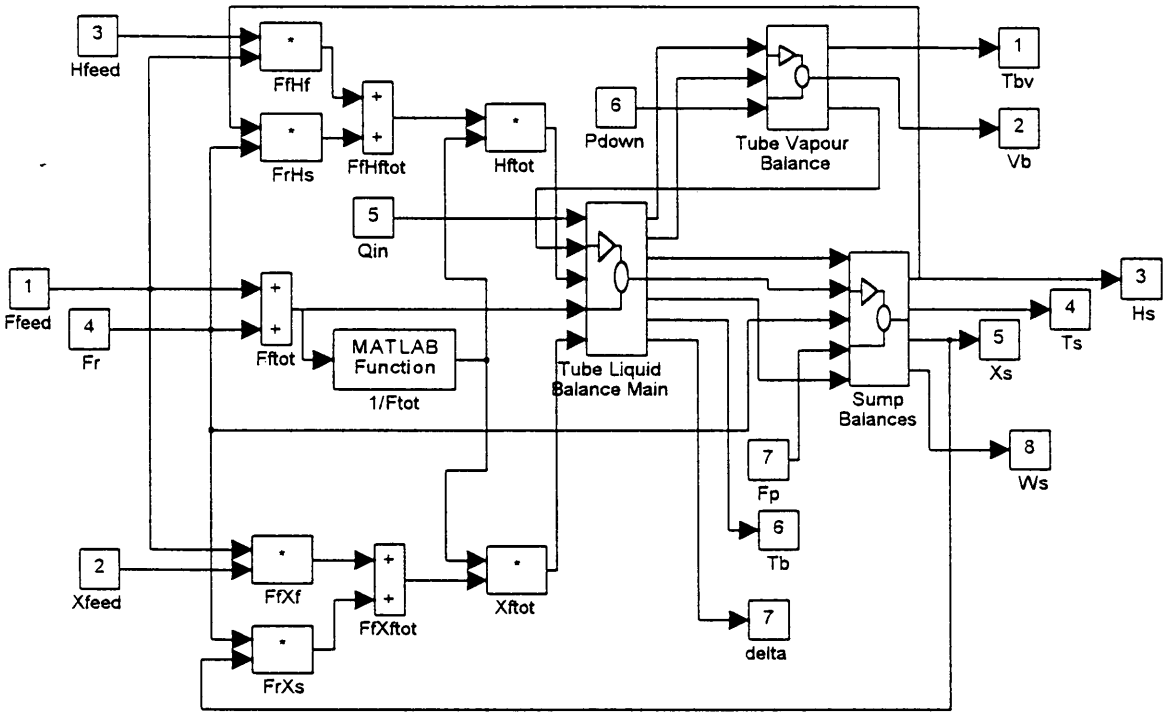

Figure 3: *Process side of a single effect*

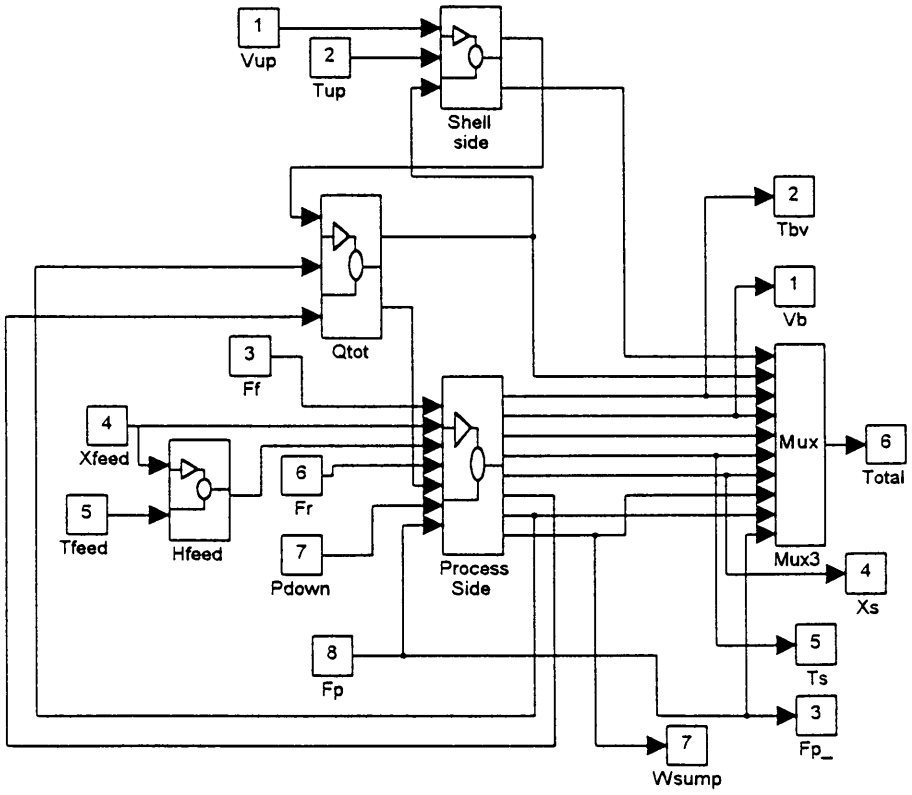

Figure 4: *A single effect*

The object denoted Qtot models the heat transfer between shell- and process sides. Three of these total effect objects (single effect 1 to 3) are now combined to model the entire process as shown in figure 5.

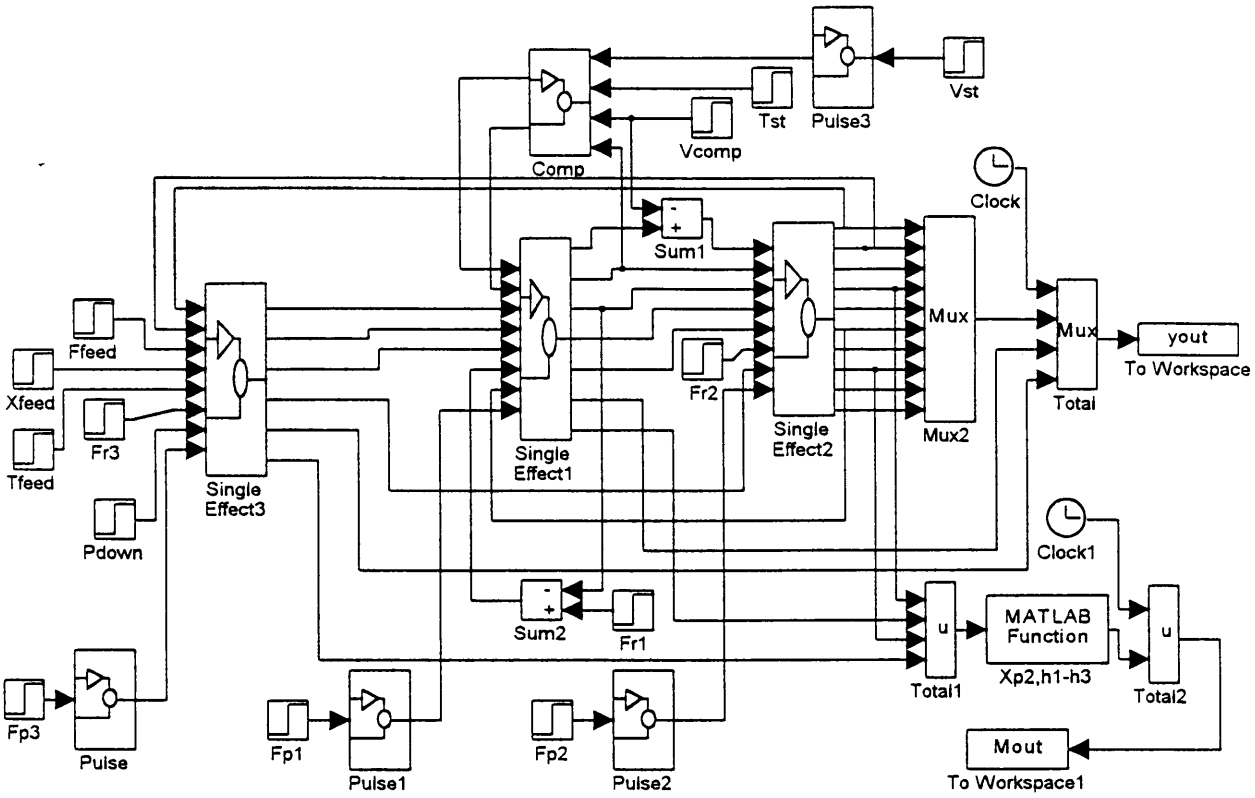

Figure 5: *Total Simulink model*

The important features of figure 5 are:

- it allows the user to insert pulse disturbances into the inputs $F_{p,1}$, $F_{p,2}$, $F_{p,3}$ and V_{st} (extension to other inputs is possible)
- it exports the simulation results to the main *Matlab* workspace through blocks To Workspace and To Workspace 1.

2. PROCESS IDENTIFICATION

The purpose of this software was to streamline process identification. The first step was to code the algorithm referred to in paragraph 2.2.1 (chapter 2) into a *Matlab* function. This function calculates the frequency response at a fixed value of frequency, given the time response. A second function was written which calls the above function to calculate the frequency response over a discrete grid of frequency values.

The identification described in paragraph 1 of chapter 3, required process identification around 16 steady state starting conditions. A number of small programs was therefore written to:

- load the relevant steady state starting point
- define the pulse disturbance
- call the *Simulink* model described in paragraph 1 which then solves the process output for the pulse disturbance
- log the output data at the required sampling rate
- transform output data to deviation variables
- if required (paragraph 2.1, chapter 2), the data is numerically differentiated

- call the *Matlab* function described above to calculate the frequency response over a specified grid of frequencies
- save the results

A further program was written to organise the 16 frequency responses for each input-output pair into a single 17-column matrix. (The first entry is the frequency, the following 16 are the frequency responses at the 16 steady state starting points.)

The algorithm described in paragraph 2.1.4 of chapter 3 was coded into a *Matlab* function. This function was applied to columns 2 to 17 of each row of each of the matrices described in the above paragraph in order to calculate the smallest circle passing through the 16 points in the complex plane. The center of this circle corresponds to the nominal plant model and its radius to the uncertainty norm-bound.

The final *Matlab* program dealing with identification performed the following tasks:
- arranges the nominal plant model for each input output pair into the *multivariable frequency response* data structure of the *Multivariable frequency domain toolbox* (Ford, Maciejowski & Boyle, 1990)
- arranges the uncertainty norm-bound into a similar data structure
- scales the nominal plant and uncertainty

3. CONTROLLER DESIGN

Matlab software was written to facilitate multivariable controller design using the Inverse Nyquist Array and Characteristic Locus design approaches. Abundant use was made of *Matlab*'s built-in graphics capabilities for the plotting of Nyquist, Nichols and Bode diagrams, to create a graphical and informative design environment. The existing *Matlab* functions were combined into a user-friendly, menu-driven suite of software. Added features include trimmings such as the ability to zoom in on certain portions of a plot by specifying a frequency range. Use is made throughout of the *multivariable frequency response* data structure.

The menu structure for the INA controller design software includes:
- Initialisation of nominal plant model frequency response.
- Determination of row dominance.
- Quasi-Gauss elimination. Use is made of a Nyquist plot to represent the frequency response of the perfect elimination function. The user decides on the form of the low order transfer function to be used and gives initial estimates of the coefficients. A performance function is then optimised over the coefficients to determine the optimal approximation. A Nyquist plot of this approximation is now given for comparison.
- The Inverse Nyquist Array. This is a plot of the inverse frequency response of plant and compensator, with Gerschgorin circles imposed on the diagonal elements.
- Diagonal controller design. Here a number of single loop controllers is designed for each diagonal input output pair. Graphical information includes Nyquist, Bode and Nichols plots. Following the total diagonal controller design, stability, performance and interaction can be evaluated using the standard Nyquist plot of the characteristic loci, the singular values of sensitivity and complimentary sensitivity, and the Ostrowski circles, respectively.

The menu structure for the CL controller design software includes
- Initialisation of nominal plant model frequency response.
- Nyquist plot of characteristic loci.

- High frequency decoupler design. The user specifies the high frequency point after which the ALIGN algorithm (paragraph 3.2, chapter 2) is used to calculate the compensator. The loci can also be further manipulated to ensure that stability is easily achievable in later design steps.
- Medium frequency decoupler design. The user specifies the frequency and phase lead to be added to the loci. Graphical aids are Bode, Nyquist and Nichols plots.
- Low frequency decoupler design. The user specifies the frequency point and α (a tuning parameter). Graphical aids include those listed at medium frequency design, as well as plots of the singular values of sensitivity and complimentary sensitivity.
- Plotting of the misalignment angles.

4. ROBUST ANALYSIS

Three programs were written for the calculation of the structured singular value (SSV), described in paragraph 1.3.2.4 of chapter 2, for robust stability, nominal performance and robust performance evaluation. The software:

- loads the nominal plant model frequency response, G_0
- loads the uncertainty norm bounds as a function of frequency
- loads the relevant controller (INA or CL) frequency response, K
- detunes the controller $K = q \cdot K$; q is specified
- plots the characteristic loci of G_0K in order to establish nominal stability
- forms the weighting matrices W_1 and W_2
- if applicable, forms W_P given the performance weighting
- forms M_{22} or M in the *multivariable frequency response* data structure
- calculates the SSV of M_{22} or M using the built in *fssv* function
- plots the SSV as a function of frequency